No. 006
September 1968

EXPERIMENTS ON THE RESISTANCE OF A FAMILY OF BOXLIKE HULL FORMS FOR AMPHIBIOUS VEHICLES

Horst Nowacki
James L. Moss
Eric D. Snyder
Bernard J. Young

THE DEPARTMENT OF NAVAL ARCHITECTURE AND MARINE ENGINEERING

THE UNIVERSITY OF MICHIGAN
COLLEGE OF ENGINEERING

THE UNIVERSITY OF MICHIGAN
College of Engineering
Department of Naval Architecture and Marine Engineering

EXPERIMENTS ON THE RESISTANCE OF A FAMILY OF BOXLIKE HULL FORMS FOR AMPHIBIOUS VEHICLES

by
Horst Nowacki
James L. Moss
Eric D. Snyder
Bernard J. Young

for
Department of the Navy
Office of Naval Research
Washington, D.C.

Nonr-1224(64)

Administered through:
Office of Research Administration

September 1968
Ann Arbor

ABSTRACT

Resistance, trim, and sinkage were measured for a family of hull shapes derived from a simple box-like parent, similar to present amphibians. The data were analyzed to reach conclusions as to the feasibility of major resistance reductions, the effects of drastic variations in hull proportions, and the presence of scale effects.

TABLE OF CONTENTS

I. Introduction

The design of tracked amphibious vehicles is governed by a multitude of operational requirements that make it very difficult to attain satisfactory hydrodynamic performance. The mobility of the vehicles on land, their obstacle-climbing capability, the geometrical properties of the track propulsion system, the desire to save space in transit shipment, all combine into design requirements that result in blunt, box-like hull shapes of unusually high displacement-length ratio and block coefficient, and correspondingly low length-beam ratio.

In water operation, such shapes are subject to great energy losses due to separation and wavemaking. In consequence of this and due to inefficient water propulsion by tracks, only moderate speeds of, say, 8 m.p.h. are reached, whereas operational requirements make speeds above 10 m.p.h., perhaps eventually 15 m.p.h., very desirable. Speed improvements will have to be brought about by genuine hydrodynamic gains by better hull form design and/or higher efficiency propulsion systems since an increase in the weight and size of the power plant can be realized only at the expense of payload reductions which are not usually acceptable. This study has concentrated on the resistance properties of such hull forms in order to examine the possibility of speed gains by hull form modifications.

Many attempts have been made to improve the hydrodynamic performance of tracked amphibians within their present geometrical constraints, either by minor alterations in hull shape that seemed permissible, or by installing special devices such as guide vanes and fins. As regards the resistance, despite a great deal of ingenuity and inventiveness the gains have unfortunately been limited to about 25 percent at best, Ref. (1). While this would be a very significant improvement with other types of ships, it is clearly not sufficient for the speed gains aimed at here. Assuming a square velocity law of the resistance, one would obtain a speed gain of about 12 percent, or about one m.p.h.

In view of this situation, two main questions were raised at the outset of the program:

1. Under the present constraints of amphibian design, is the high level of resistance a physical necessity?

2. If the current design constraints were to be alleviated, what improvements could be expected and what would be the most promising geometric alterations? The changes contemplated in this context went beyond what may seem compatible with land operations. It was thought that this was justifiable, however, in trying to anticipate innovative designs and operational schemes such as inflatable, detachable, retractable, or otherwise expendable vehicle segments, or flotilla arrangements of amphibians.

One major difficulty in answering the above two questions is the fact that very little reliable and systematic knowledge exists regarding the magnitude of the resistance components

of box-like shapes, i.e., primarily separation and wavemaking resistance. The picture is further obscured in that most model tests with amphibians have been conducted with tracks, wheels, fenders, skirts, or other parts of the propulsion system fitted to the main hull. This added some coincidental features to the hull shape whose influence on the resistance components could not be separated.

It has also been observed that the customary way of extrapolating model test data simply according to Froude's law may have led to wrong predictions of the full-scale resistance, Ref. (2), which points to the presence of scale effects on separation resistance or other viscous phenomena.

In order to obtain a better insight into the resistance components or energy loss mechanisms of amphibians and the pertinent scaling laws, and to provide the designer with information on physical bounds and trends, a series of simple box-like hull shapes without any appendages was tested. Their resistance components and the influence of scale were investigated.

Any questions of propulsive performance were thus deliberately left aside since it is already known that improvements in the propulsive efficiency of track-propelled amphibians are possible with the use of other propulsion systems such as pump jets or propellers.

It was thought important, however, to collect some information on sinkage and trim which is scarce in the literature. Excessive sinkage and trim are indicative of poor hydrodynamic performance and may also be objectionable from the operational viewpoint.

II. Test Program

Seven models were built and tested. The principal dimensions and form parameters are summarized in Table 1. Models 1 through 6 were each tested at three drafts corresponding to beam draft ratios of 2, 3, and 4. The beam was the same for all six models. Model 7 was tested at two drafts (Beam-draft ratios of 3 and 4). The model series was planned and designed as follows. (See Figures 1-4 for sketches and body plans.)

Model No. 1: This model is the parent model of the series. Its hull parameters were selected to be representative of present amphibians: L/B = 2.5, heavy draft B/T = 2.0. Amphibian hull shape was idealized as a rectangular box (parallelepiped) to bring out the typical physical effects.

All corners were rounded (radius r = 0.1042 ft., r/B = 0.0866) as on actual amphibians; otherwise the amount of separation at the corners would have been much higher than on actual amphibians. Ref. 4, p. 3-13, Figure 23, and p. 11-6, Figure 5, shows, for example, that a certain amount of nose rounding is necessary to avoid excessive nose separation drag. This will be discussed further in section IV.

Model No. 2: Hull shape essentially the same as Model No. 1, except that this model was lengthened by a factor of 1.4 to study the effect of length-beam ratio.

Model No. 3: This model was further lengthened to be 1.8 times as long as Model No. 1.

TABLE 1: MODEL DIMENSIONS AND PROPORTIONS

Quant.	Dim.	Model No.																					
		1			2			3			4			5			6			7			
L	ft	3.00			4.20			5.406			4.20			4.20			5.406			5.0			
B	ft	1.203			1.203			1.203			1.203			1.203			1.203			2.0			
L/B	--	2.5			3.5			4.5			3.5			3.5			4.5			2.5			
T	ft	.30	.40	.60	.30	.40	.60	.30	.40	.60	.30	.40	.60	.30	.40	.60	.30	.40	.60	.667	1.00		
V	ft^3	1.06	1.43	2.15	1.49	2.00	3.01	1.92	2.58	3.88	1.24	1.74	2.75	1.27	1.75	2.70	1.46	2.07	3.30	6.60	9.94		
B/T	--	4	3	2	4	3	2	4	3	2	4	3	2	4	3	2	4	3	2	3	2		
$\Delta/(0.01L)^3$	$LTSW/ft^3$	1126	1509	2271	574	769	1160	349	468	700	480	669	1060	491	674	1037	263	374	597	1509	2271		
C_B	--	.980	.984	.989	.983	.986	.990	.984	.987	.991	.822	.857	.904	.838	.865	.886	.746	.793	.843	.984	.989		
C_P	--	.992	.994	.995	.995	.996	.996	.996	.997	.997	.832	.866	.910	.848	.873	.892	.756	.800	.849	.994	.995		
C_M	--	.988	.990	.994	.988	.990	.994	.988	.990	.994	.988	.990	.994	.988	.990	.994	.988	.990	.994	.990	.994		
C_{WP}	--	.998	.998	.998	.998	.998	.998	.999	.999	.999	.998	.998	.998	.966	.904	.903	.920	.925	.924	.998	.998		
C_{VP}	--	.982	.987	.991	.984	.988	.992	.985	.989	.992	.824	.859	.906	.867	.957	.981	.811	.857	.913	.987	.991		
A_M	ft^2	.357	.478	.719	.357	.478	.719	.357	.478	.719	.357	.478	.719	.357	.478	.719	.357	.478	.719	1.33	2.00		
S	ft^2	5.71	6.53	8.18	7.77	8.84	11.0	9.83	11.4	13.8	6.83	8.05	9.91	6.89	8.06	10.1	8.01	9.58	11.8	18.1	22.7		
$S/V^{2/3}$	--	5.48	5.16	4.92	5.95	5.57	5.27	6.36	6.08	5.57	5.88	5.58	5.06	5.86	5.55	5.19	6.22	5.90	5.31	5.16	4.92		

Model No. 4: This model consists of "Model No. 1" as blunt leading part and a raked stern. The length of the raked part of the stern is 24 percent of the model length, (excluding transition radius) the rake angle 20 degrees, and the stern ends in a flat vertical transom. See Figure 2.

Model No. 5: This model has the same length as Model No. 2, but has been obtained by fitting a ship-shaped bow to Model No. 1, rather than a box-shaped extension. Its block and prismatic coefficients are consequently less. See Figures 3 and 4.

The design of the forebody was governed by the aim of obtaining a smooth pressure distribution over the nose to reduce nose separation. The sectional area curve of the forward part of the axisymmetric body "4", Series 58, Ref. 3, showed a favorable gentle transition of the pressure distribution into the midship domain. It was therefore adopted as a guideline for the bow design. Figure 5 shows corresponding segments of the two sectional area curves.

Model No. 6: This model combines the ship-shaped bow of Model No. 5, Model No. 1 as middle part except for the rounded end plates, and the stern of Model no. 4 as end segment. Its form parameters approach those of conventional ships. See Table 1.

Model No. 7: This model is a five foot geosim of Model No. 1. It was included in the series to investigate scale influences.

III. Test Procedure

Model resistance tests were performed on the seven box-like hull forms in the towing basin of The University of Michigan Ship Hydrodynamics Laboratory. During the resistance tests the trim and sinkage of the models were also measured. Figure 6 shows the model as attached to the towing carriage. It was constrained at each end by devices ("grasshoppers") which prevented side sway and yaw, while permitting freedom to heave and trim. The resistance force was taken up by a dynamometer fixed to the carriage near the mid-length of the models and was measured in a horizontal direction from a point 22.85% of the beam above the baseline.

The resistance force was transmitted through a bell crank to a differential transformer type load cell. The load cell was excited by a Sanborn 350-1100B carrier preamplifier, and the output was displayed on an X-Y (X-axis time base) recorder. The calibration of the instrumentation was checked about once every half-hour to insure the accuracy of the resistance data.

Sinkage and trim were measured with direct recording dials connected to the model by strings. The instrument was balanced so that no appreciable forces were exerted on the model.

No turbulence stimulators were installed on Models 1, 2, 3, 4 and 7 because laminar-turbulent transition played a secondary role, if any, relative to the separation at the

front corners of the models. Model 5 and 6, with the bow segment, were fitted with a 0.036 inch diameter trip wire, 0.625 feet aft of the fore perpendicular.

IV. General Observations on the Flow Around Blunt Bodies and Their Resistance

The following remarks are in general based on knowledge contained in the hydrodynamic literature, but include some special observations made during the test program.

a. Deeply submerged bodies

Slender streamlined forms with fine ends are known to have a pressure distribution as shown in the upper part of Figure 7. Because of some turbulent diffusion in the afterbody the pressure at the rear end does not quite reach the stagnation pressure, $\Delta p/q = 1$, but $\Delta p/q$ usually remains positive. The viscous pressure resistance which is due to the pressure deficiency at the stern is therefore relatively small in comparison to the skin friction of such bodies.

For bluff bodies, on the contrary, separation becomes the predominant flow phenomenon. It will occur at the front corners of the body unless the rounding radius there is of the order of at least 0.1 body height, Ref. 4, p. 3-13, Figure 23. It will also occur at the rear corners of a flat, cut-off stern if the body is long enough for the flow to become reattached between bow and stern.

The resistance effects corresponding to these two types of separation are appreciable and may be referred to as <u>forebody pressure drag</u> and <u>base drag</u>.

At a sharp-edged nose, bow separation occurs, and the forebody pressure drag is the more significant

drag component of the two. As a rounding radius is introduced the trends are gradually reversed. In Figure 8, which is reproduced from Ref. 4, p. 3-12, Figure 21, one sees that forebody pressure drag and base drag for intermediate length-diameter ratios relate as 0.65:0.2. Note that the drag coefficients in the context of blunt objects are usually defined with projected frontal area as a reference area.

The flat disk constitutes an extreme case in which reattachment is impossible and separation occurs only once. The pressure on the rear side of the disk drops to about $\Delta p/q = -0.45$, which also represents the base drag coefficients. The forward side contributes another $\Delta C_D = 0.7$ to the pressure resistance so that the total is $C_D = 1.15$. This may serve as an upper bound for blunt body pressure drag.

It is interesting to note that this component of the drag is practically constant with Reynolds number above $R_N = 10^3$ [Ref. 4, p. 3-15, Figure 26].

The frictional resistance of blunt bodies is relatively small, or even negligible if the bodies are short. See Figure 8.

Observations during the experiments confirmed the general nature of the bluff body flow phenomena. The resistance data will be discussed later, but a few further comments may be added here.

At any except the lowest speeds, the flow picture contained two large eddying regions, one near the

front shoulders, the other in the wake of the flat stern. Reattachment seemed to occur at about 1/3 to 1/2 model length from the bow, further aft with increasing speed. About half a model length behind the stern, one observed an upward flow like a well, apparently the underbottom flow, which was in part deflected from the region where it surfaced toward the stern of the model. This demonstrates the presence of low pressures ($\Delta p/q<0$) at the stern.

b. Floating bodies

The additional complexities introduced by the free surface are related to the effects of the displacement flow (primary disturbance) and of secondary wavemaking. They manifest themselves in considerable effects on sinkage, trim, and resistance.

Although it is clear that blunt, boxy shapes have poor wave resistance characteristics, no systematic knowledge on this matter seems to exist in the literature.

The following observations which were made during this test program may be typical for the general nature of the flow.

The primary disturbance differs significantly from the case of slender bodies because of separation effects. The bow stagnation point and the associated high pressure domain results in a very pronounced local wave elevation. The low pressure area seems to extend from the front corner throughout the length of the body. The flow separating at the rear end did not recover positive pressures. Figure 7,

lower part, illustrates this situation qualitatively.

It was also typical that the models experienced a relatively large sinkage and trim by the bow. The sinkage is explained by the extended low pressure area under the bottom, and the trim seems to indicate that the pressures in the separated regime behind the front corners were lower than at corresponding points near the stern.

The wavemaking is governed by the nature of the primary disturbance just described, and is certainly influenced by the presence of sinkage and trim effects. The secondary wave system originating at the bow was very pronounced (bow wave). The other secondary wave systems were much less evident. Their strength and location varied to some extent with Froude number as shown in the photographs 1-6 for two box-like hull shapes [L/B = 2.5 and 3.5].

V. Results

The results of model resistance, sinkage, and trim measurements for the seven models tested in this program are shown in Figures 9 to 48. Figures 9 to 28 show the faired model resistance R in pounds versus model speed in feet per second, with the individual data points also plotted. Figures 49 to 68 show the model total resistance coefficient, C_T, (which is based on the total static wetted surface of the model) versus Froude number and Reynolds number. The ratio $\frac{W.S.}{\nabla^{2/3}}$ is given for each test to facilitate a comparison with other forms on a volume basis. Figures 29 to 48 give model sinkage and trim versus model speed and Froude number, with the individual data points also plotted.

Figures 69 to 71 show the total resistance coefficient for models 1 through 6 for each of the three values of B/T. Figures 72 to 76 are similar, and give the total drag coefficient, C_D, which is based on the maximum section area of the underwater form. This drag coefficient is useful for comparing the resistance data of blunt bodies where separation drag is the major component of resistance.

V-1. Discussion of Results

Model No. 1: Model No. 1, the parent, is the boxiest shape investigated and has proportions similar to actual amphibians. Its resistance coefficient C_T is higher than any of the others. At the lower speeds, this is primarily due to separation. The drag coefficients there obtained are between C_D = 0.4 and 0.6. This is a level that one might reasonably expect for boxy shapes with some rounding of the front end. Figure 8 shows, for example, that some axially symmetric bodies of similar length-beam ratio have drag coefficients between 0.2 and 0.8 depending on front end streamlining. The lower level is only attainable if front end separation is completely eliminated, which was not the case in our tests.

Figure 8 also shows the friction resistance is small for short bodies, e.g., length to beam ratio equal to that of Model 1, L/B = 2.5. One should keep in mind two effects which tend to reduce friction significantly:

a. Tangential forces in the front and rear end planes have no longitudinal components, so that these surfaces cannot contribute to the frictional resistance.

b. Flow observation during the tests showed reverse flows over the forward one third of the model inside the front shoulder eddy (see Pictures 1-6). This would result in negative friction over a considerable area of the sides

and the bottom, and only the remaining part where the flow is reattached is subject to positive friction.

The ITTC line is hence most likely too high for the pure frictional resistance of the model.

Regarding wavemaking effects, the results show a rapid increase of C_D with Froude number, which is most significant at the lower drafts.

It is not quite certain if the whole increase is due to wavemaking or perhaps in part to further separation triggered by greater trim and sinkage. But it is rather clear that both wavemaking and viscous pressure drag due to separation are about equally significant at $F_n \approx 0.45$.

For projected amphibians of significantly higher speeds, wavemaking may assume the more important role.

Model No. 2: Model 2 is the box-shaped model (square bow and square stern) of length to beam ratio L/B = 3.5. One must be careful in comparing this model with Model 1 on the basis of drag coefficient, C_D, vs. Froude number because the length is different. But a comparison on the basis of total resistance versus speed (Figures 9 to 14) shows Model 2 is superior to Model 1. This effect is most pronounced at the lightest drafts, and diminishes as the draft is increased.

The effect of increasing the displacement by lengthening Model 1 has resulted in a decrease in resistance, a significant result. This may be explained in terms of the

pressure distribution on the bottom of the two models. If one accepts the premise that the pressure distribution (dip in $\Delta p/q$) near the bow of blunt bodies is nearly identical for length to beam ratios of about 2.5 and greater, (see Figures 7 and 8) then it is clear that there will be a greater moment to trim by the bow for the smaller body (which has less bottom area experiencing a moment to trim by the stern). Also, there is less longitudinal stability for the shorter form, which has a smaller longitudinal metacentric height and less displacement. Sinkage would also be greater for the shorter model, where the highly negative portion of the pressure distribution ($\Delta p/q$), exists over a proportionally greater part of the bottom.

The increase in sinkage and trim by the bow increases the submerged frontal area of the model and results in an increase of the base drag. The trim by the bow also promotes more separation under the bottom, which increases the resistance of the shorter form still further.

The change in length and draft of the box-like forms does of course affect the wave resistance, too. The changes in the humps and hollows of the resistance curve suggest that one may find favorable combinations of length and draft for any given beam and design speed.

The decrease in resistance of Model 2, which was obtained by lengthening Model 1 and increasing displacement, results

in a decrease in resistance per ton displacement of about 35% on the average, at a model speed of 4 feet per second.

Model No. 3: Model 3 was the longest box-like hull form tested, L/B = 4.5. It compares with Model 2 generally in the same way that Model 2 compares with Model 1.

Model No. 4: With Model No. 4, L/B = 3.5, a raked, barge-like stern was introduced, with the intention of eliminating, or at least reducing, the base drag of the box-like form. An angle of 20° was chosen, a value which barge resistance data suggest to be the maximum permissible angle for this purpose. Comparing drag coefficients with Model No. 2, also of L/B = 3.5, shows that over a wide range of Froude numbers the drag coefficient of Model 4 is less than that of Model 2 by an almost constant amount. This suggests that we have been successful in decreasing the base drag by refining the run. However, the resistance reduction was parallelled by a loss of displacement in raking the stern. If the comparison is based on resistance per ton displacement one has to make the conversion

$$\frac{R_T}{\Delta} = C_D \frac{F_N^2}{2\, C_p}$$

At any given Froude number, the C_D - curves are reduced in inverse proportion to C_p. Model 2 has considerably higher prismatic coefficients than Model 4 (Table 1). The advantages

due to the raked stern are therefore almost vanishing on a resistance per ton basis.

Raking the stern as perfomed in this program is therefore of questionable value from the resistance viewpoint.

Model No. 5: The introduction of a ship-shaped bow on model 5, L/B = 3.5, effects a significant decrease in resistance when comparing to Models 2 and 4, also of L/B = 3.5. At Froude numbers less than 0.3, the resistance coefficients are almost independent of speed, indicating that the wave-making resistance is insignificant in this speed range. Also, the shaping of the bow has decreased the viscous pressure resistance of the forebody and resulted in much lower values of resistance. A reduction in sinkage and trim also points to a more favorable pressure distribution about the entrance. See also pictures 7-9.

On the basis of drag coefficient Model 5 is superior to all other models of the series except for Model 6 whose greater length and volume were beneficial. Using resistance per ton for the comparison would bring the two models closer together, but not enough to reverse the conclusion.

It seems further that Model 5 has reached a hump speed at Froude numbers around 0.4. This suggests taking advantage of the following hollow for speed increases. This is not economically feasible with current amphibians whose maximum speed corresponds to $F_N = 0.4$ where the resistance curve of

these shapes shows a steep increase. Compare the corresponding case of Model 1.

Model No. 6: Model 6, L/B = 4.5, is the form that results when ship bow and barge stern are both included in the design.

This form has the lowest total resistance and drag coefficients (C_T and C_D). The model obviously has benefitted from its greater length which minimized its forebody pressure drag, base drag and wavemaking resistance.

As mentioned before, the superiority of Model 6 over Model 5 is retained, although somewhat reduced, on a resistance per ton basis. But Model 6 is considerably longer (L/B = 4.5 versus 3.5). It may be conjectured from the other results that the hull form of Model 6, reduced down to L/B = 3.5, would have been inferior to Model 5 because the sharper curvatures in the forebody would have reintroduced some forebody separation and pressure resistance.

V-2. The Scaling Question

It is current practice to extrapolate amphibian model test data strictly according to Froude's law (force scale equal to length scale to the third power) without accounting in any manner for the presence of viscous scale-dependent effects.

The reason for this practice may be found stated about like this:

> "The frictional resistance is negligible ($C_{F_{ITTC}} << C_T$), and the residuary resistance follows Froude's law as we customarily assume."

This reasoning is subject to some fundamental doubts. The residuary resistance is composed of wave-making and viscous pressure drag ("eddy resistance"):

$$R_R = R_W + R_{PV}$$

While R_W as a gravity phenomenon clearly follows Froude's law, this is questionable for R_{PV}. This may go undebated with conventional hull forms where R_{PV} is relatively small, but for amphibians it constitutes about 50 percent of the total, or more at lower speeds, so that the scale relationship for R_{PV} is of great importance.

It might be argued that tests with bluff bodies, deeply immersed in an airstream (Ref. 4, section 3, Figure 26) do not show any Reynolds number dependence of C_D above a certain

R_N, say $R_N = 1{,}000$. Hence, one might say:

$$C_{D_{Model}} = C_{D_{Ship}}$$

$$\text{or } R_{T_{Ship}} = R_{T_{Model}} \frac{V^2_{Ship} \cdot A_{o_{Ship}}}{V^2_{Model} \cdot A_{o_{Model}}} = R_{T_{Model}} \cdot \lambda^3$$

This is Froude's law.

But for surface ships this is not fully conclusive:

a. Sinkage and trim may trigger new separation patterns so that the basic assumption of geometrically similar flows breaks down.

b. Gravity-viscous interference effects are ignored in the above reasoning, but may be significant with these shapes. It is possible that the wave flow influences the point of separation as well as its extent.

For these basic reasons it can not be taken for granted that Froude's law is correct in the extrapolation even though skin friction is very small.

Unfortunately, conventional techniques of scale effect studies could not be applied to this case where the scaling relation for the viscous pressure drag was the issue. Neither would it be correct for any single model to represent the viscous pressure drag as a multiple of the skin friction of a flat plate (k-factor or Hughes method):

$$C_{PV} = (1 + k) \cdot C_{F_o}$$

This contradicts the above statement that at least for some shapes the separation drag was found to be independent of R_N. Besides, the equation was conceived for turbulent diffusion in thick boundary layers rather than separation or base drag.

Nor can one extend geosim evaluation techniques without further verification. Separability of resistance components by Froude-and Reynolds-dependent terms

$$C_T = C_1(F_N) + C_2(R_N)$$

is fundamental to this method, and the viscous pressure drag due to separation may not fit this description. Perhaps:

$$C_{PV} = f(F_N, R_N).$$

For example, if at any given Froude number trim and sinkage differ for two scales because of gravity-viscous interference effects and/or differing separation patterns, the fundamental assumption of the geosim method breaks down.

A scale comparison was conducted to investigate if the aforementioned hypothetical effects were of significance. It was hoped that they would be small enough to justify the

use of Froude's law in the present case.

Unfortunately this was not borne out by the tests. Figs. 55 and 56 show the resistance coefficients C_D versus R_N for the geosim models no. 1 and no. 7. It can be seen that the larger model (5 ft.) has a lower C_D than the smaller one (3 ft.). This puzzling result is paralleled by two other observations:

a. The larger model had the greater sinkage, but it was less than a factor of λ greater than the sinkage of the smaller model. The trim of the smaller model was larger, which might explain the larger resistance coefficient of the smaller model.

b. In the tests of Ref. 1 with a 1/2 and a 1/4 scale model, resistance, trim and sinkage showed scale effects in the same direction.

Explanations for these differences may be sought as follows:

α. Measurement errors due to instrumentation: The tests with the big box were difficult to conduct, the box being relatively heavy and unstable in its course. Grasshoppers were used to keep it from yawing, and this system undoubtedly experienced some side forces and moments. While this may have increased grasshopper bearing friction so that trim and sinkage might have been influenced there was not enough of this effect to lead to binding. In fact, the model kept undergoing some vertical motions of small amplitudes during the tests. The authors, therefore, do not believe this influence could explain the existing discrepancy.

β. Blockage:
May have had an influence, but points in the wrong direction.

γ. Laminar effects:
The smaller model had a fairly small Reynolds number. But since the front and rear corners were setting the separation region, and skin friction itself was negligible, laminar effects are not believed to be of the necessary magnitude to explain the observation.

δ. Influence of towing force on trim:
All models were towed from a point 22.85% of the beam above the baseline. If we assume the resultant of the resistance forces acts at a point one half the draft above the baseline, we can calculate approximate trimming moments caused by the difference in height of resistance and towing force. In the speed range of interest, say, $V/\sqrt{gL} > 0.1$, the moments are less than 1% of the static moments needed to produce the trim the model assumes while moving. Therefore, moments induced by the difference in height between resistance and towing forces are too small to produce the scale effects noted.

ε. Differing separation patterns:
A hypothetical argument shall be offered how the differences in sinkage and trim may have contributed to those in resistance.

Small changes in the separation point at the bottom nose radius may have triggered larger changes in

the reattachment under the bottom. For example, the smaller model might have had the whole bottom in separated (low pressure) flow whereas the larger model might have had reattachment near midship section.

In any event, for some reason the pressures under the bottom of the smaller model must have been appreciably lower than according to scale to explain the disproportionately great sinkage. The trim may have played a role in setting a pressure level.

This pressure scale effect in conjunction with the trim of the models by the bow must have caused a scale effect on the bottom force resultant and its resistance component. Moreover, the frontal wetted area, the immersed displacement, and the immersed part of the transom responsible for the base drag all differed in favor of the larger model because of the sinkage scale effect.

It is of course very difficult to assess the magnitude of the combined effects. Crude estimates indicate that the resistance scale effects may be attributable primarily to trim and sinkage effects in the case of B/T = 2.0. But for B/T = 3.0 the resistance scale effects are much greater, and a full explanation is alack.

No definitive conclusions will be reached without some further test, preferably including direct flow observations and measurements around the model.

In summary, caution is in place regarding scaling relationships for amphibians although the effects are most likely less pronounced there than with the box-like shapes trimming heavily by the bow. In any correlation work, trim and sinkage should be regarded as significant scale effect indicators.

ζ. Local scale effects at bow and stern:
In the early stages of the project one other attempt was made to get further evidence on scale effects. The big box was instrumented so that its front and end plane normal forces could be measured together with the total resistance. Fig.77 shows the arrangement. The purpose was to test the model constrained at level trim, and:

a. Identify the small amount of skin friction by direct measurement and subtraction: $R_F = R_T - (R_{Front} + R_{Rear})$.

b. Study scale influences on R_{Front} and R_{Rear}. Both results would have permitted checking the validity of the Froude method of extrapolation.

But despite great efforts the tests failed because of instrumentation difficulties (bearing alignment, cross flow and static head variation in gap, model course unsteadiness, etc.). It was felt that after laboring through with some developments the trouble spots were recognized so that corrective measures could have been taken. But at this time the project had progressed too far, and this side track had to be abandoned to do justice to the parametric hull variation series.

VI. Design Conclusions

VI1. Resistance of Bluff Shapes

In this section the resistance data obtained in this program are viewed in the broader context of a variety of shapes compared in Figure 78. This leads to some design conclusions as to the effect of major parametric variations in hull proportions upon resistance.

Some separation is obviously inevitable with bluff bodies. The amount of viscous pressure resistance due to separation hence determines the lower limit of resistance of the hull shape. What level of viscous pressure drag one may reasonably expect for some given hull proportions is best discussed by means of the C_D - representation, Fig. 78. Of course, in the higher speed range ($F_N \geq 0.4$) one may also aim to accomplish wave resistance reductions, for example about 25% for the series tested in Ref. 1. But more drastic improvements seem to be possible only if the viscous pressure drag is also reduced by adequate variations in hull proportions. The following therefore concentrates on viscous resistance aspects.

The shapes compared in Figure 78, and described in more detail in Table 2 are, in the order of ascending drag coefficient:

1. Series 60 hull, $C_B = 0.8$, $L/B = 7$, as tested in Ref. 5.

TABLE 2: FORM PARAMETERS OF SHAPES COMPARED IN FIGURE

Quant.	Dim.	Series 60 $C_B = 0.8$ Ref. 5	Rounded Axisymm. Body Ref. 4	Barge B-1 Ref. 6	Model 5 This Series	Model B-5 Ref. 1	Model 2 This Series	Blunt Axisymm. Body Ref. 4	Circular Plate Ref. 4
L	ft	14		4.0	4.20	~ 1.33	4.20		0
B	ft	2		1.14	1.203	0.525	1.203		
L/B	--	7.0	$\geq 2.$	3.25	3.5	~ 2.54	3.5	$\geq 2.$	
T	ft	0.8		0.28	.60	0.192	.60		
∇	ft^3	17.9		1.11	2.70		2.70		0
B/T	--	2.5	1.	4.15	2.0	2.74	2.0	1.	1.
$\Delta/(0.01L)^3$	$LTSW/ft^3$	187.		489	1037.	~1086.	1160.		
C_B	--	0.8		0.872	.886		.990		
C_P	--	0.805		0.900	.892		.996		
C_M	--	0.994	0.785	0.969	.994		.994	0.785	
C_{WP}	--	0.871		0.988	.903		.998	1.	
C_{VP}	--	0.92		0.883	.981		.992		
A_M	ft^2	1.59		0.31	.719		.719		
S	ft^2	42.2			10.1		11.0		
$S/\nabla^{2/3}$	--	6.16			5.19		5.27		

This hull is full, but has a rather generous length constraint permitting sufficient rounding of entrance and run. The viscous resistance, corresponding to $C_D = \sim 0.12$, is relatively low, and consists of a major amount of friction as well as some separation.

2. Axisymmetric body in axial flow, rounded head, Ref. 4, same as in Figure 8, $L/B \geq 2.5$, deeply submerged.

Forebody pressure drag completely eliminated due to rounding, only base drag and friction left. $C_D = \sim 0.2$.

3. Barge B-1, Ref. 6, $C_B = 0.87$, $L/B = 3.25$. This barge is rather short, but not extremely full. Entrance and run are faired into the parallel middlebody gently, the buttocks having the shape of the segment of a circle in these regions. The bottom is flat with very little deadrise.

The hull form shows favorable resistance properties, minimizing separation, $C_D = \sim 0.2$.

4. Model 5 of this report, $C_B = 0.886$, $L/B = 3.5$. The best hull of this program for $L/B = 3.5$. The ship-shaped bow ensures small forebody separation, but some base drag is present. $C_D = \sim 0.23$.

5. Model B-5, Ref. 1, $C_B = 0.9$ (estimated), $L/B = 2.54$ (estimated). The best hull of the Hydronautics program. Special bow design ensures favorable high-speed performance, but drag coefficient

at low speeds apparently $C_D \geq \sim 0.3$.

6. Model 2 of this report, $C_B = 0.99$, $L/B = 3.5$. Representative of present amphibian proportions. Extremely full shape. Separation drag much above ship-shaped Model 2. $C_D = \sim 0.58$.

7. Axisymmetric body, in axial flow, blunt nose, Ref. 4, same as in Figure 8, $L/B \geq 2$, deeply submerged.

Fully developed forebody and base pressure drag, reattachment present, $C_D = \sim 0.85$.

8. Circular plate in perpendicular flow, Ref. 4, deeply submerged.

Extreme case of separation without reattachment, $C_D = \sim 1.17$.

VI-2. Design Parameters

Length - beam ratio: One of the most important parameters. Significant improvements are possible by increasing L/B. This is most apparent when comparing the resistance per ton of Models 1, 2, 3 (L/B = 2.5, 3.5, 4.5) at constant speed (rather than Froude number).

Beam-draft ratio: This parameter had little effect upon C_D in the range investigated here, B/T = 2 to 4. It plays a role in determining sinkage and trim.

Fullness: High block or prismatic coefficient, and displacement-length ratio all create problems relative to separation and wavemaking.

Model 5 with the ship bow and the barge B-1 of Figure demonstrate that it is greatly desirable to lower the fullness enough to permit incorporating a rounded forebody.

Forebody rounding: Essential to minimize forebody pressure drag, and most likely bow wave system.

As a minimum the radii at the bow should be r/d = 0.1 where d is to be taken as the greater dimension of beam and draft. This radius ensures reattachment of the flow along the sides and under the bottom. See Figure 8.

It is even better to use a ship bow as in Model 5, and provide a gentle variation of the pressures over the nose.

The magnitude of the effect is clear from Figures 8 or by comparing the bluff and rounded nose data.

Wetted surface: Not significant since skin friction of bluff bodies is low.

Rake: May be beneficial, but is of secondary importance relative to bow rounding. Propulsion aspects may change picture.

Center of buoyancy: Has not been investigated. But initial trim by the stern ought to be favorable in delaying separation under the bottom.

VII. Summary and Recommendations

*Under the present design constraints on amphibian proportions, a drag coefficient of C_D = 0.3 to 0.4 seems to be the absolute lower limit since a certain amount of viscous pressure drag is inevitable. At higher speeds, due to wavemaking, C_D has typically twice that order of magnitude.

*The most promising drastic changes of amphibian proportions lie in the direction of greater length to beam ratios and sufficient forebody rounding.

*While skin friction is insignificant in short, bluff shapes there is evidence of scale effects on viscous pressure drag. The exact nature of these effects must be further substantiated. Froude's law of extrapolation should be used with caution.

*Trim and sinkage are important indicators of hull performance and should be determined systematically under model and full scale conditions.

*A forebody design method aiming at gentle pressure variations using suitable sectional area curves from axisymmetric bodies has proven successful in reducing the forebody pressure drag.

*Sufficient initial trim by the stern to compensate against dynamic trimming moments by the bow is advantageous. The operator might benefit from trim control devices.

*It seems possible and desirable to develop a method for

estimating the resistance of amphibians departing from data for simple shapes such as those of this program. This would necessitate corrections for special hull form features and appendages. Identifying these effects and seeking favorable arrangements in a systematic manner would be a valuable extension of this work.

VIII. List of Symbols

Symbol	Dimension	Definition	Meaning
A_M	ft^2		Frontal static area of maximum section
B	ft		Beam
C_B		∇/LBT	Block coefficient
C_D		R_T/qA_M	Drag coefficient
C_{F_o}		R_{F_o}/qS	Plate friction coefficient, Hughes 2D base line
$C_{F_{ITTC}}$		$R_{F_{ITTC}}/qS$	ITTC friction coefficient
C_M		A_M/BT	Maximum section coefficient
C_P		∇/LA_M	Prismatic coefficient
C_{PV}		R_{PV}/qS	Viscous pressure resistance coefficient
C_T		R_T/qS	Total resistance coefficient
C_{VP}		$\nabla/A_{WP}\ T$	Vertical prismatic coefficient
C_{WP}		A_{WP}/BL	Waterplane coefficient
F_N		$V/\sqrt{gL}$	Froude number
g	ft/sec^2		Acceleration of gravity
H	ft		Draft, alternative to T
k			Form factor
L	ft		Length, generally in the waterline
q	psi	$\frac{\rho}{2}V^2$	Stagnation pressure
r	ft		Rounding radius
R	lb		Total resistance of model

Symbol	Dimension	Definition	Meaning
R_F	lb		Frictional Resistance
R_{Front}	lb		Front end plane resistance force of constrained box
R_N		VL/ν	Reynolds number
R_{PV}	lb		Viscous pressure resistance
R_R	lb		Residuary resistance
R_{Rear}	lb		Rear end plane resistance of constrained box
R_T	lb		Total resistance
R_W	lb		Wavemaking resistance
S	ft^2	= W.S.	Static wetted surface
T	ft	= H	Draft
V	ft/sec		Speed, in general
V_M	ft/sec		Model speed
∇	ft^3		Static submerged volume
Δ	lbs		Displacement
Δp	psi		Difference between local pressure and pressure at infinity on the same streamline
λ			Model scale
δ	lb $sec^2 ft^{-4}$		Density of fluid

IX REFERENCES

1. Contractor, D.N., and Love, R.H., "An Experimental Investigation of Devices for Reducing the Hydrodynamic Resistance of Amphibious Vehicles," Technical Report 501-1 (Laurel, Md.: Hydronautics, Inc., October 1965).

2. Kilgore, U., "Hydrodynamic Aspects of Tracked Amphibians," Presented at the First International Conference of Vehicle Mechanics, Wayne State University, Detroit (July 1968).

3. Landweber, L., and Macagno, M., "Potential Flow About Series 58 Bodies in General Translational and Rotational Motion," Report 2505 (Washington, D.C.: Naval Ship Research and Development Center, June 1967).

4. Hoerner, S.F., Fluid Dynamic Drag (Published by the author, 1965).

5. Couch, R.B., and Moss, J.L., "Application of Large Protruding Bulbs to Ships of High Block Coefficient" (New York: The Society of Naval Architects and Marine Engineers, 1966).

6. Taggart, R., "A Study of Barge Hull Forms," Journal of the American Society of Naval Engineers (November 1956).

X. Appendix of Figures and Pictures

BOX-LIKE MODEL FAMILY

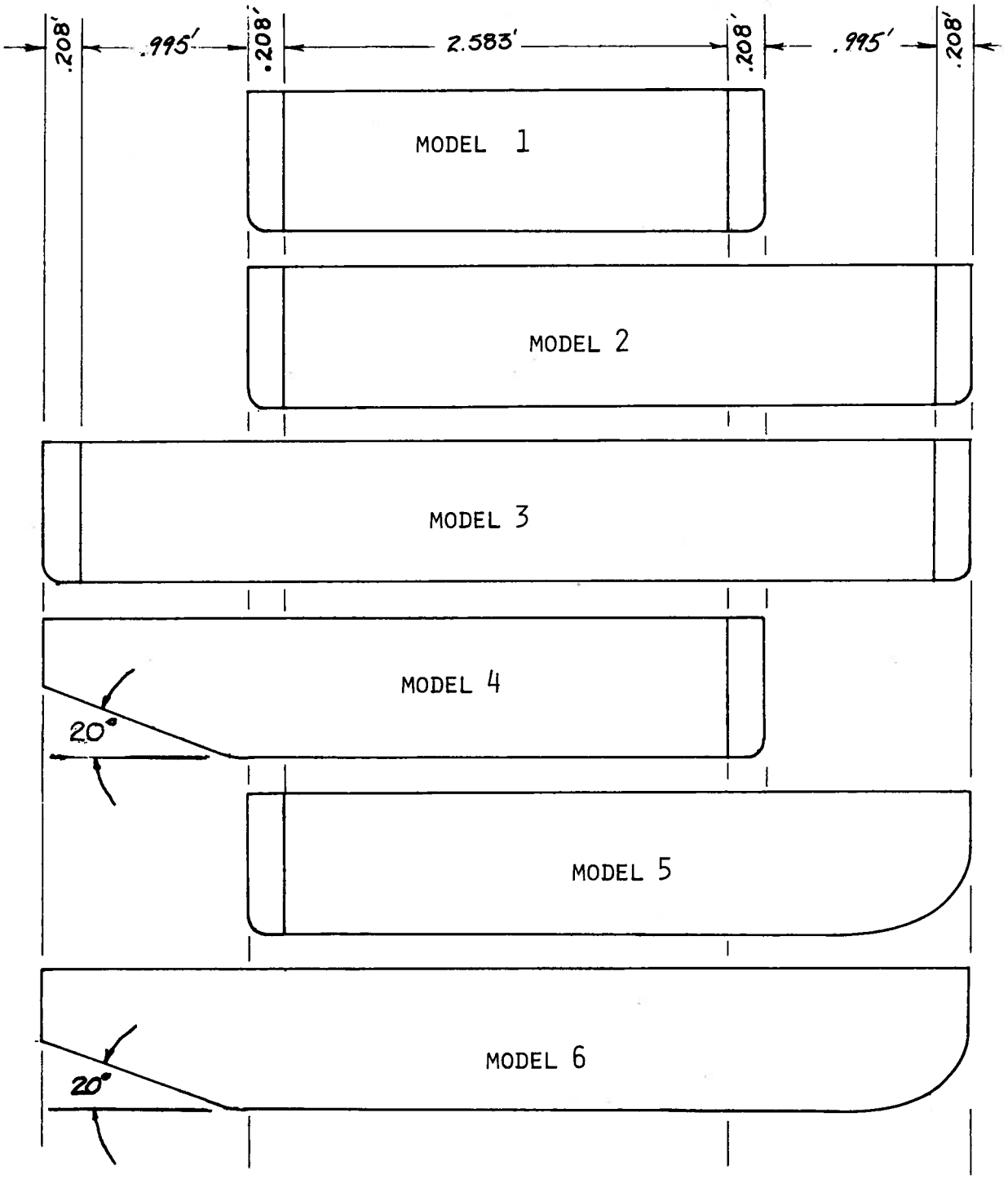

FIGURE 1

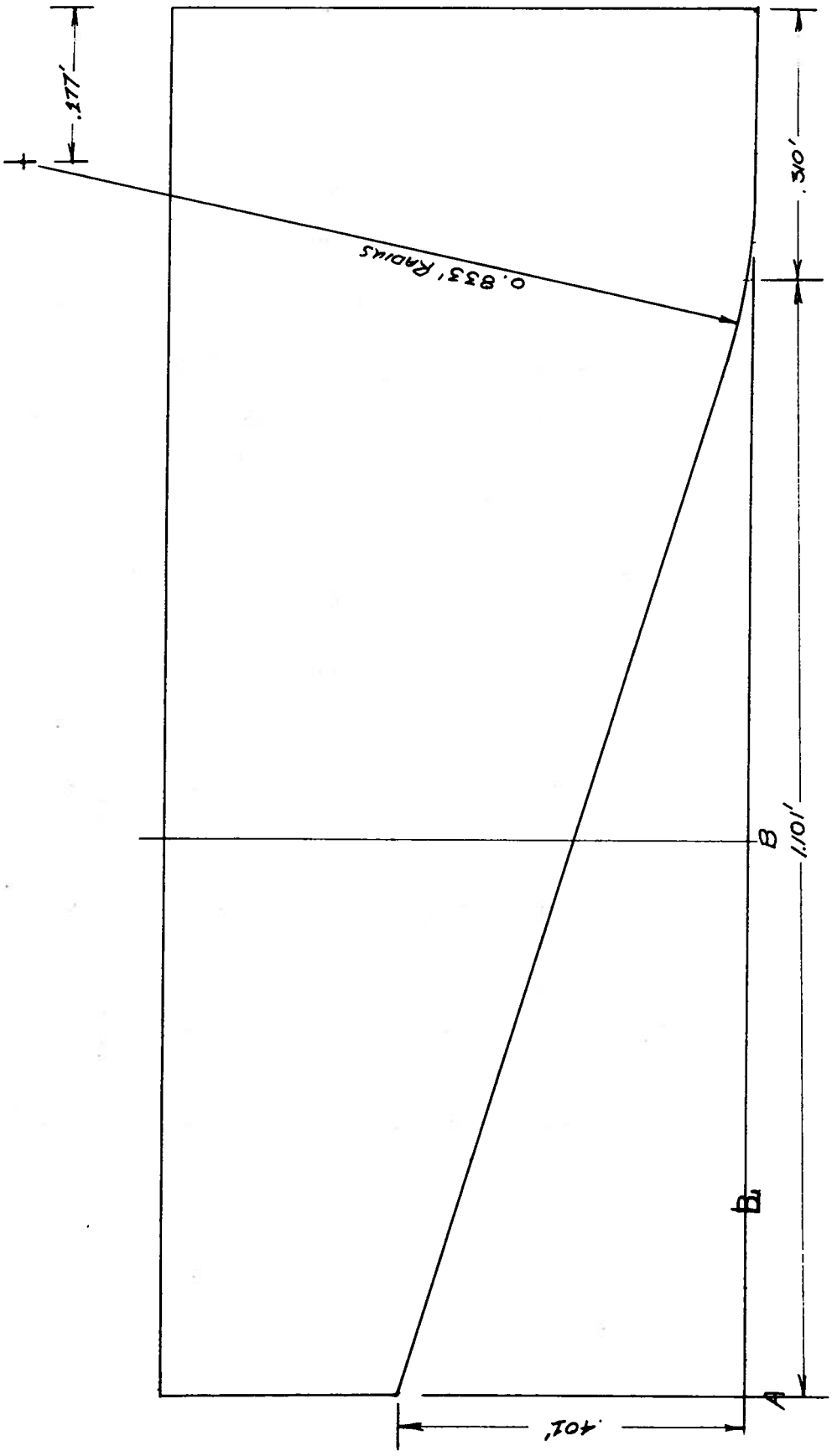

DIMENSIONS OF RAKED STERN
(PART OF MODELS 4 & 6)

FIGURE 2

FOREBODY BUTTOCKS AND WATERLINES OF MODELS 5 AND 6

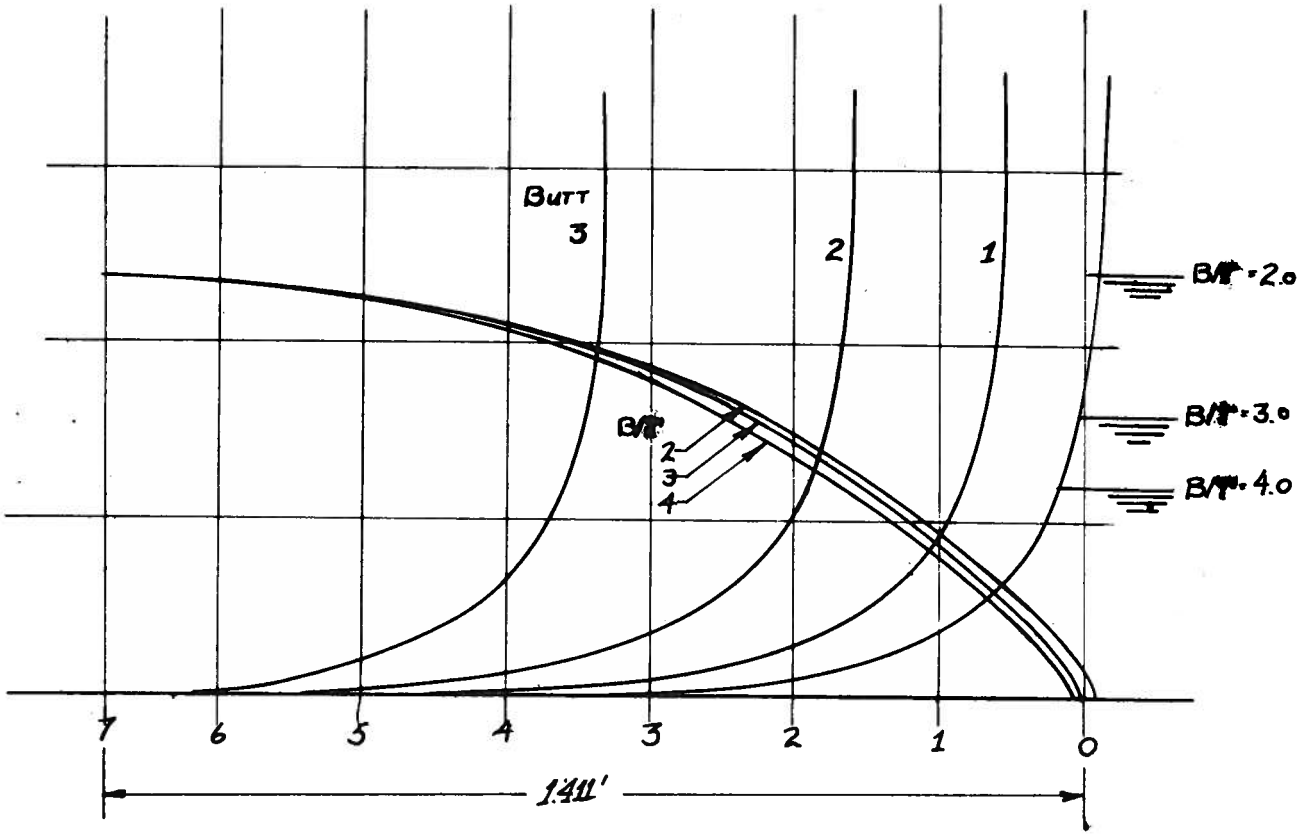

FIGURE 3

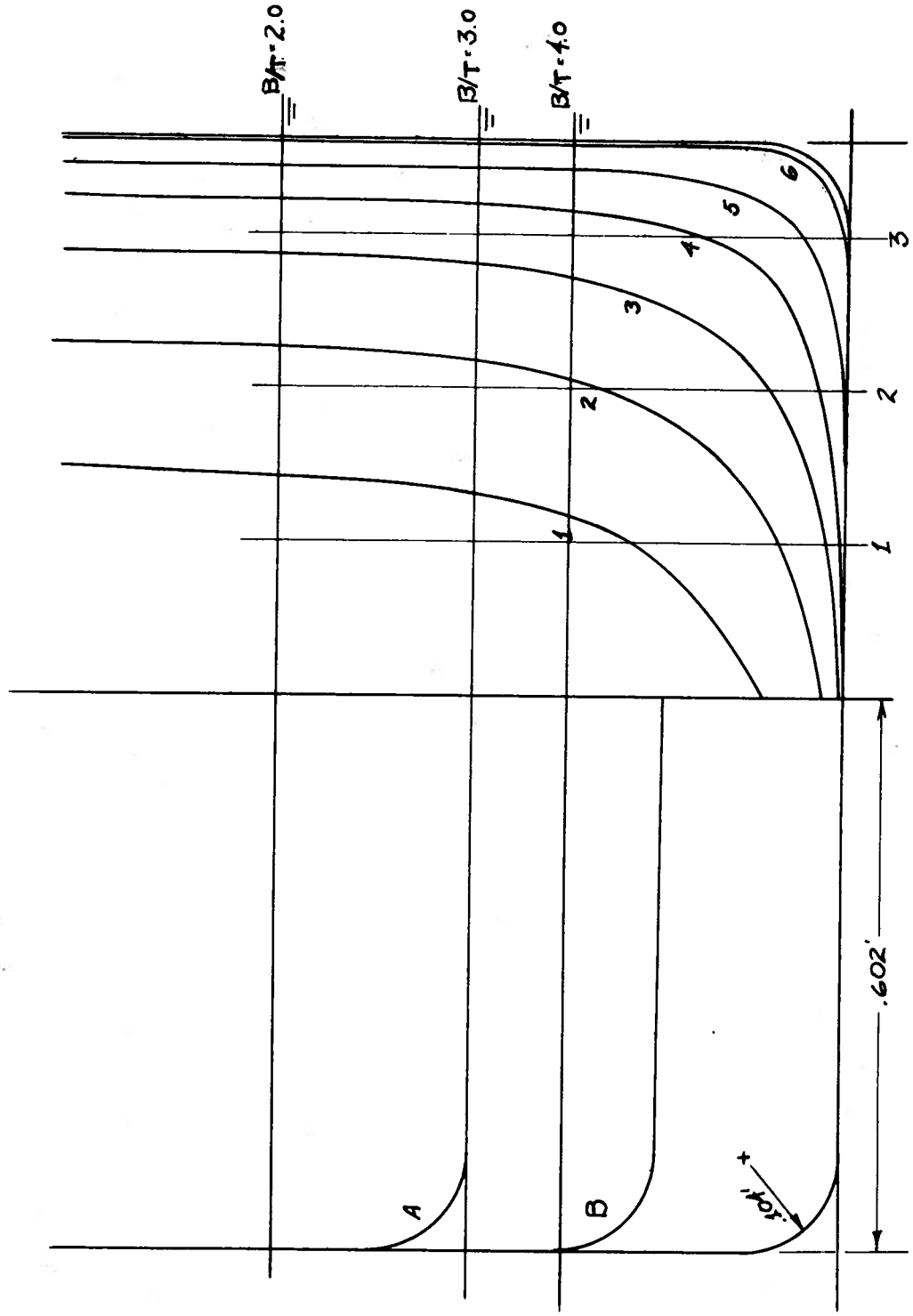

BODY PLAN OF MODEL 6

FIGURE 4

SECTIONAL AREA CURVES USED IN DESIGN OF MODEL Nº 5

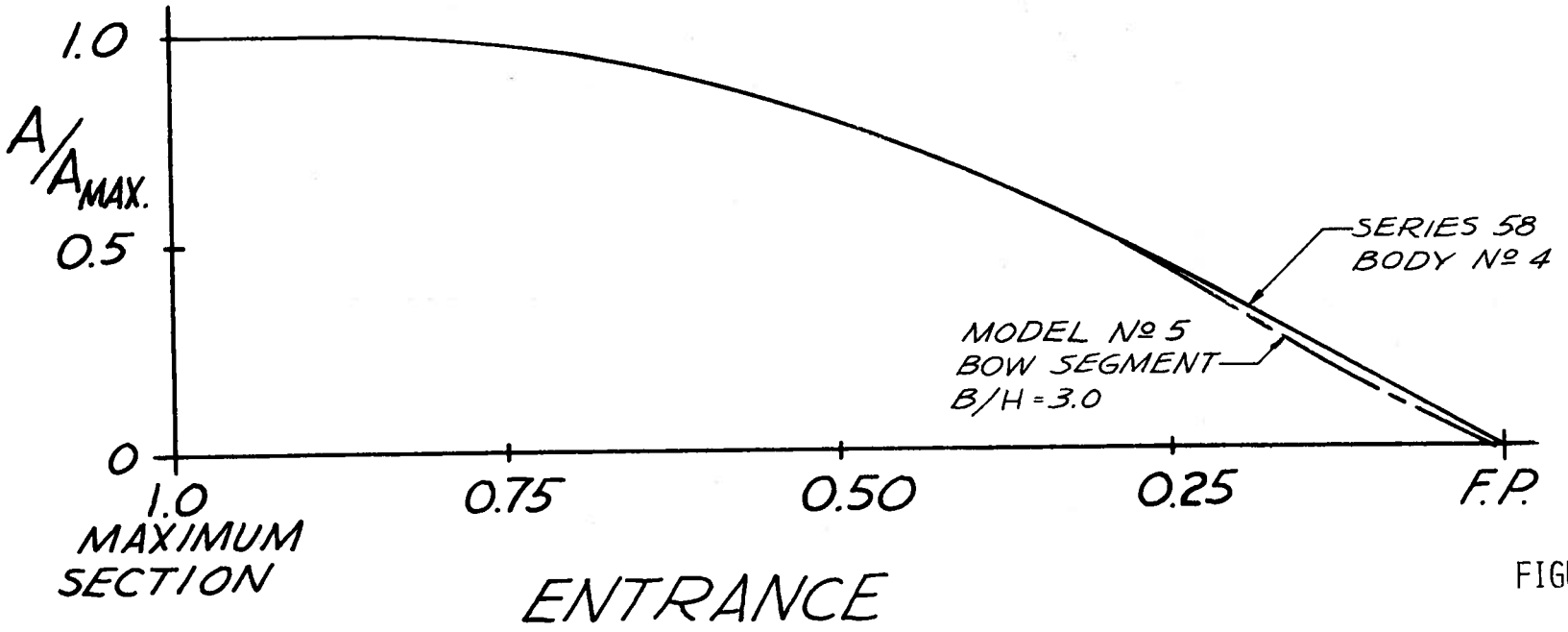

FIGURE 5

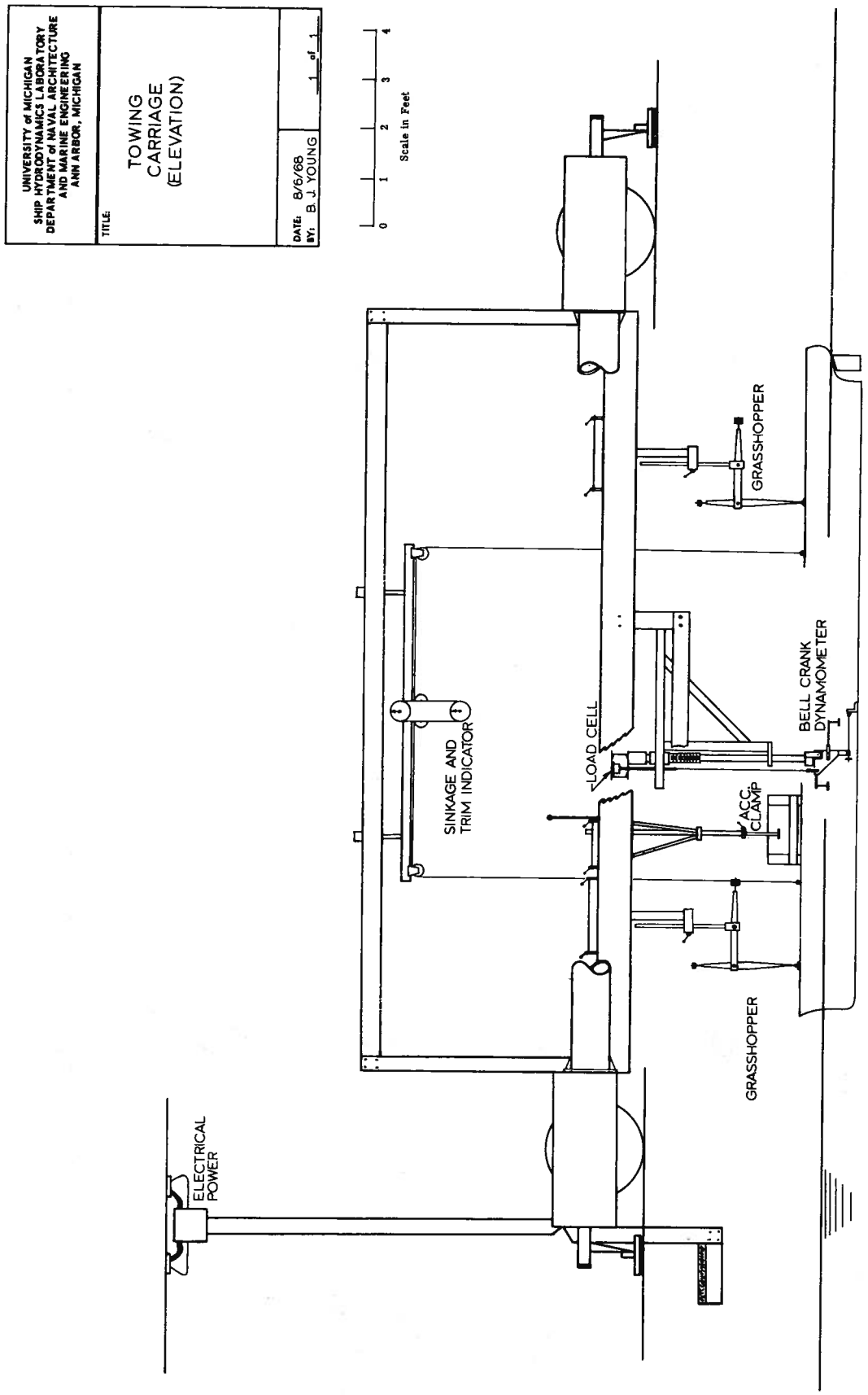
UNIVERSITY of MICHIGAN
SHIP HYDRODYNAMICS LABORATORY
DEPARTMENT of NAVAL ARCHITECTURE
AND MARINE ENGINEERING
ANN ARBOR, MICHIGAN
TITLE:
TOWING
CARRIAGE
(ELEVATION)
DATE: 8/6/68
BY: B. J. YOUNG
1 of 1
0 1 2 3 4
Scale in Feet
ELECTRICAL
POWER
SINKAGE AND
TRIM INDICATOR
LOAD CELL
ACC.
CLAMP
BELL CRANK
DYNAMOMETER
GRASSHOPPER
GRASSHOPPER

FIGURE 6

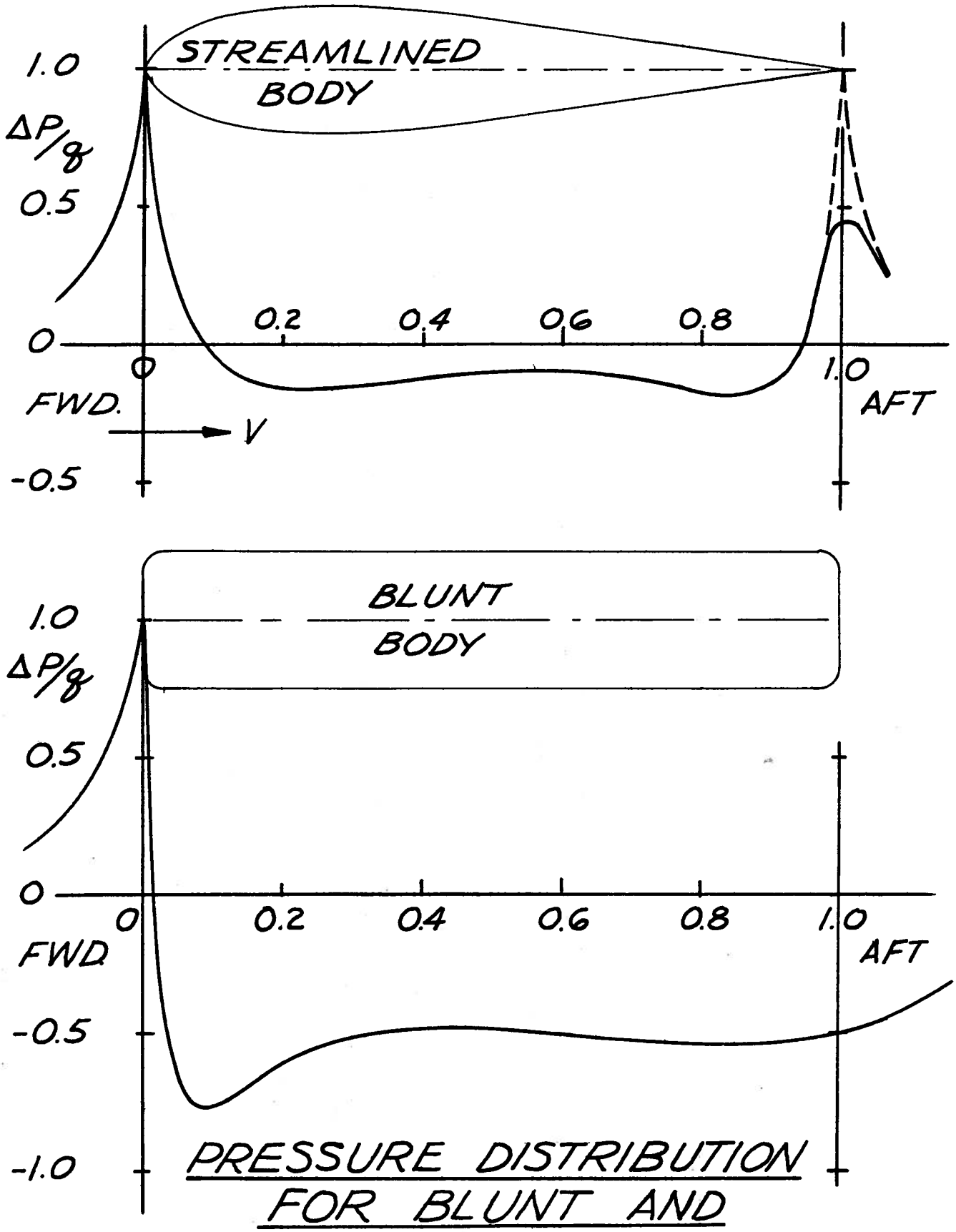

PRESSURE DISTRIBUTION FOR BLUNT AND STREAMLINED BODIES

FIGURE 7

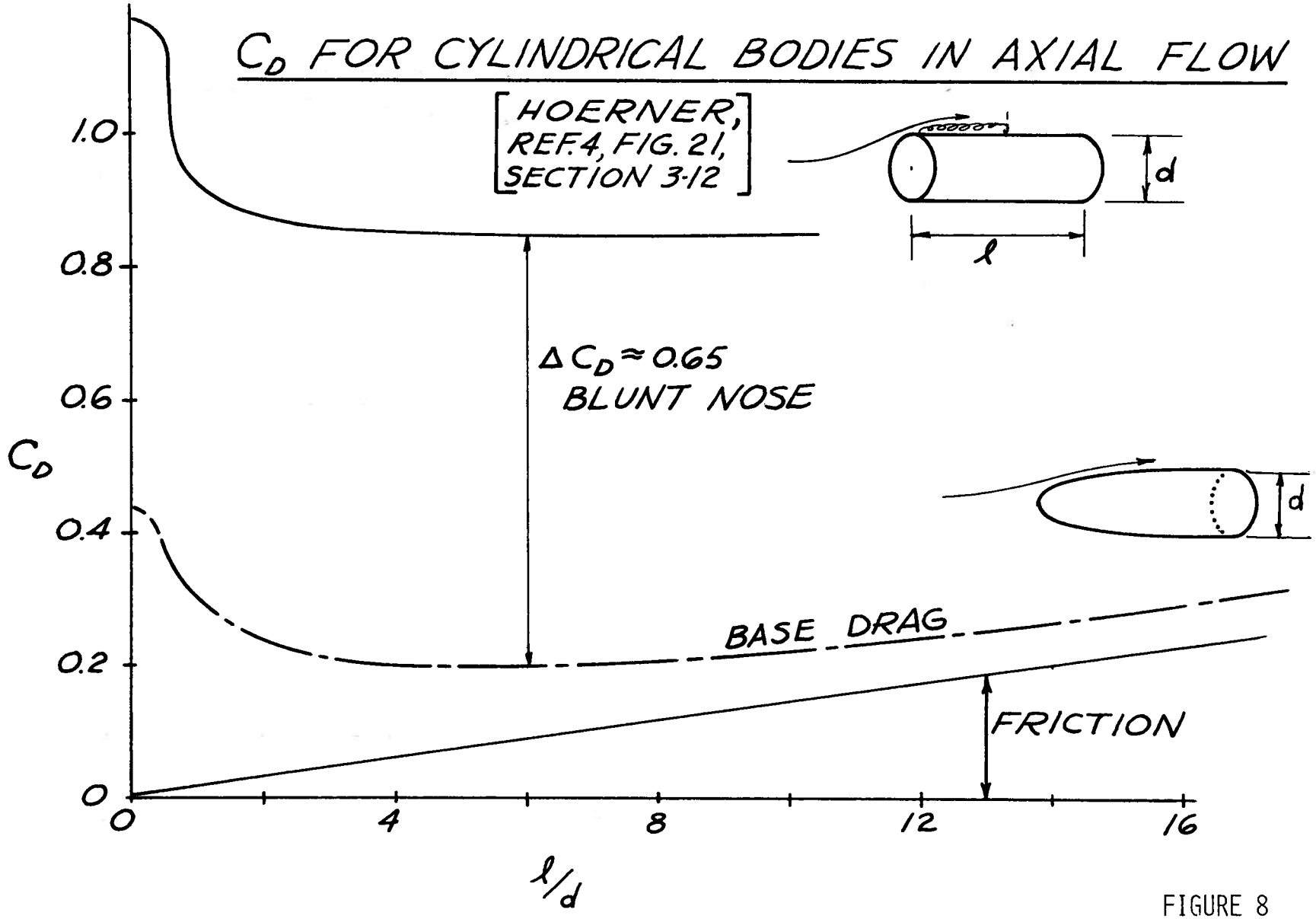
C_D FOR CYLINDRICAL BODIES IN AXIAL FLOW
[HOERNER, REF.4, FIG. 21, SECTION 3-12]
1.0
0.8
0.6
0.4
0.2
0
C_D
$\Delta C_D \approx 0.65$
BLUNT NOSE
d
ℓ
d
BASE DRAG
FRICTION
0
4
8
12
16
ℓ/d

FIGURE 8

RESISTANCE vs. SPEED

ONR Amphibious Vehicles

MODEL Nº 1

$L/B = 2.5$

$B/H = 4.0$

$T = 67°F$

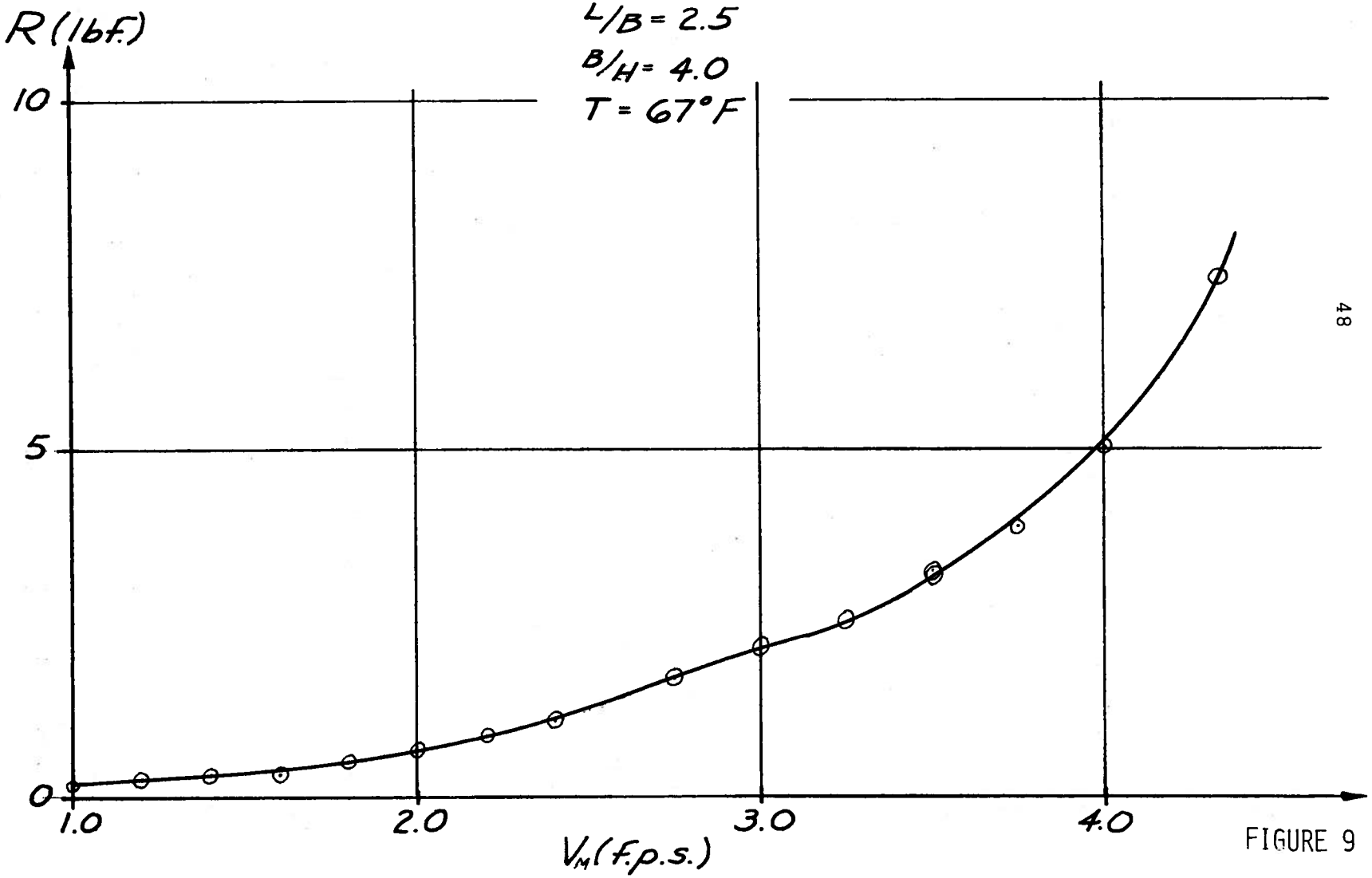

FIGURE 9

RESISTANCE vs. SPEED

ONR Amphibious Vehicles

MODEL Nº 1

$L/B = 2.5$

$B/H = 3.0$

$T = 67°F$

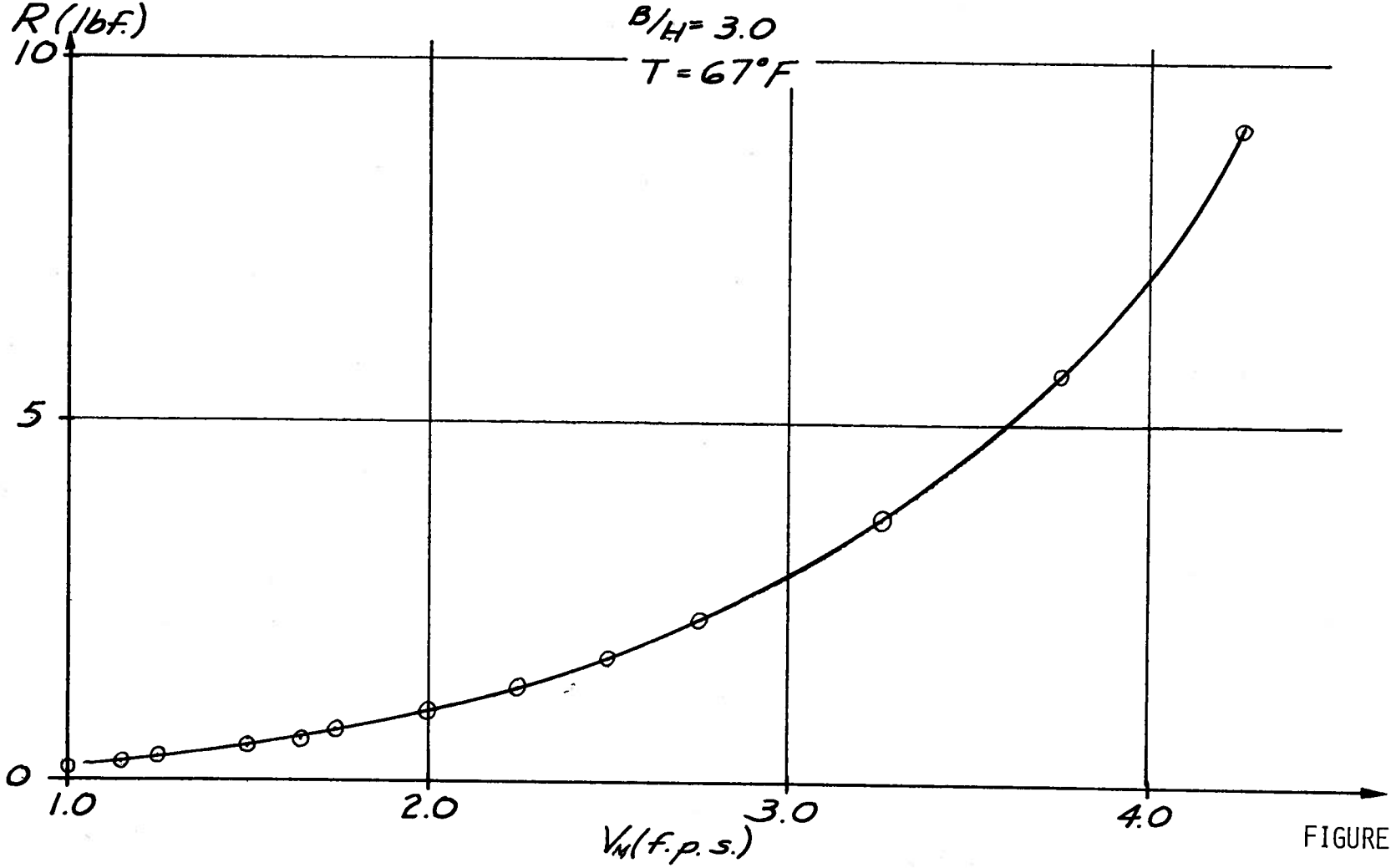

FIGURE 10

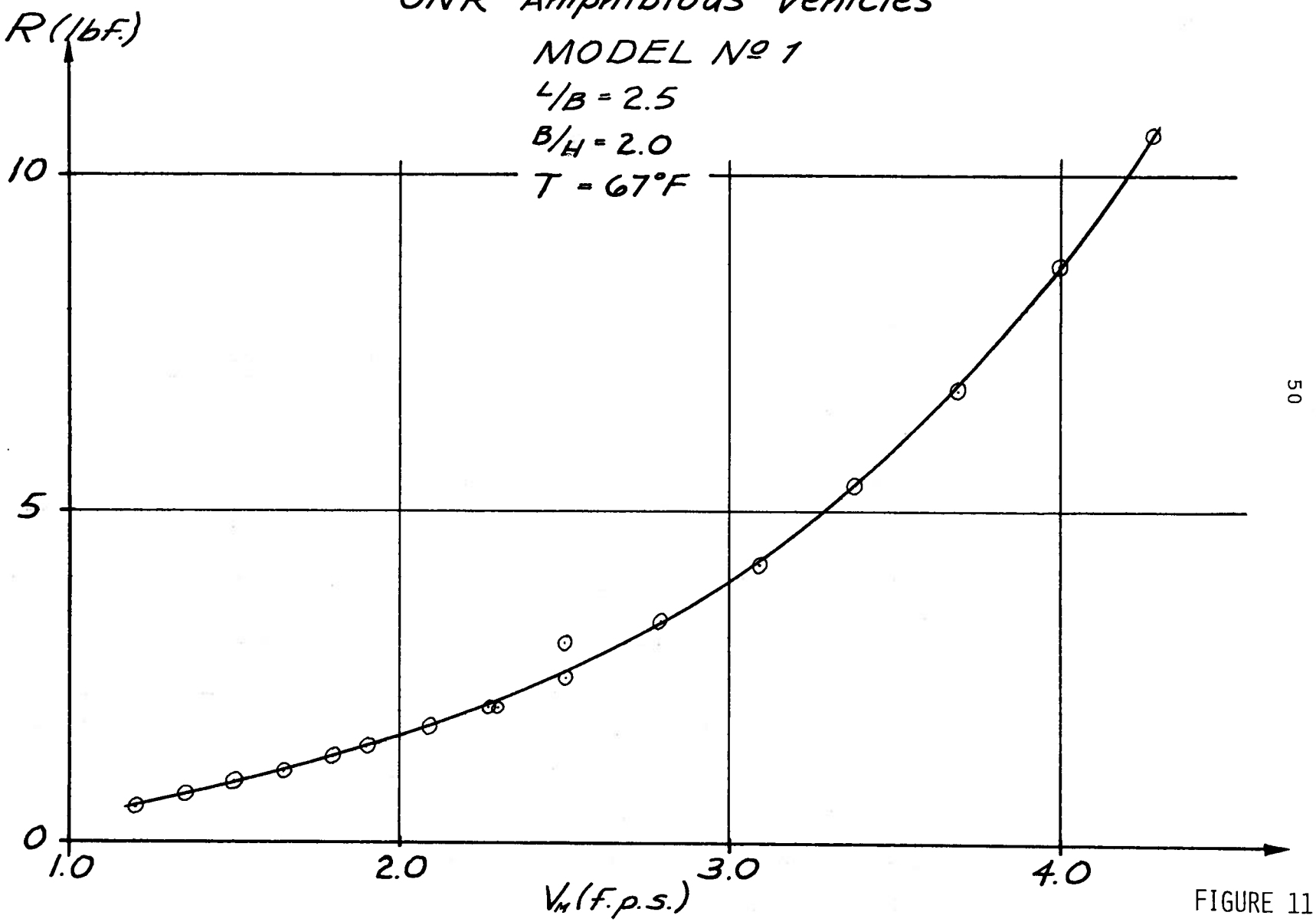
RESISTANCE vs. SPEED
ONR Amphibious Vehicles
MODEL Nº 1
L/B = 2.5
B/H = 2.0
T = 67°F
R (lbf.)
10
5
0
1.0
2.0
3.0
4.0
VM (f.p.s.)

FIGURE 11

RESISTANCE vs. SPEED

ONR Amphibious Vehicles

MODEL № 2

$L/B = 3.5$

$B/H = 4.0$

$T = 67°F$

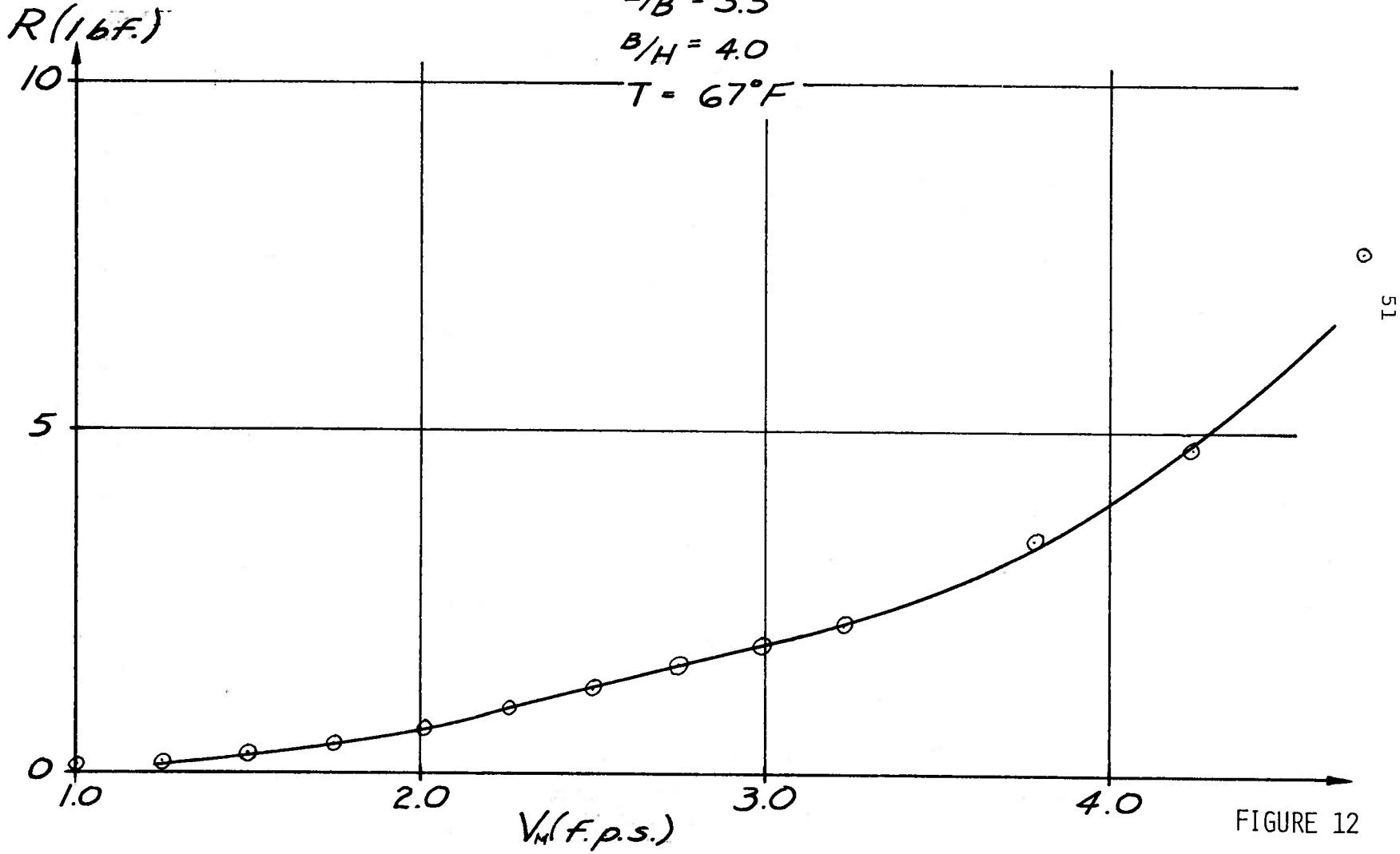

FIGURE 12

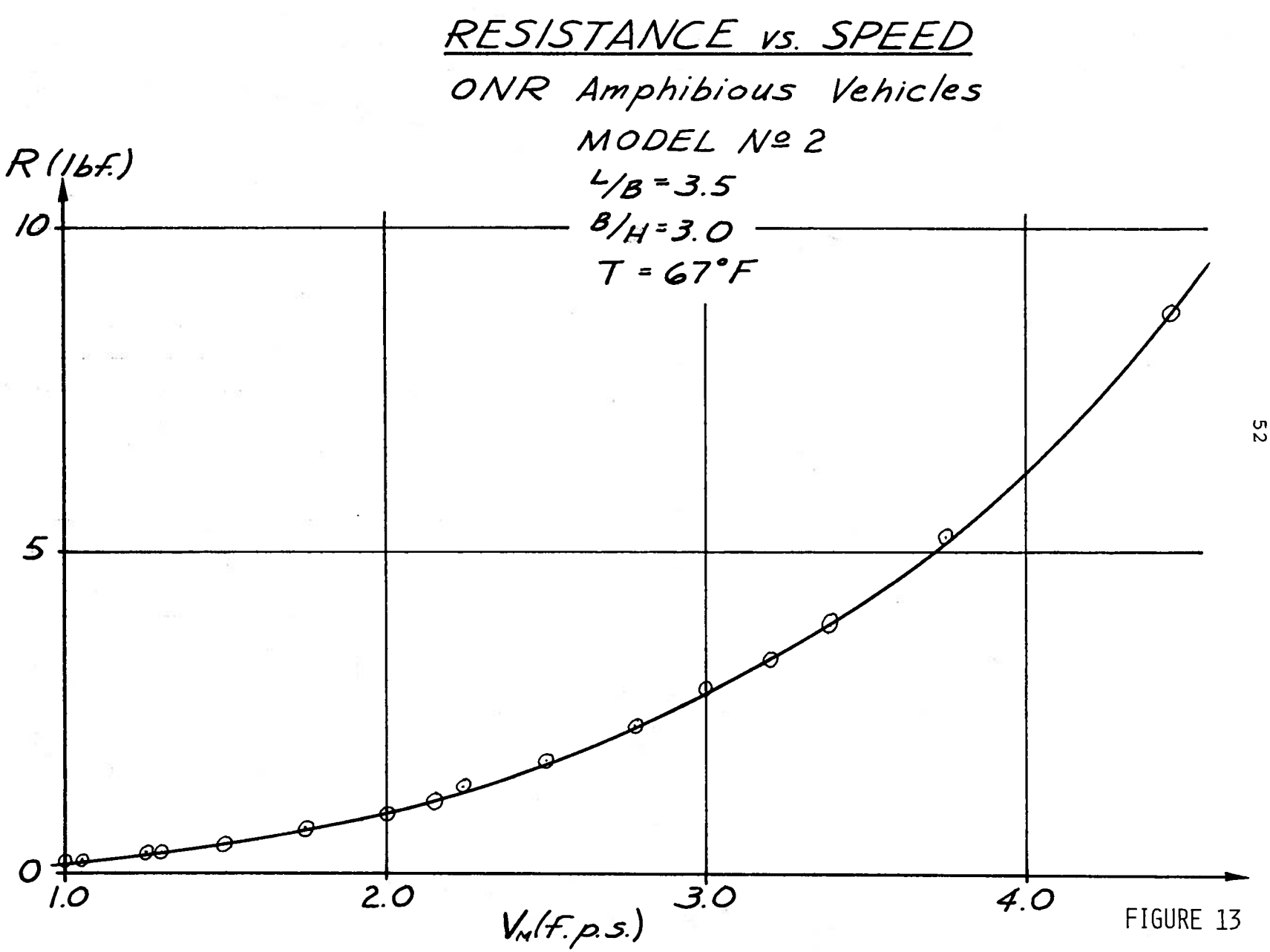
RESISTANCE vs. SPEED
ONR Amphibious Vehicles
MODEL Nº 2
L/B = 3.5
B/H = 3.0
T = 67°F
R (lbf.)
10
5
0
1.0
2.0
3.0
4.0
VM (f.p.s.)

FIGURE 13

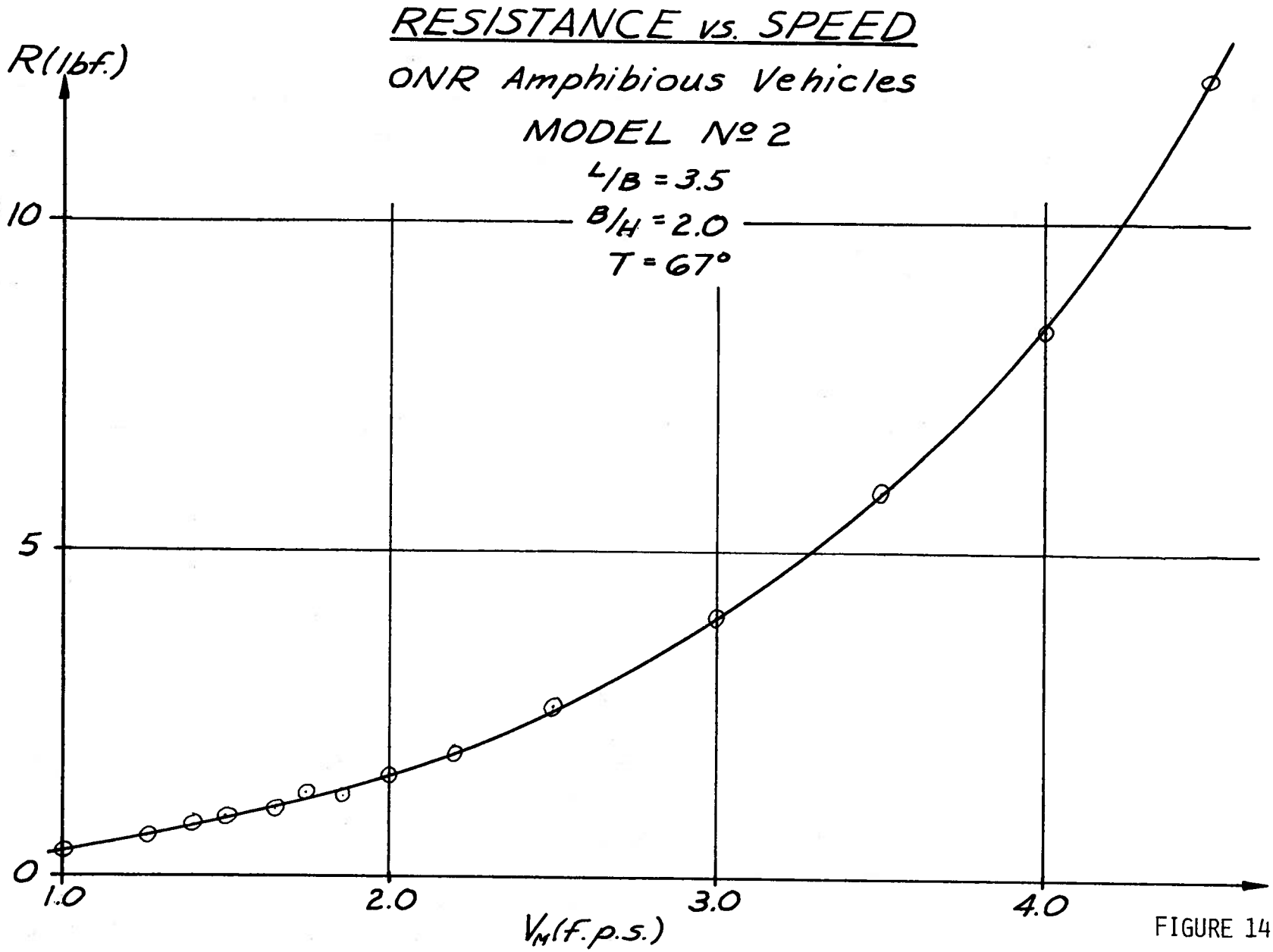
RESISTANCE vs. SPEED
ONR Amphibious Vehicles
MODEL Nº 2
L/B = 3.5
B/H = 2.0
T = 67°
R(lbf.)
10
5
0
1.0
2.0
3.0
4.0
VM(f.p.s.)

FIGURE 14

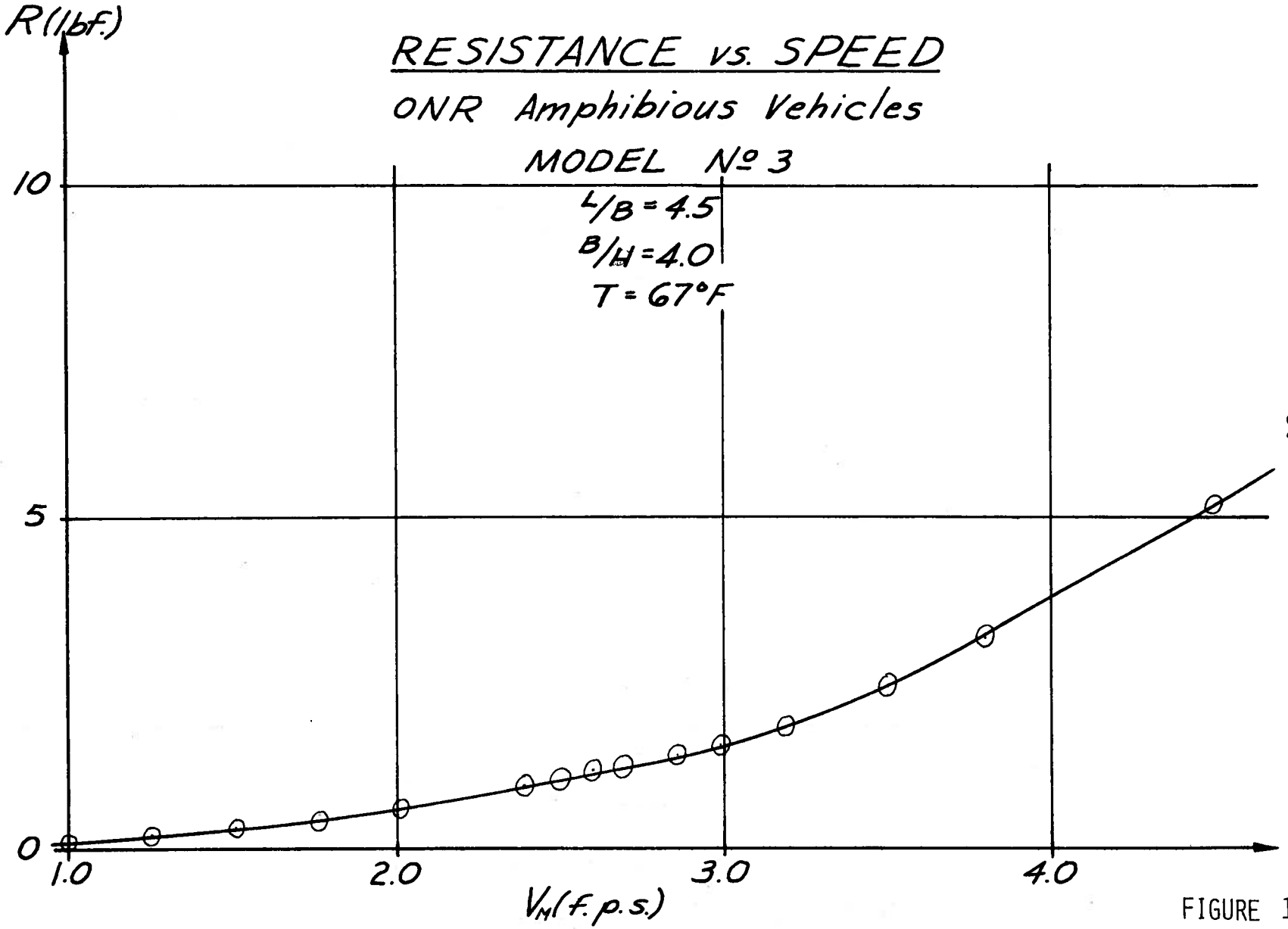
R(lbf.)
RESISTANCE vs. SPEED
ONR Amphibious Vehicles
MODEL Nº 3
L/B = 4.5
B/H = 4.0
T = 67°F
10
5
0
1.0
2.0
3.0
4.0
V_M(f.p.s.)

FIGURE 15

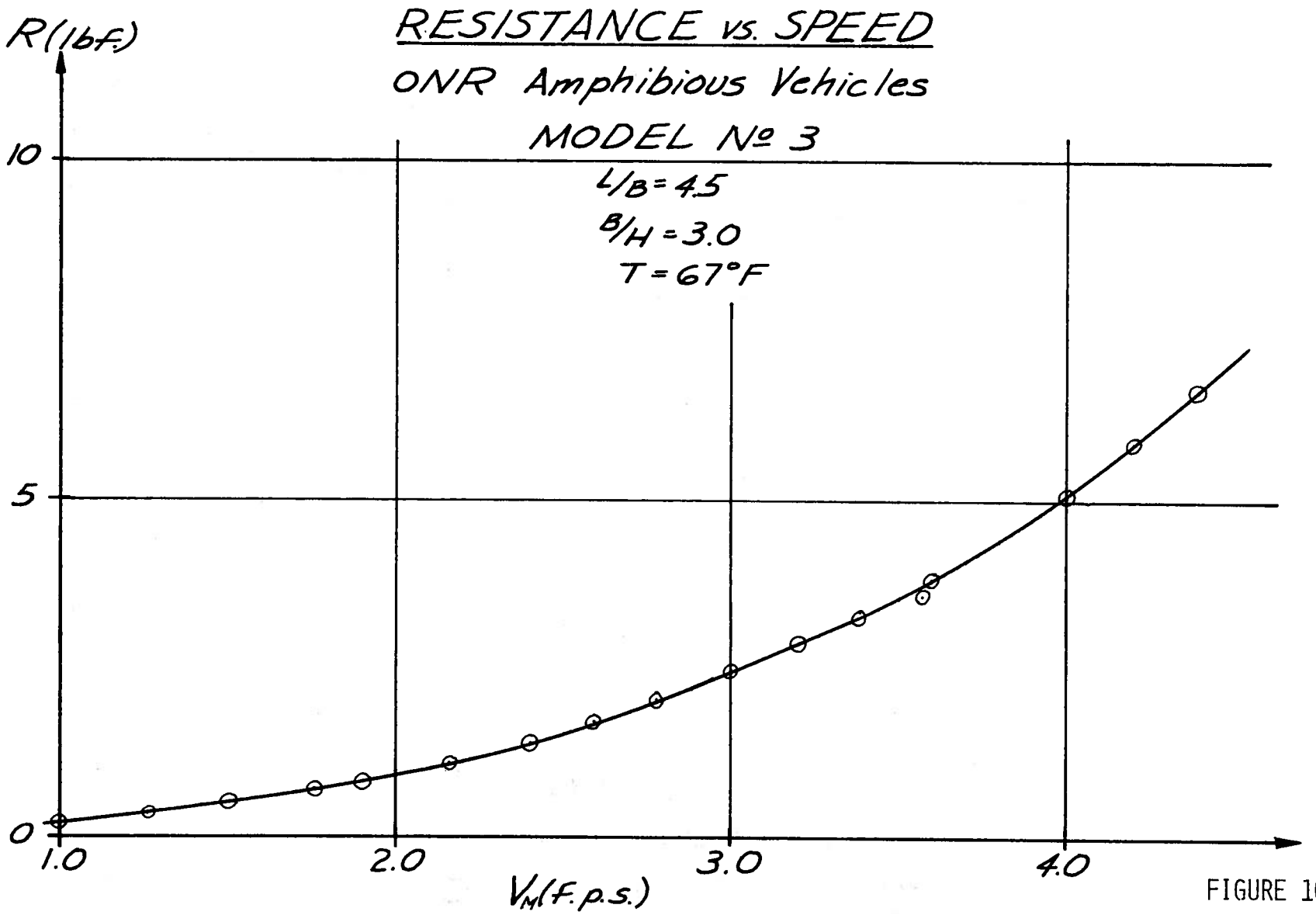
RESISTANCE vs. SPEED
ONR Amphibious Vehicles
MODEL Nº 3
L/B = 4.5
B/H = 3.0
T = 67°F
R(lbf.)
10
5
0
1.0
2.0
3.0
4.0
VM(F.p.s.)

FIGURE 16

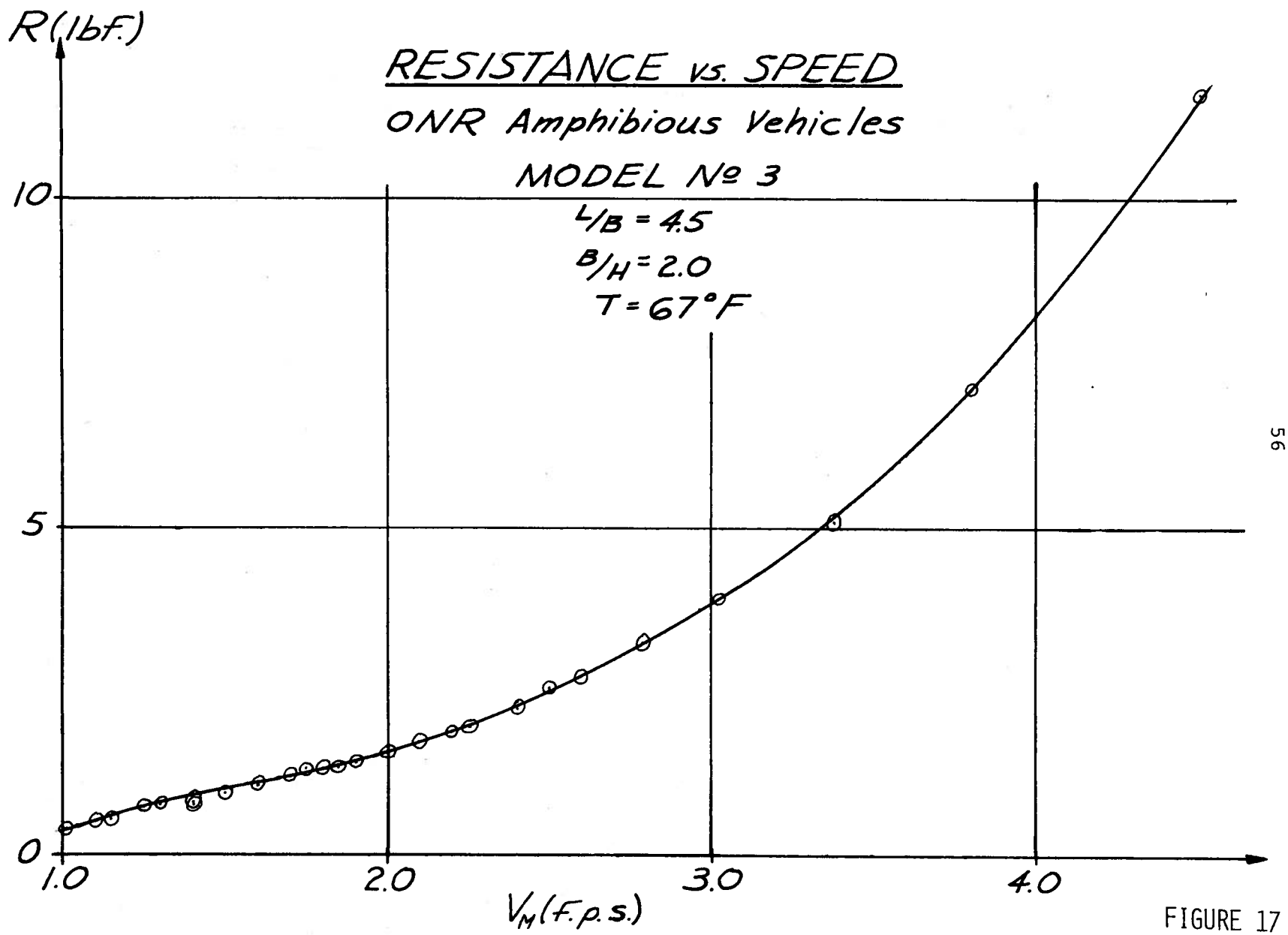
R(lbf.)
RESISTANCE vs. SPEED
ONR Amphibious Vehicles
MODEL Nº 3
L/B = 4.5
B/H = 2.0
T = 67°F
10
5
0
1.0
2.0
3.0
4.0
VM(f.p.s.)

FIGURE 17

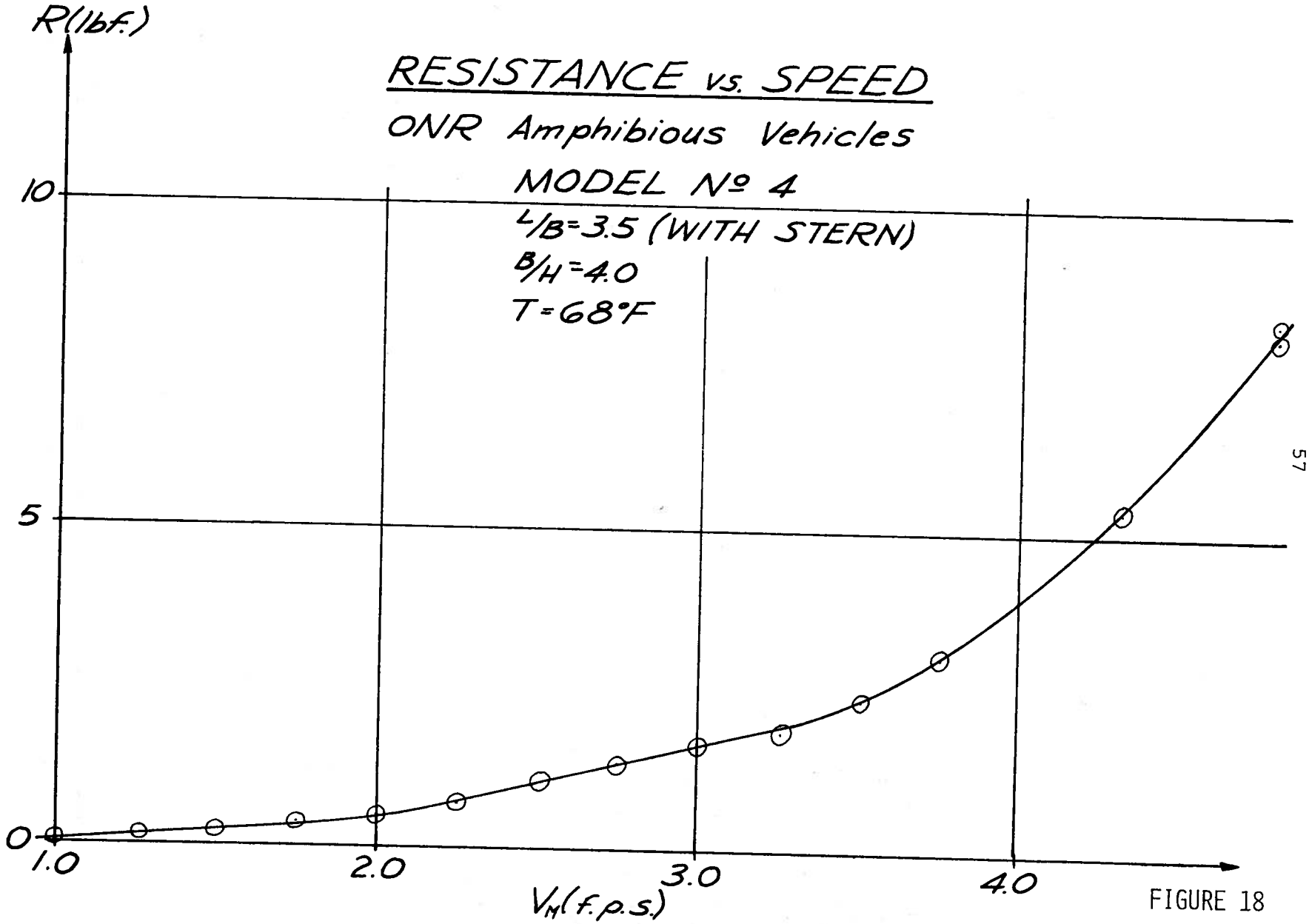
R(lbf.)
RESISTANCE vs. SPEED
ONR Amphibious Vehicles
MODEL Nº 4
L/B=3.5 (WITH STERN)
B/H=4.0
T=68°F
10
5
0
1.0
2.0
3.0
4.0
V_M(f.p.s.)

FIGURE 18

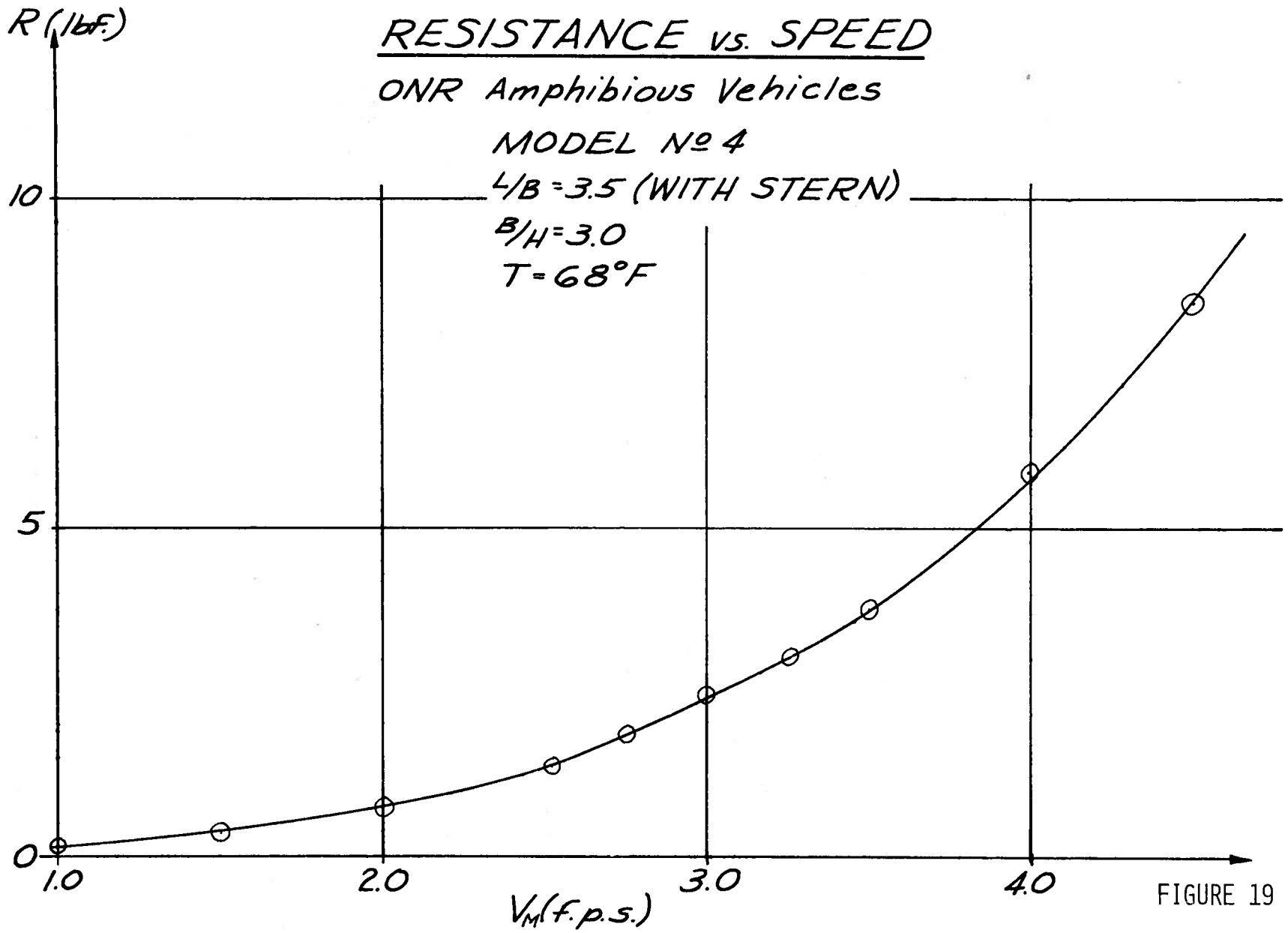
RESISTANCE vs. SPEED
ONR Amphibious Vehicles
MODEL Nº 4
L/B = 3.5 (WITH STERN)
B/H = 3.0
T = 68°F
R (lbf.)
10
5
0
1.0
2.0
3.0
4.0
V_M (f.p.s.)

FIGURE 19

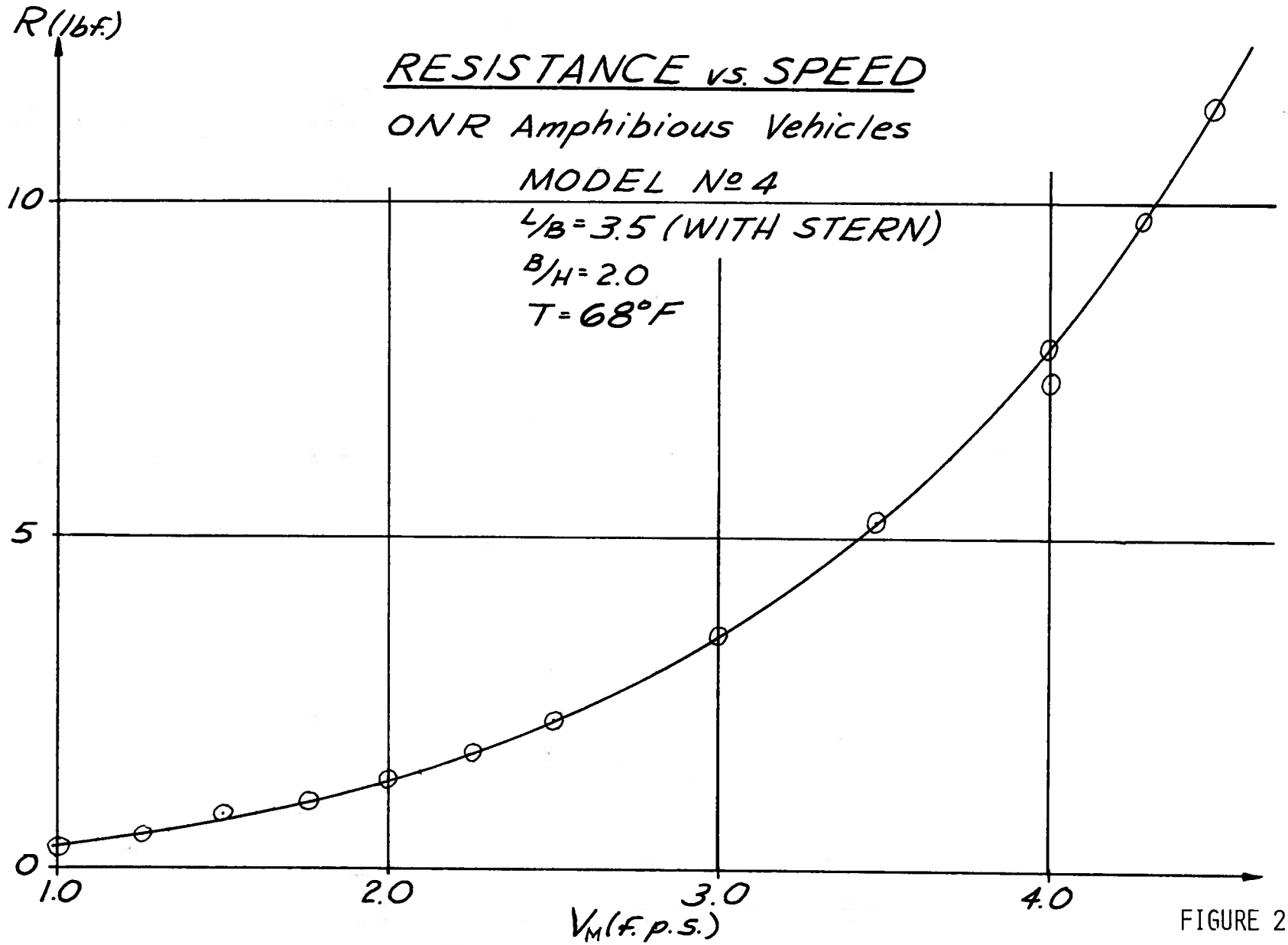
R(lbf.)
RESISTANCE vs. SPEED
ONR Amphibious Vehicles
MODEL Nº 4
L/B = 3.5 (WITH STERN)
B/H = 2.0
T = 68°F
10
5
0
1.0
2.0
3.0
4.0
VM(F.P.S.)

FIGURE 20

RESISTANCE vs. SPEED

ONR Amphibious Vehicles

MODEL Nº 5

$L/B = 3.5$ (WITH BOW)

$B/H = 4.0$

$T = 68°F$

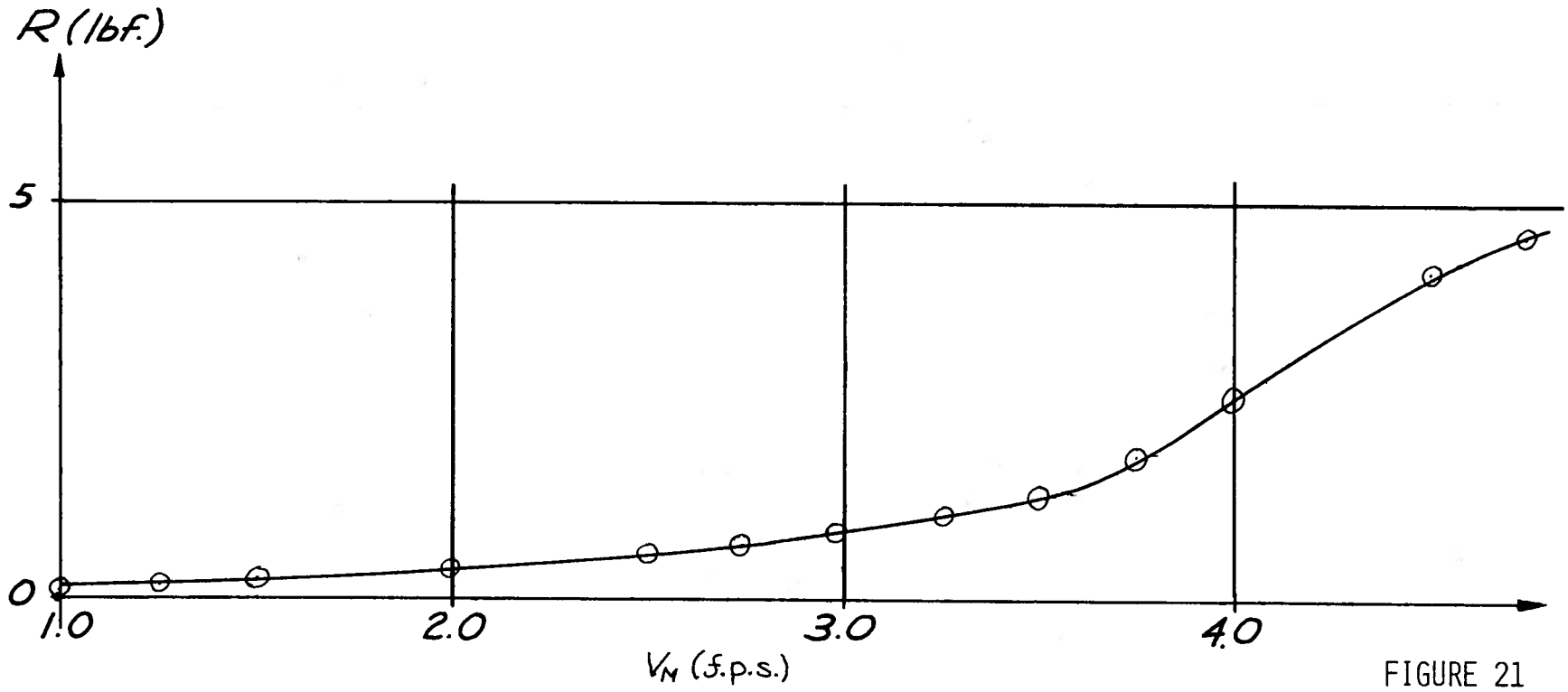

FIGURE 21

RESISTANCE vs. SPEED

ONR Amphibious Vehicles

MODEL Nº 5

$L/B = 3.5$ (WITH BOW)

$B/H = 3.0$

$T = 68°F$

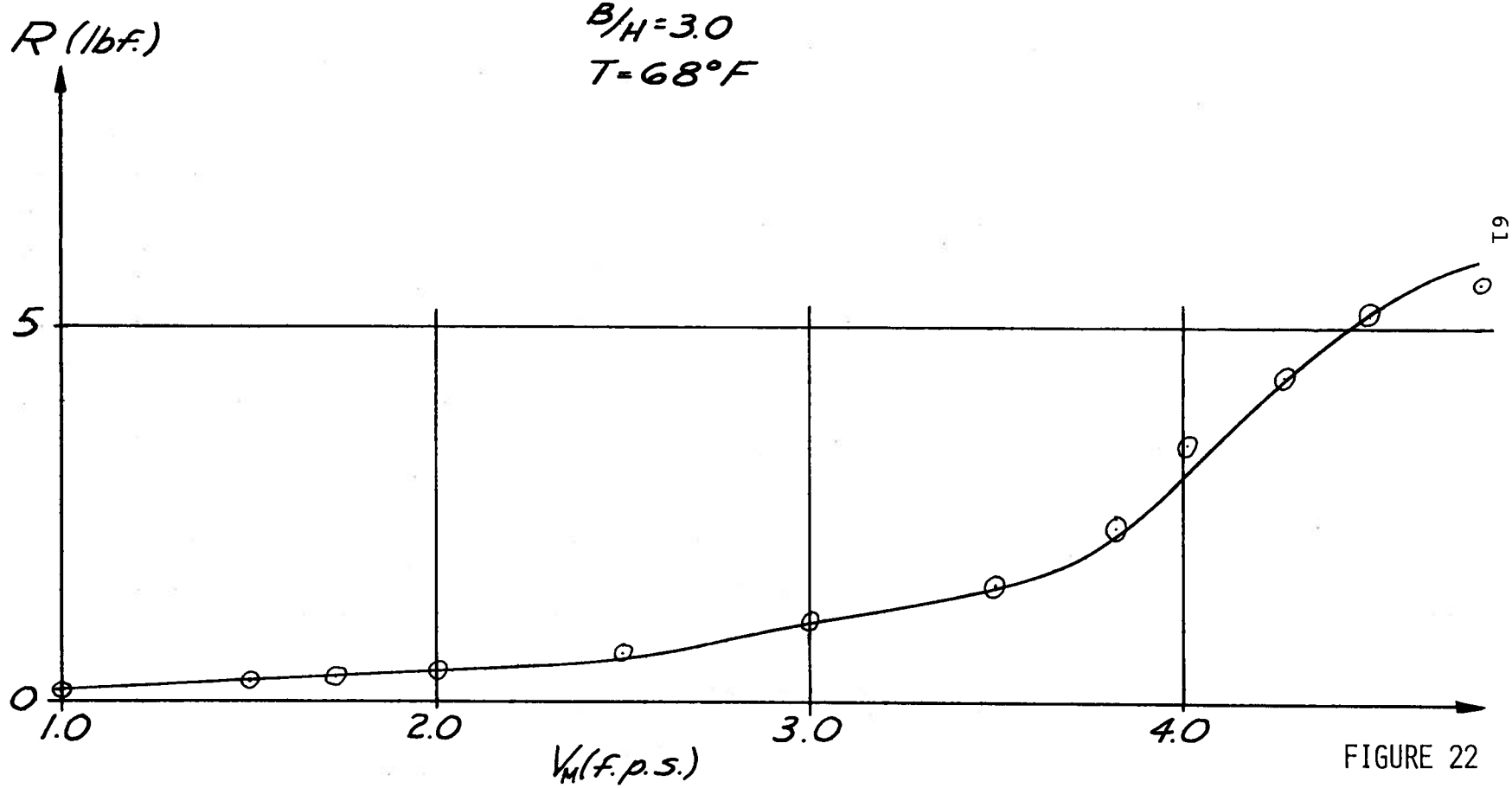

FIGURE 22

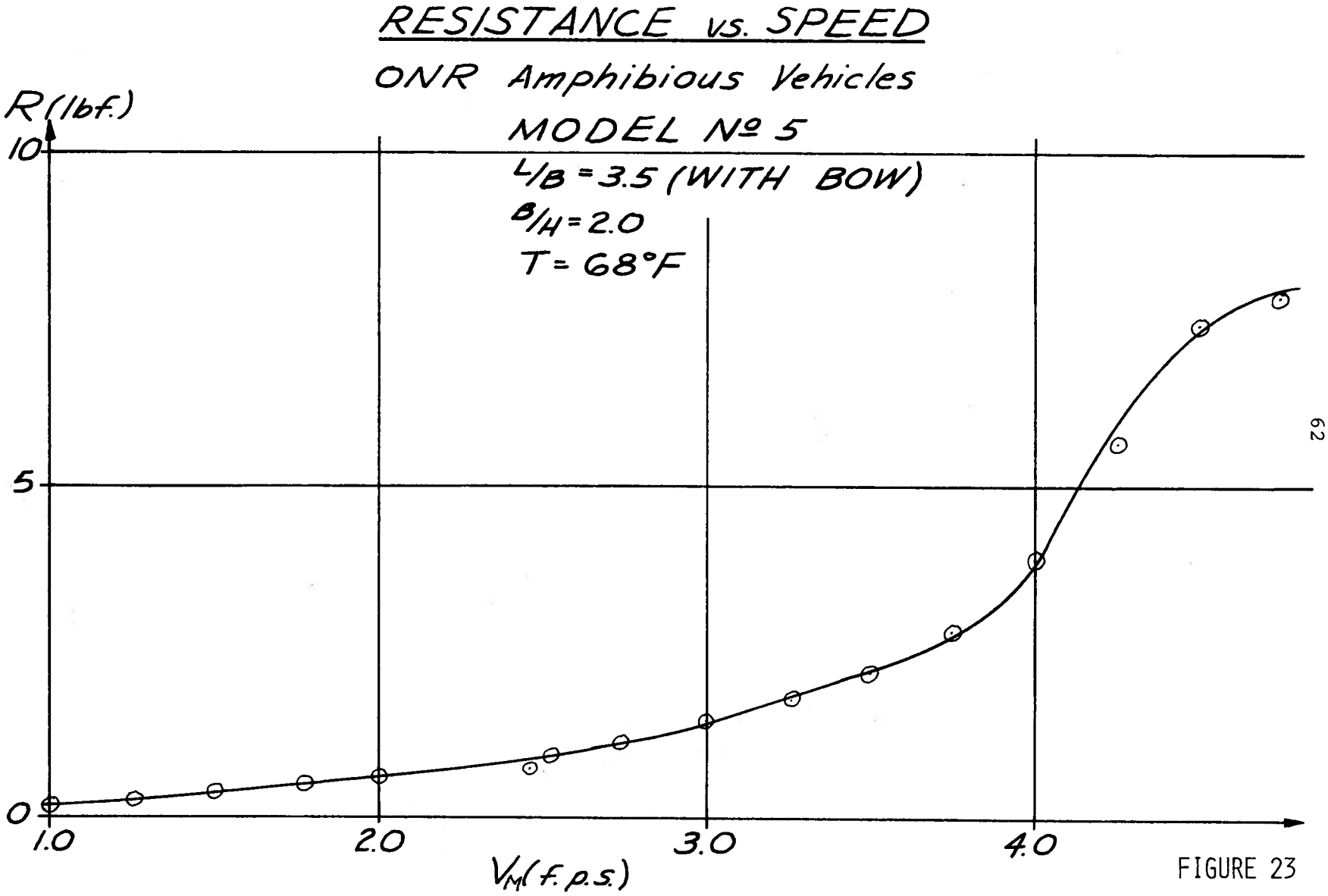
RESISTANCE vs. SPEED
ONR Amphibious Vehicles
MODEL Nº 5
L/B = 3.5 (WITH BOW)
B/H = 2.0
T = 68°F
R (lbf.)
10
5
0
1.0
2.0
3.0
4.0
VM (f.p.s.)
62

FIGURE 23

RESISTANCE vs. SPEED

ONR Amphibious Vehicles

MODEL Nº 6

$L/B = 4.5$ (BOW AND STERN)

$B/H = 4.0$

$T = 69°F$

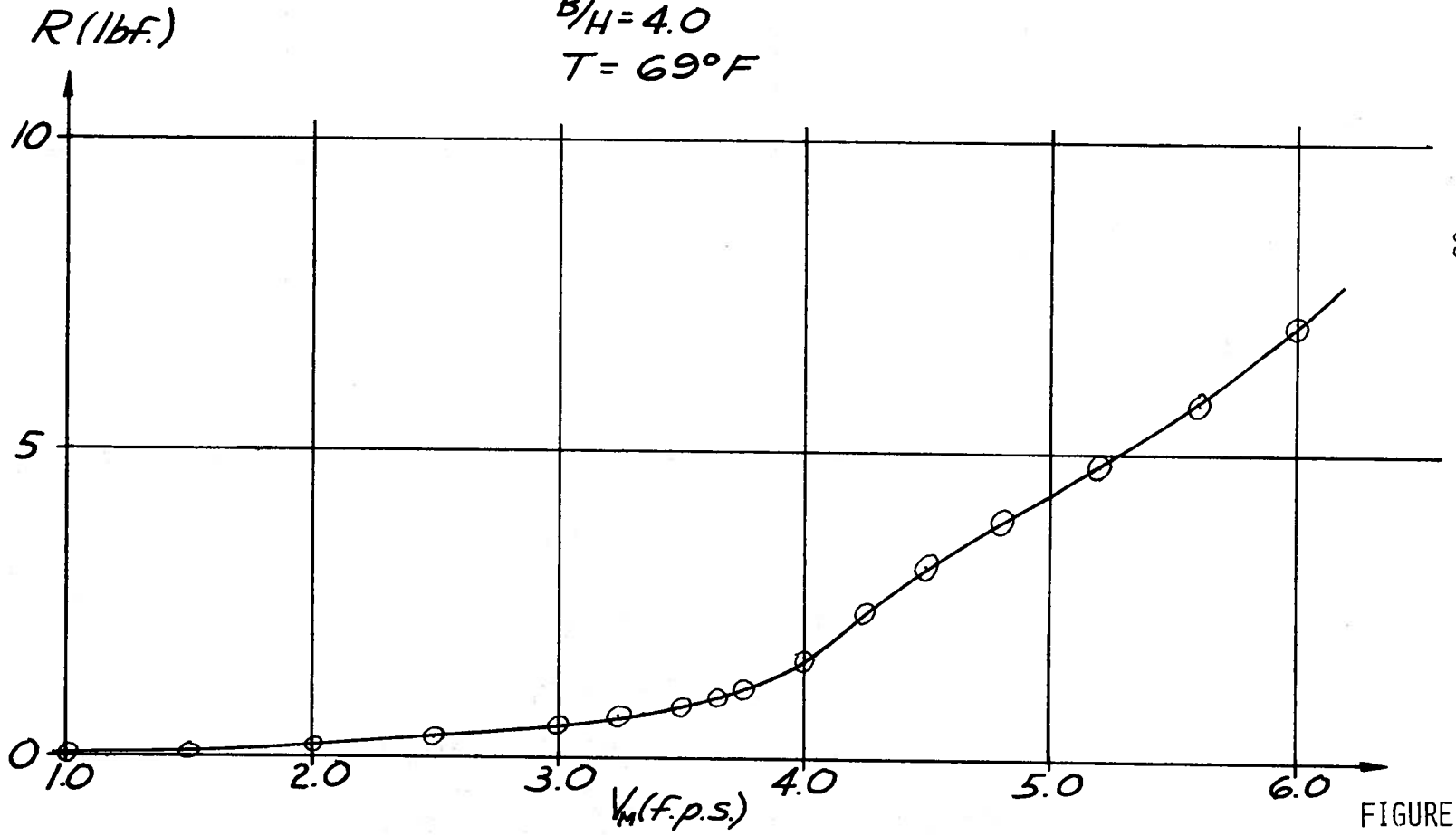

FIGURE 24

RESISTANCE vs. SPEED

ONR Amphibious Vehicles

MODEL Nº 6

L/B = 4.5 (BOW AND STERN)

B/H = 3.0

T = 69°F

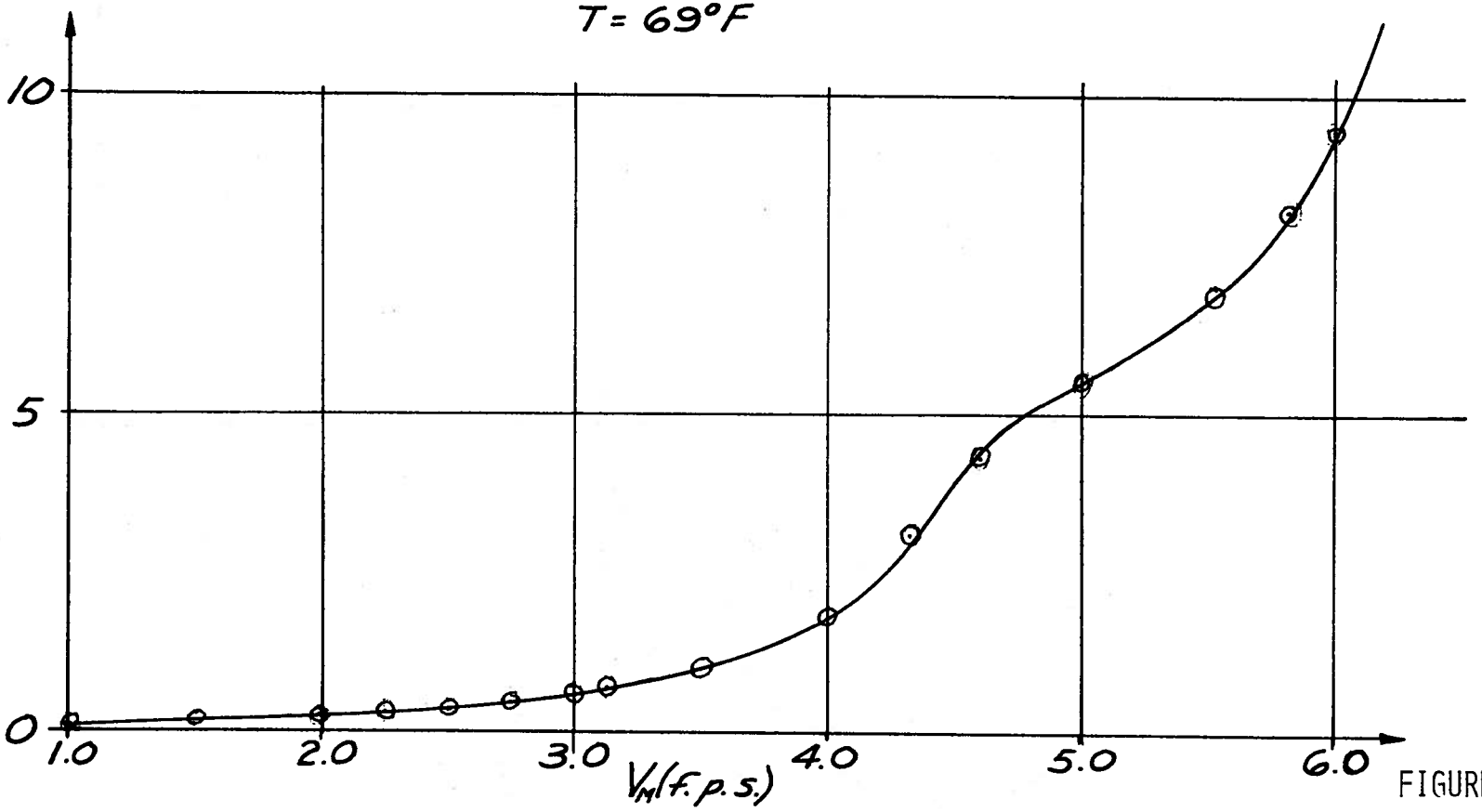

FIGURE 25

RESISTANCE vs. SPEED

ONR Amphibious Vehicles

MODEL Nº 6

$L/B = 4.5$ (BOW AND STERN)

$B/H = 2.0$

$T = 69°F$

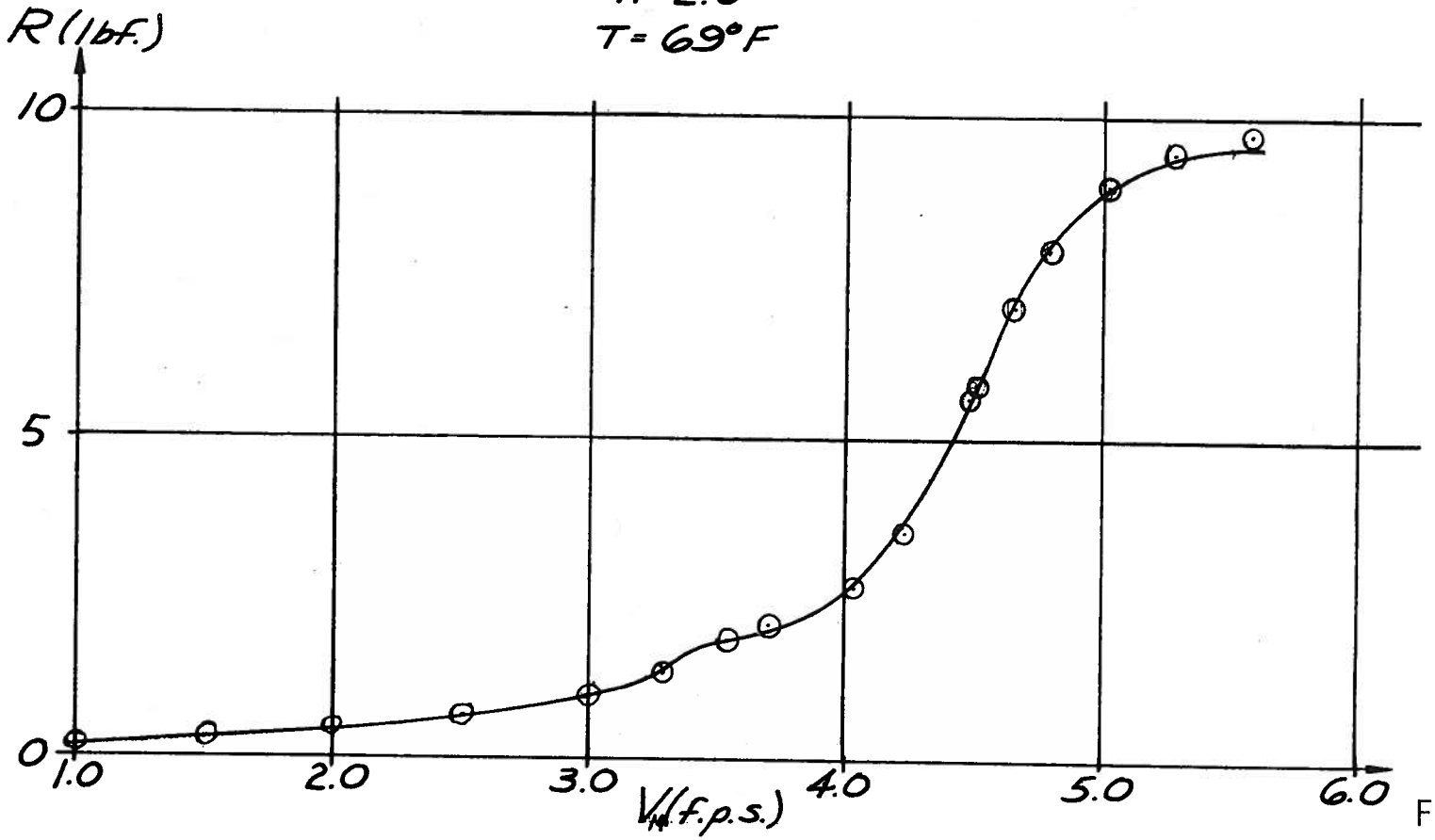

FIGURE 26

RESISTANCE vs. SPEED

ONR Amphibious Vehicles

MODEL Nº 7

$L/B = 2.5$

$B/H = 3.0$

$T = 70°F$

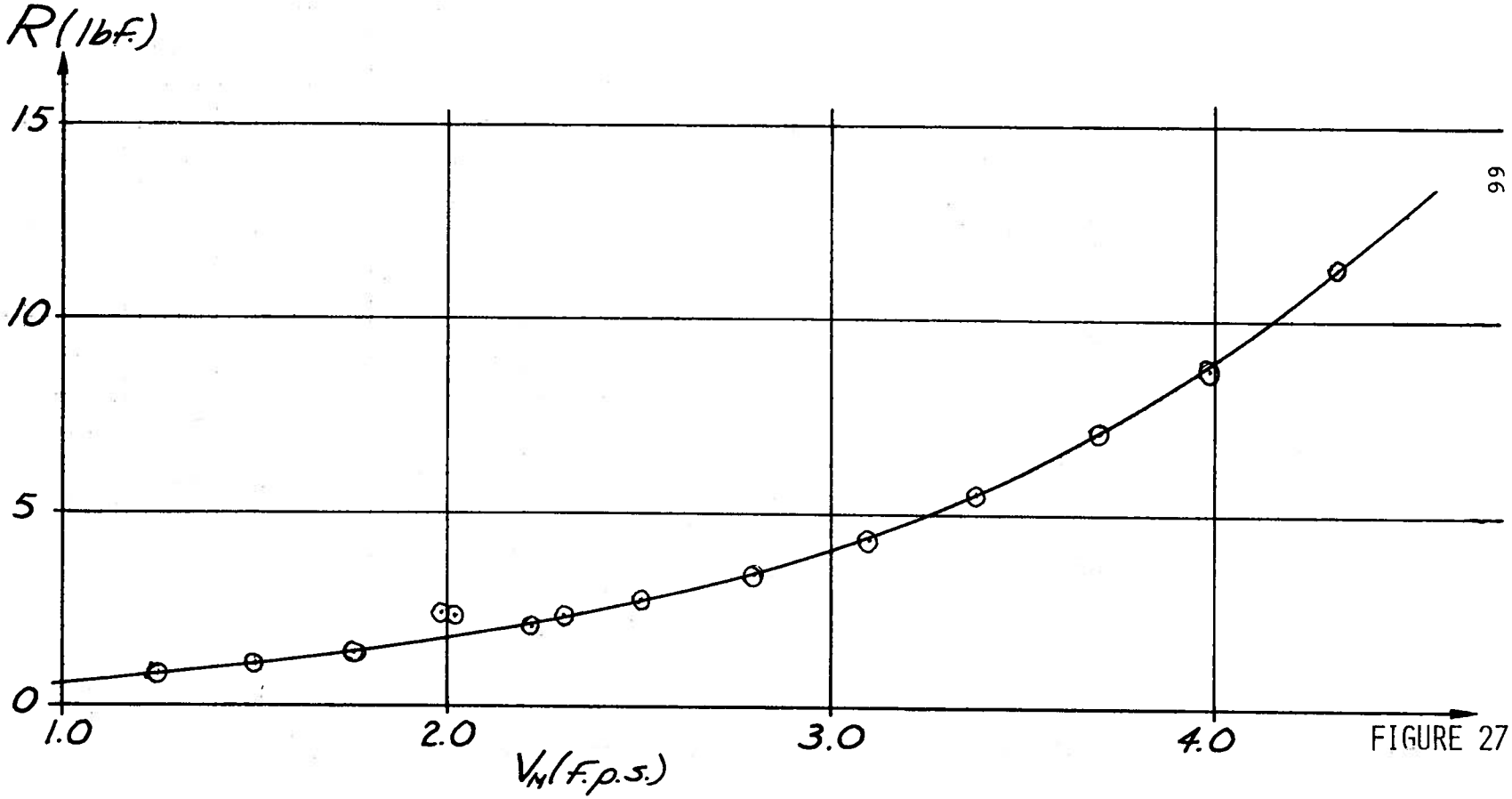

FIGURE 27

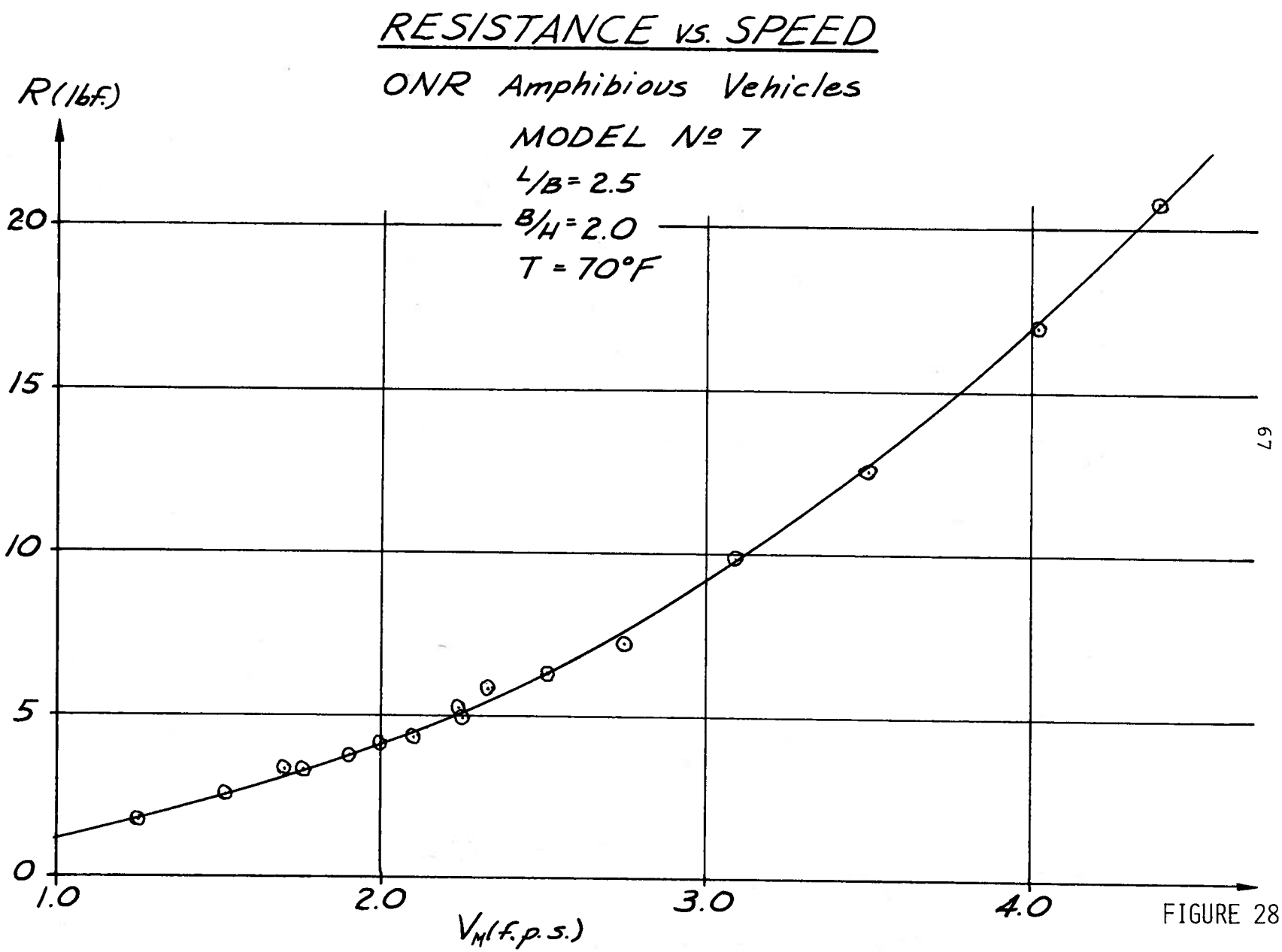
RESISTANCE vs. SPEED
ONR Amphibious Vehicles
MODEL Nº 7
L/B = 2.5
B/H = 2.0
T = 70°F
R(lbf.)
20
15
10
5
0
1.0
2.0
3.0
4.0
V_M(f.p.s.)
67

FIGURE 28

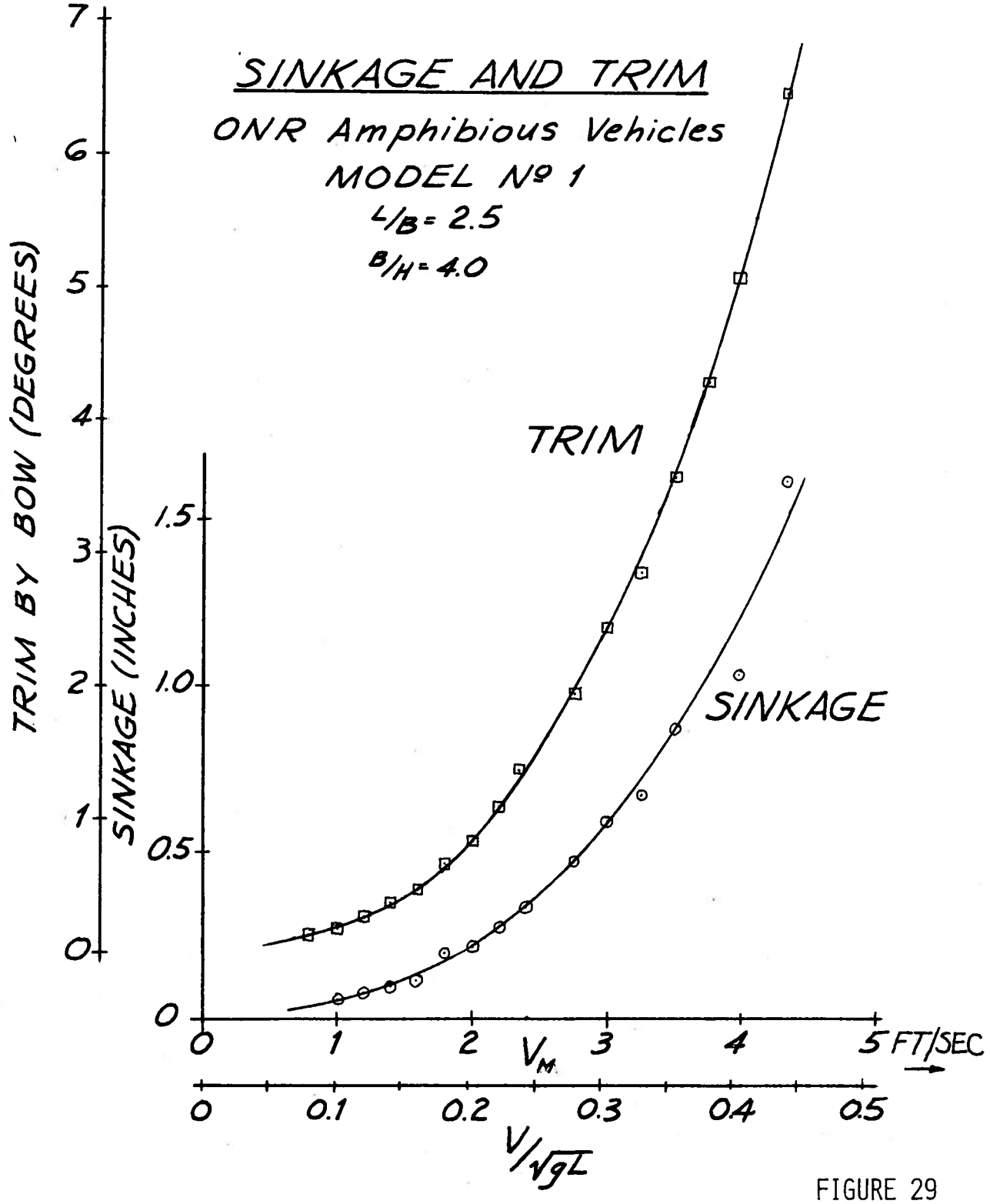
SINKAGE AND TRIM
ONR Amphibious Vehicles
MODEL Nº 1
L/B = 2.5
B/H = 4.0
TRIM
SINKAGE
TRIM BY BOW (DEGREES)
SINKAGE (INCHES)
0
1
2
3
4
5
6
7
0.5
1.0
1.5
V_M
FT/SEC
0.1
0.2
0.3
0.4
0.5
$V/\sqrt{gL}$

FIGURE 29

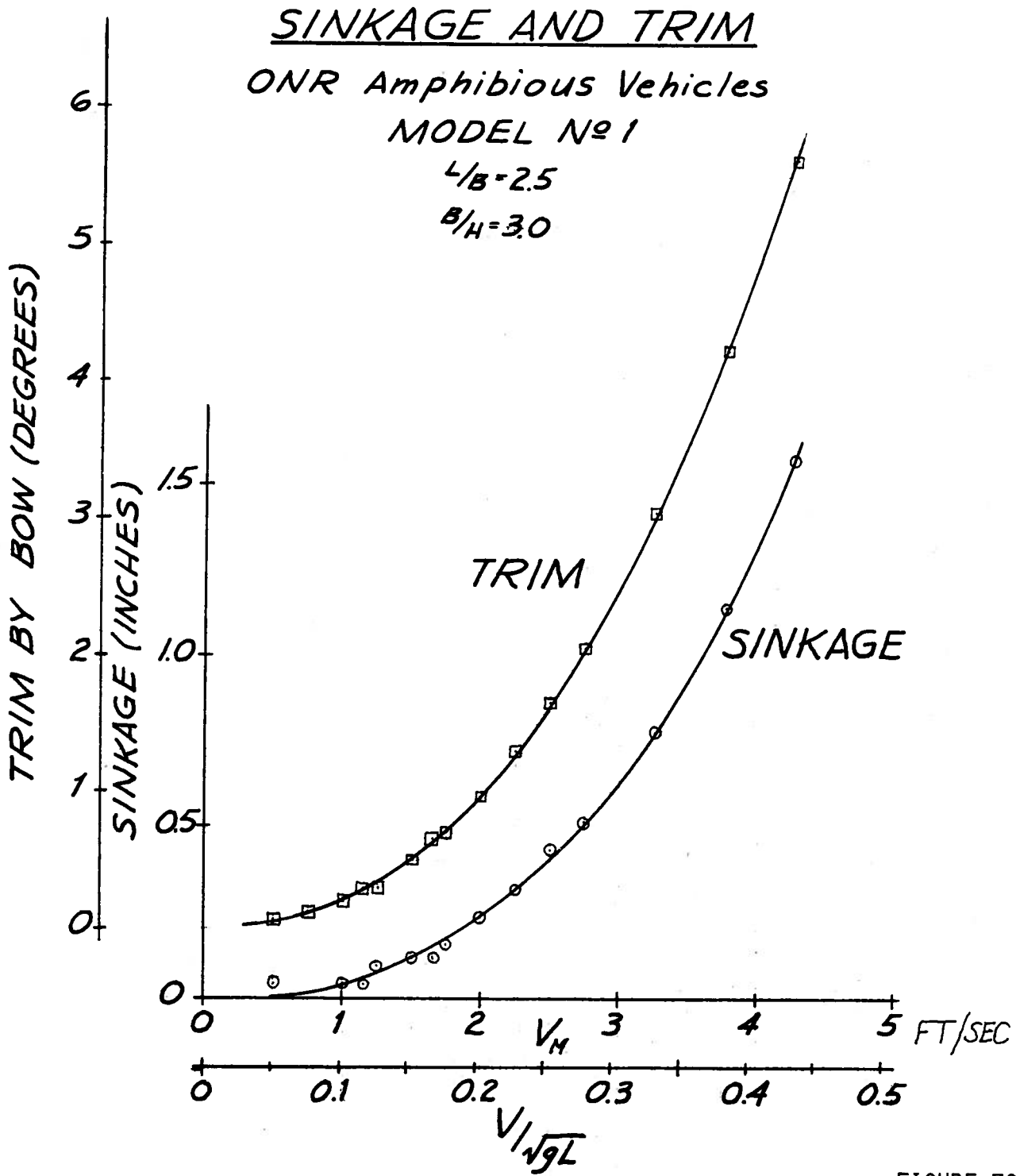
SINKAGE AND TRIM
ONR Amphibious Vehicles
MODEL Nº 1
L/B = 2.5
B/H = 3.0
TRIM BY BOW (DEGREES)
SINKAGE (INCHES)
TRIM
SINKAGE
0
1
2
3
4
5
6
0.5
1.0
1.5
V_H
FT/SEC
0.1
0.2
0.3
0.4
0.5
$V/\sqrt{gL}$

FIGURE 30

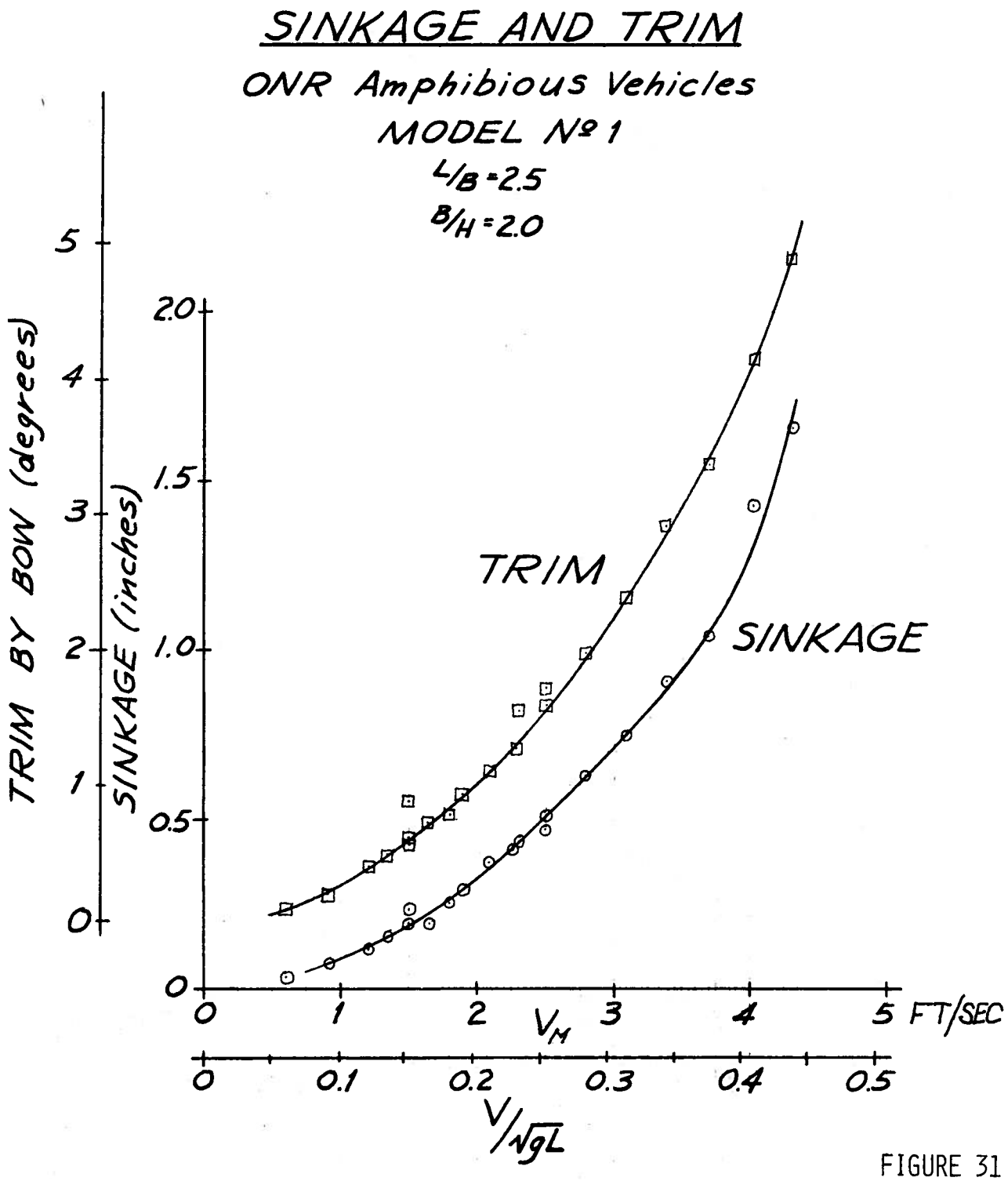
SINKAGE AND TRIM
ONR Amphibious Vehicles
MODEL Nº 1
L/B = 2.5
B/H = 2.0
TRIM BY BOW (degrees)
SINKAGE (inches)
TRIM
SINKAGE
0
1
2
3
4
5
0.5
1.0
1.5
2.0
V_M
FT/SEC
0.1
0.2
0.3
0.4
0.5
$V/\sqrt{gL}$

FIGURE 31

SINKAGE AND TRIM

ONR Amphibious Vehicles

MODEL Nº 2

$L/B = 3.5$

$B/H = 4.0$

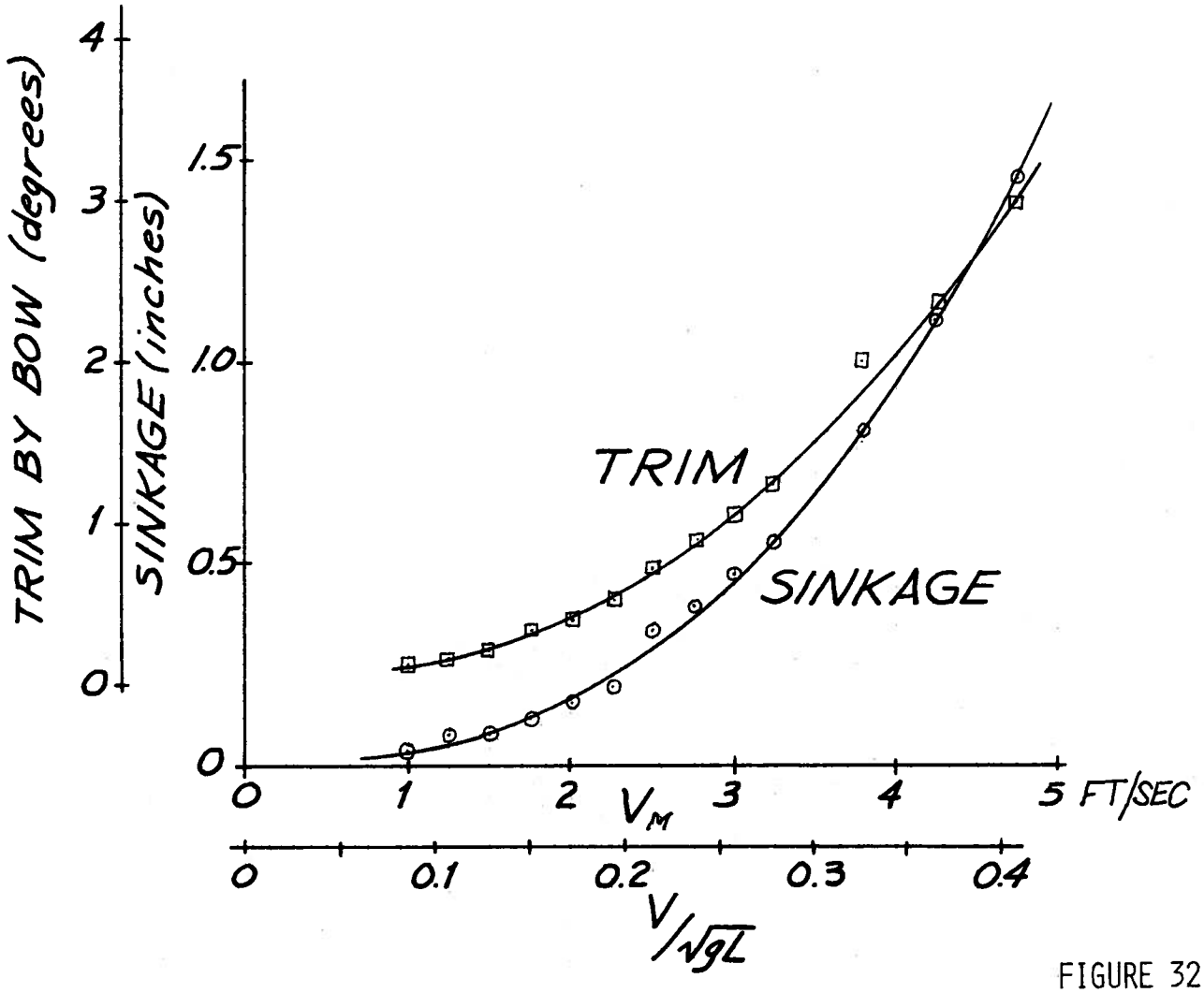

FIGURE 32

SINKAGE AND TRIM

ONR Amphibious Vehicles

MODEL Nº 2

$L/B = 3.5$

$B/H = 3.0$

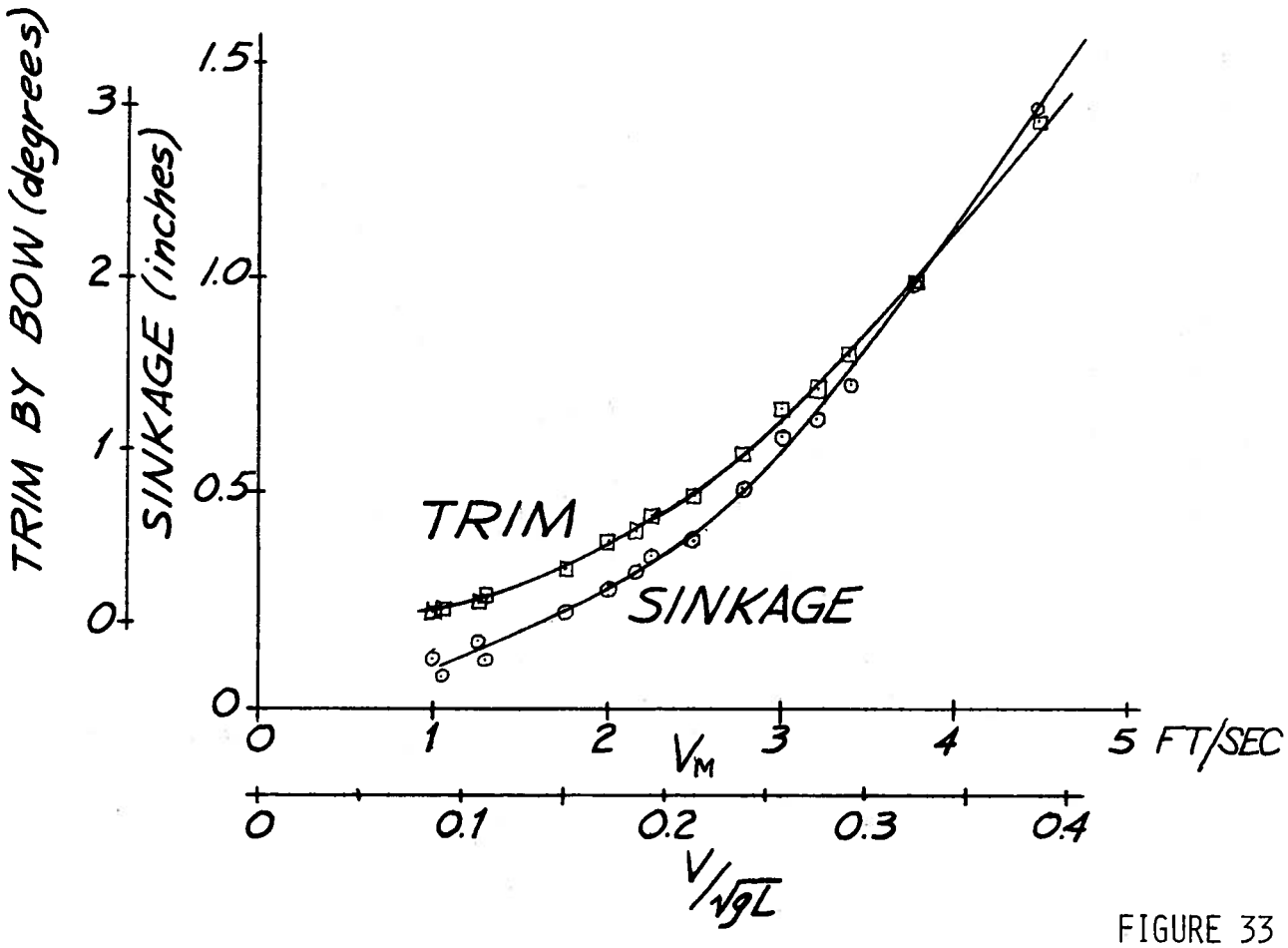

FIGURE 33

SINKAGE AND TRIM

ONR Amphibious Vehicles

MODEL Nº 2

$L/B = 3.5$

$B/H = 2.0$

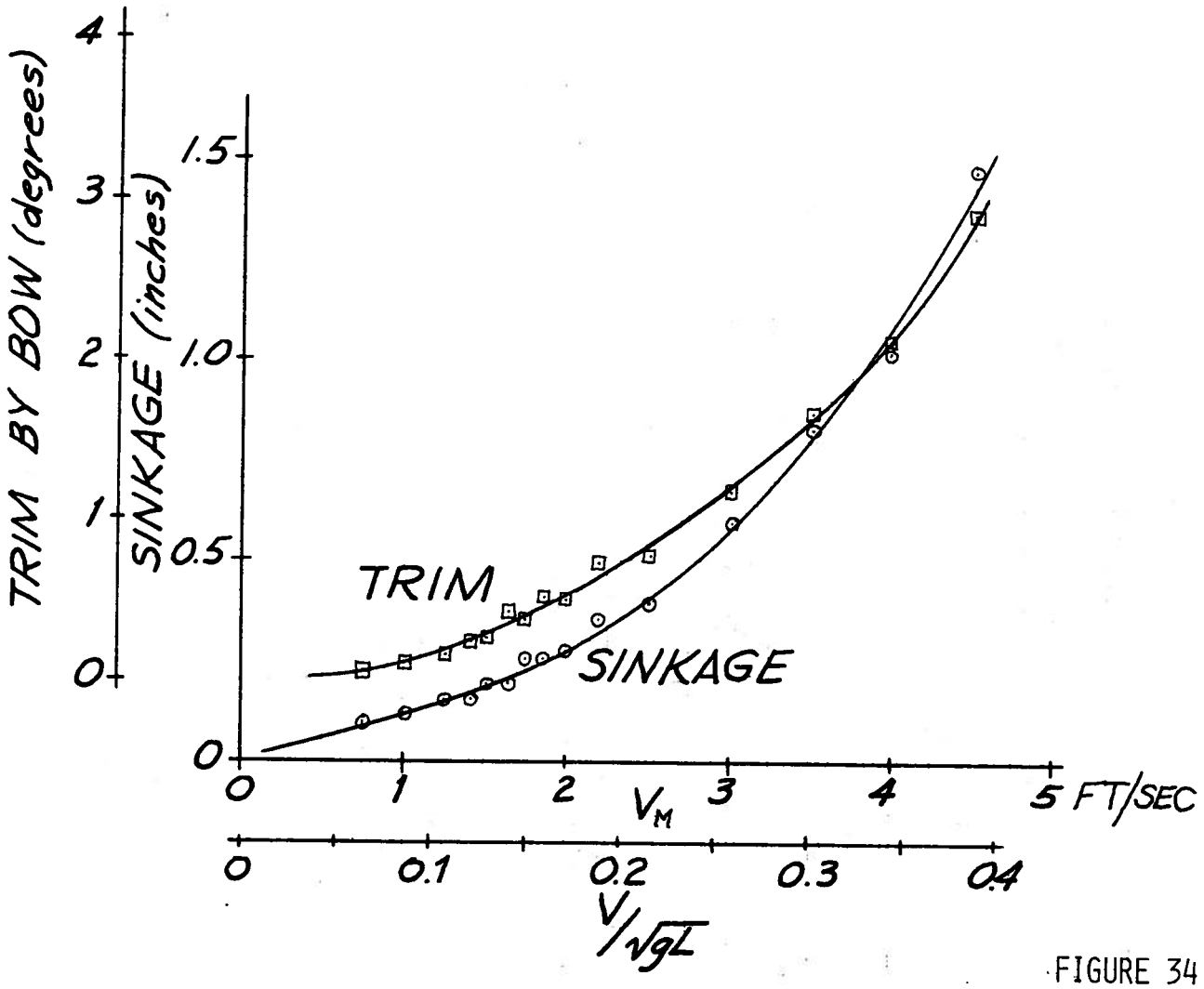

FIGURE 34

SINKAGE AND TRIM

ONR Amphibious Vehicles

MODEL Nº 3

$L/B = 4.5$

$B/H = 4.0$

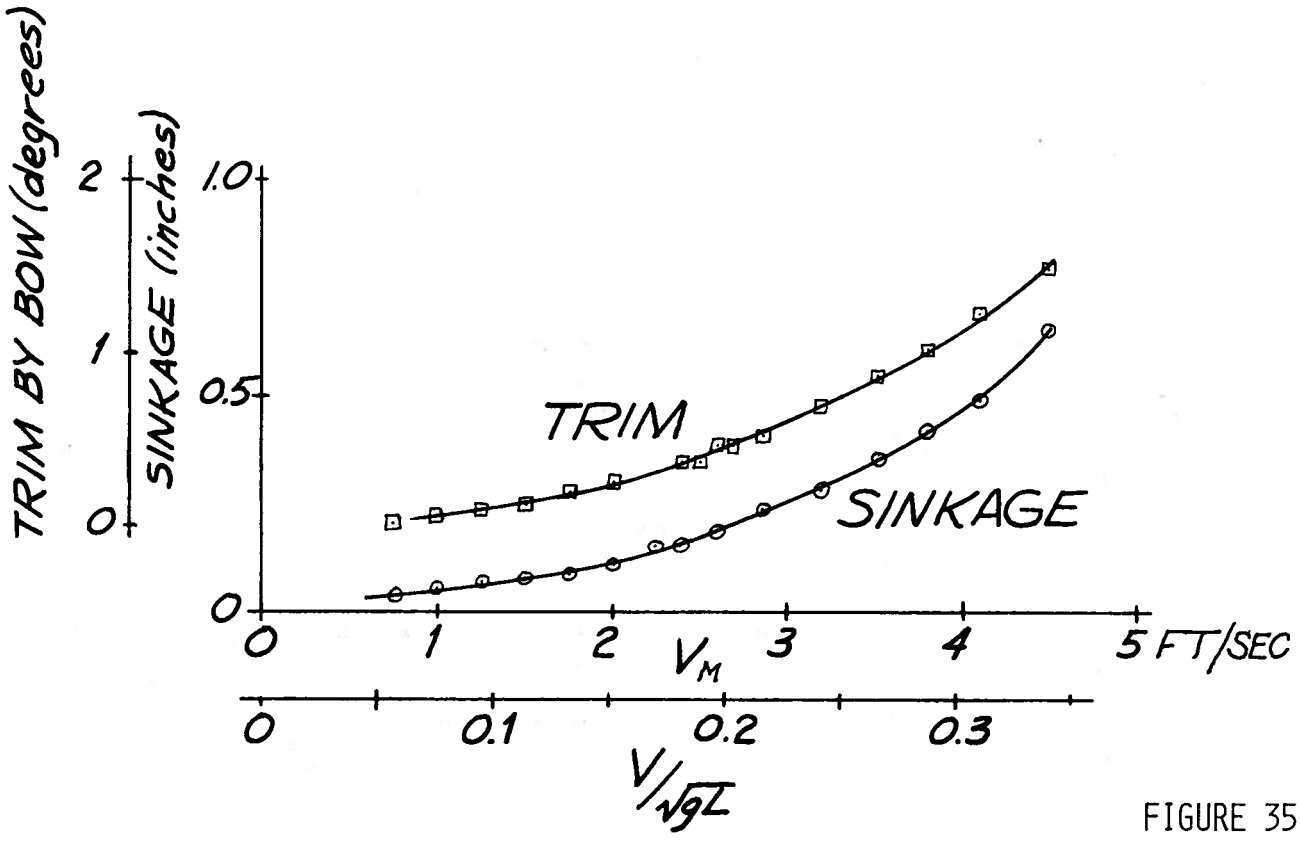

FIGURE 35

SINKAGE AND TRIM

ONR Amphibious Vehicles

MODEL Nº3

$L/B = 4.5$

$B/H = 3.0$

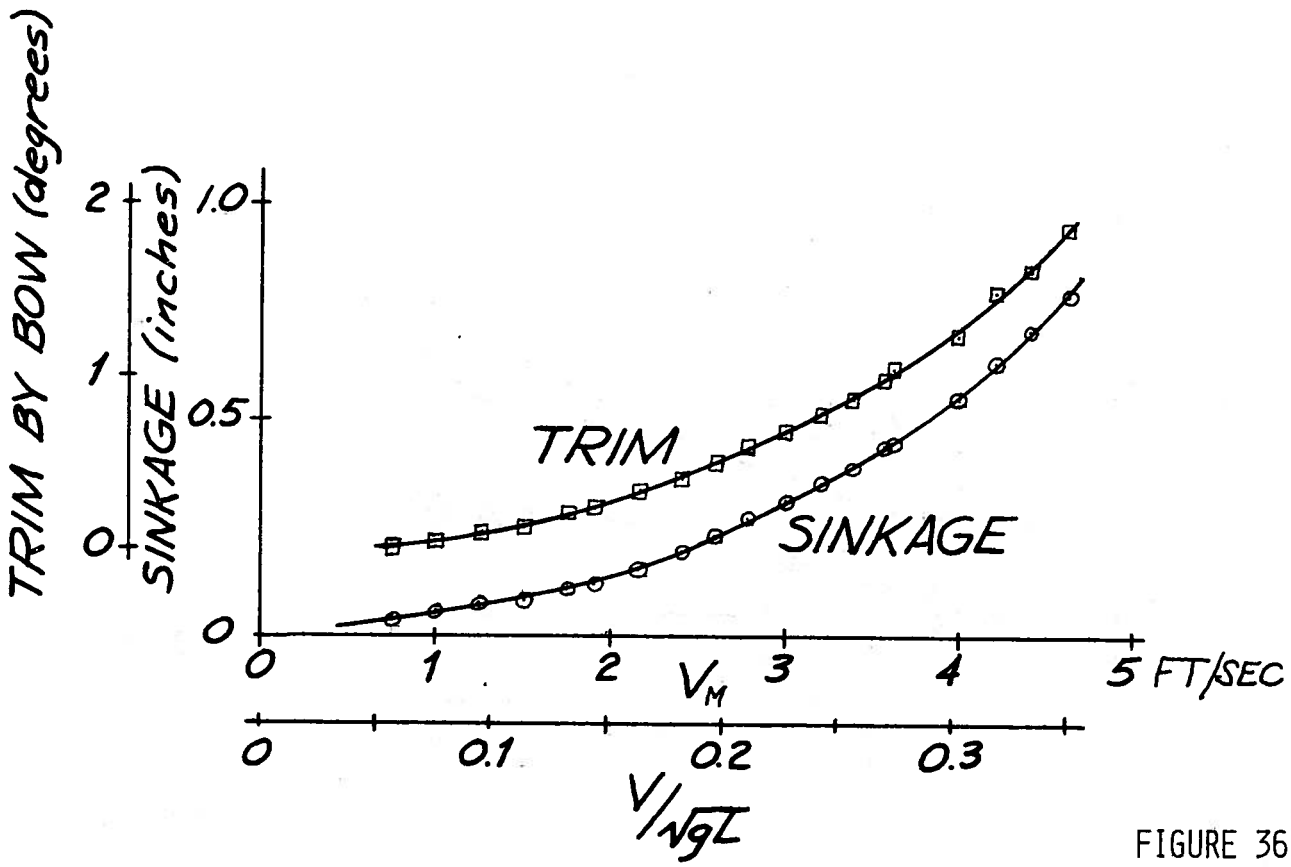

FIGURE 36

SINKAGE AND TRIM

ONR Amphibious Vehicles

MODEL Nº3

$L/B = 4.5$

$B/H = 2.0$

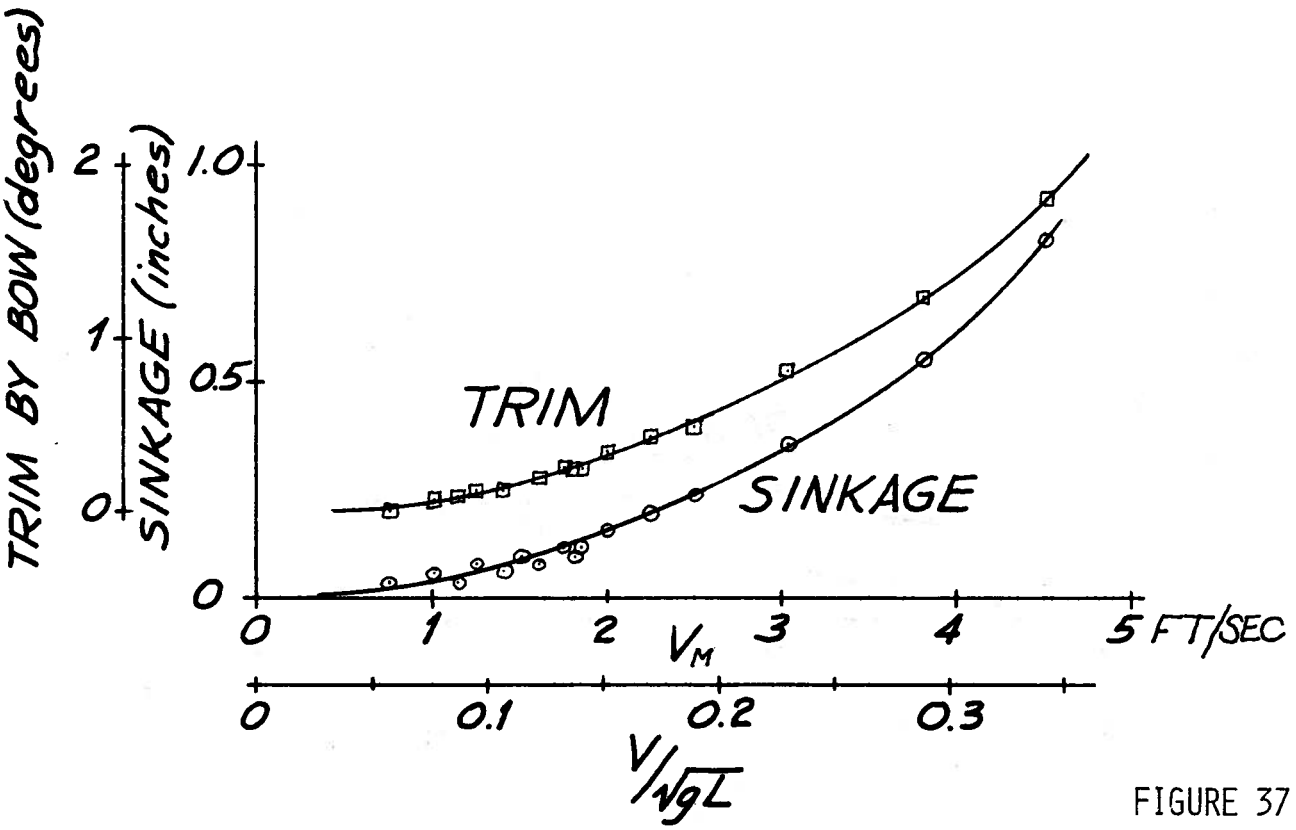

FIGURE 37

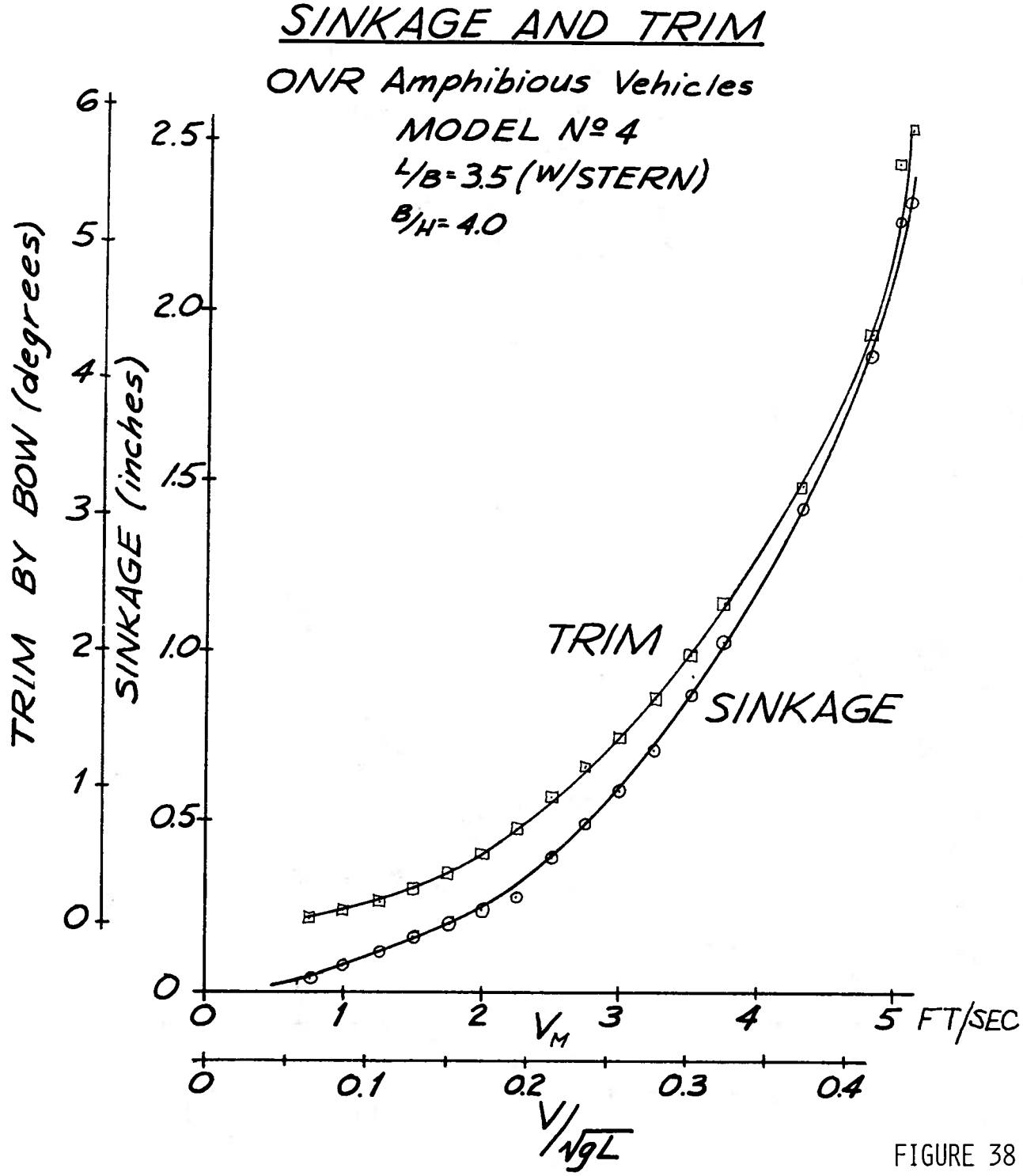
SINKAGE AND TRIM
ONR Amphibious Vehicles
MODEL Nº 4
L/B = 3.5 (W/STERN)
B/H = 4.0
TRIM BY BOW (degrees)
SINKAGE (inches)
TRIM
SINKAGE
0
1
2
3
4
5
6
0.5
1.0
1.5
2.0
2.5
V_M
FT/SEC
0.1
0.2
0.3
0.4
$V/\sqrt{gL}$

FIGURE 38

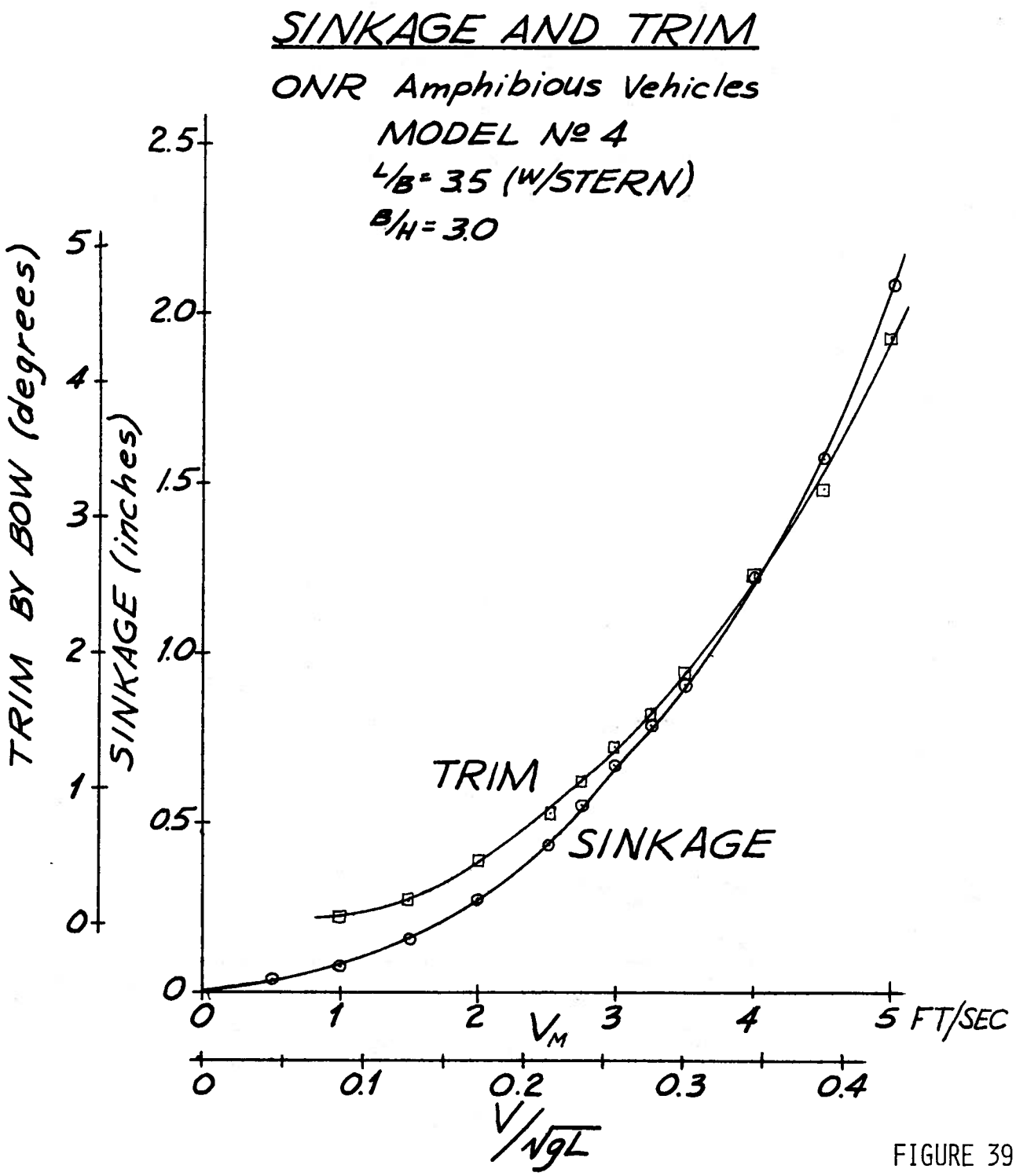
SINKAGE AND TRIM
ONR Amphibious Vehicles
MODEL Nº 4
L/B = 3.5 (W/STERN)
B/H = 3.0
TRIM BY BOW (degrees)
SINKAGE (inches)
TRIM
SINKAGE
0
1
2
3
4
5 FT/SEC
V_M
0
0.1
0.2
0.3
0.4
$V/\sqrt{gL}$

FIGURE 39

SINKAGE AND TRIM

ONR Amphibious Vehicles

MODEL Nº 4

$L/B = 3.5$ (W/STERN)

$B/H = 2.0$

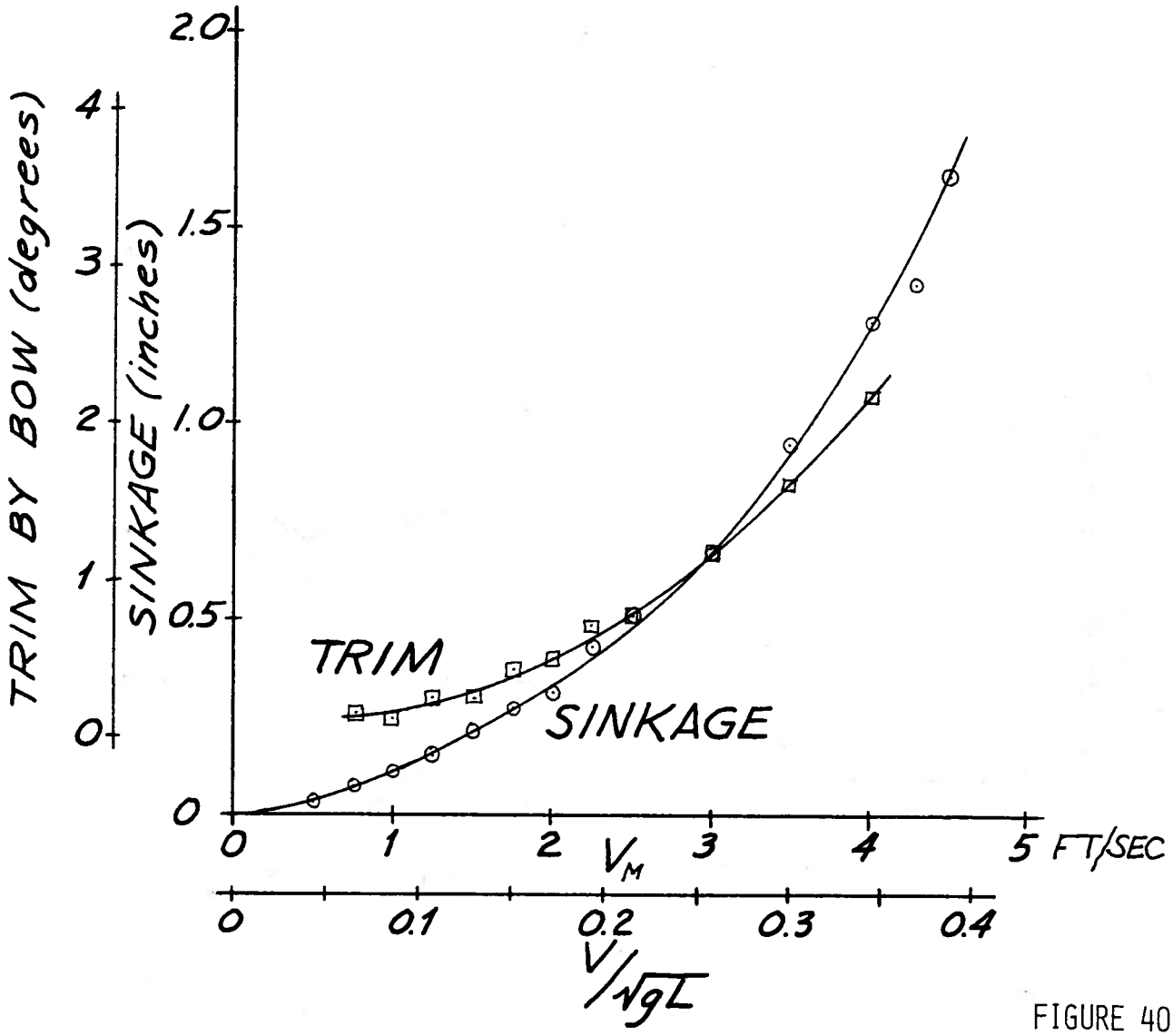

FIGURE 40

SINKAGE AND TRIM

ONR Amphibious Vehicles

MODEL Nº5

$L/B = 3.5$ (W/BOW)

$B/H = 4.0$

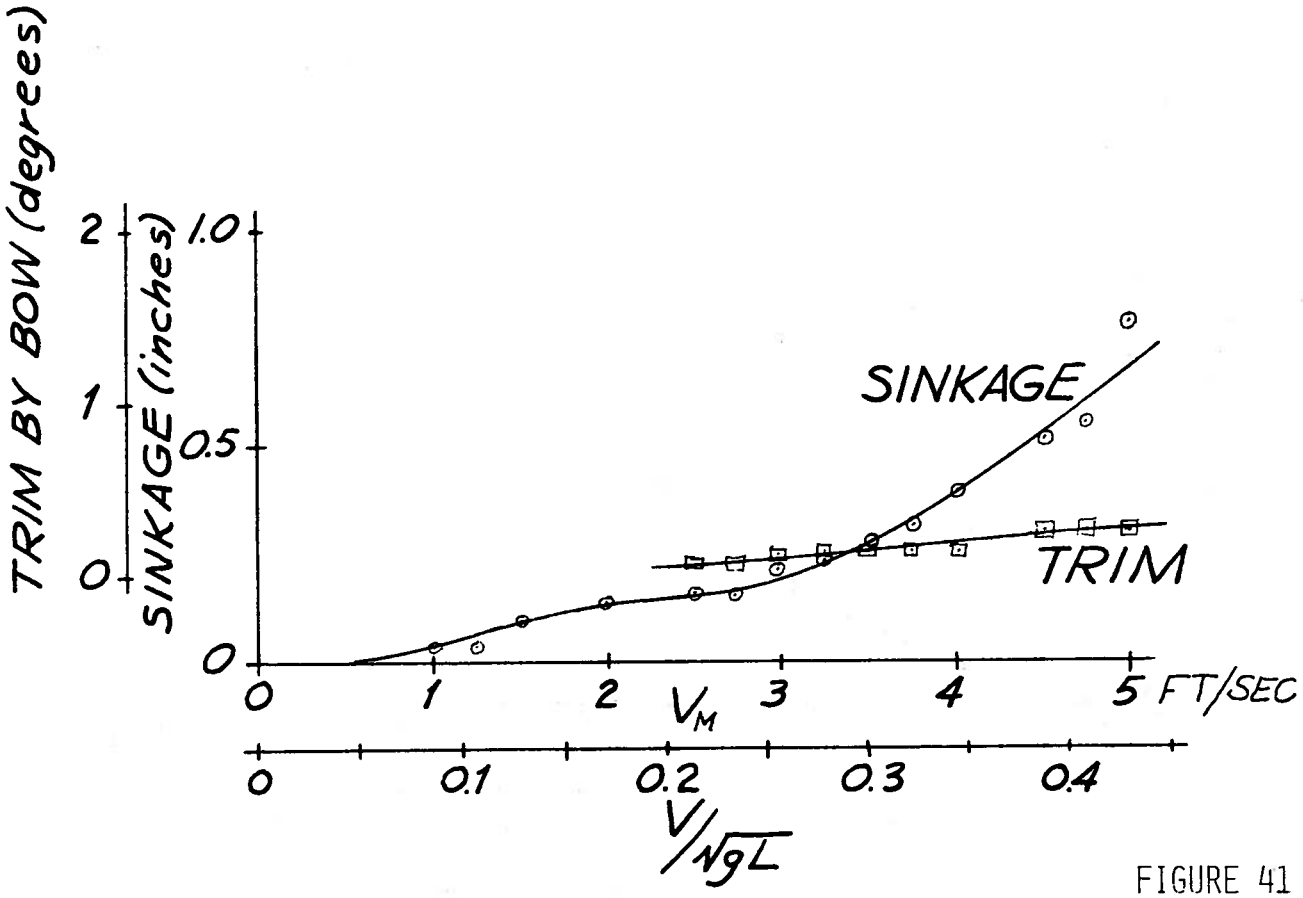

FIGURE 41

SINKAGE AND TRIM

ONR Amphibious Vehicles
MODEL Nº5
$L/B = 3.5$ (W/BOW)
$B/H = 3.0$

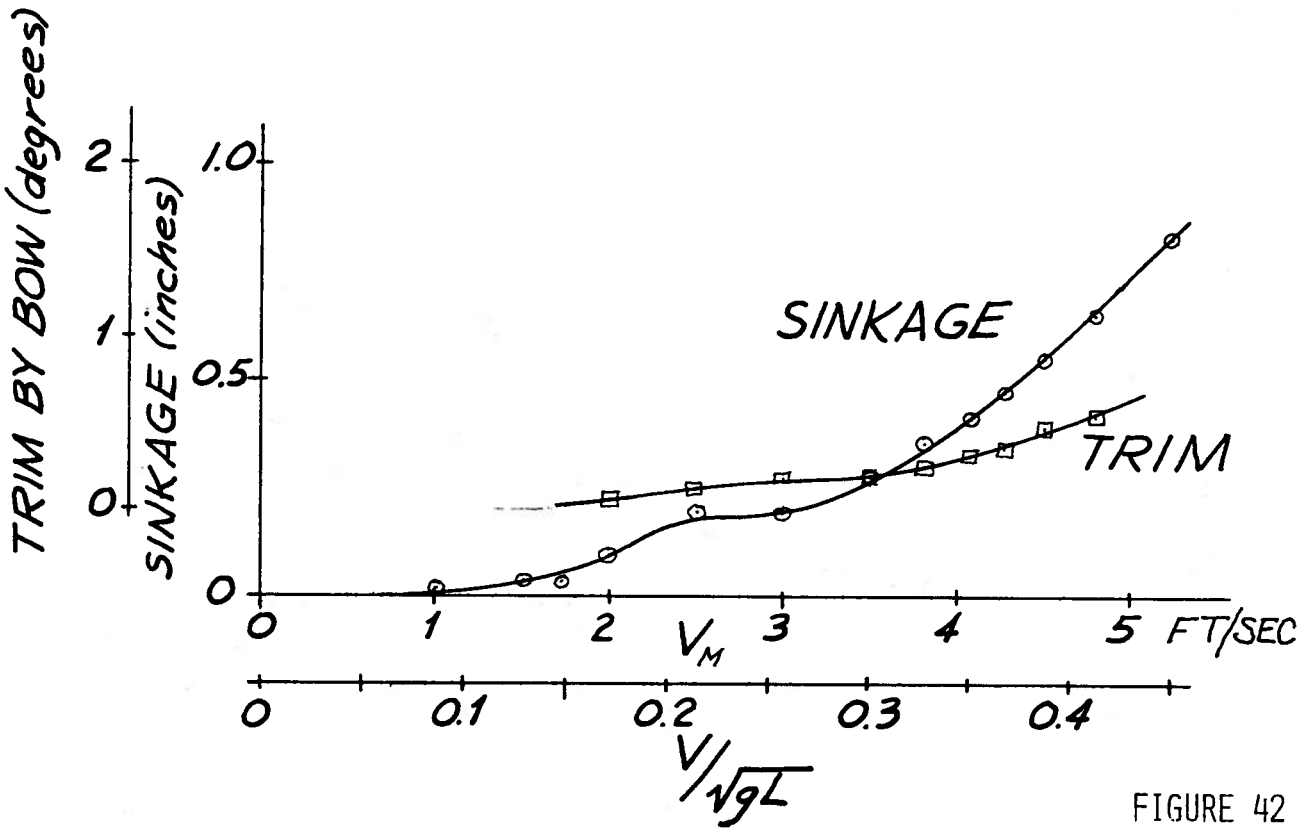

FIGURE 42

SINKAGE AND TRIM

ONR Amphibious Vehicles
MODEL Nº5
$L/B = 3.5$ (W/BOW)
$B/H = 2.0$

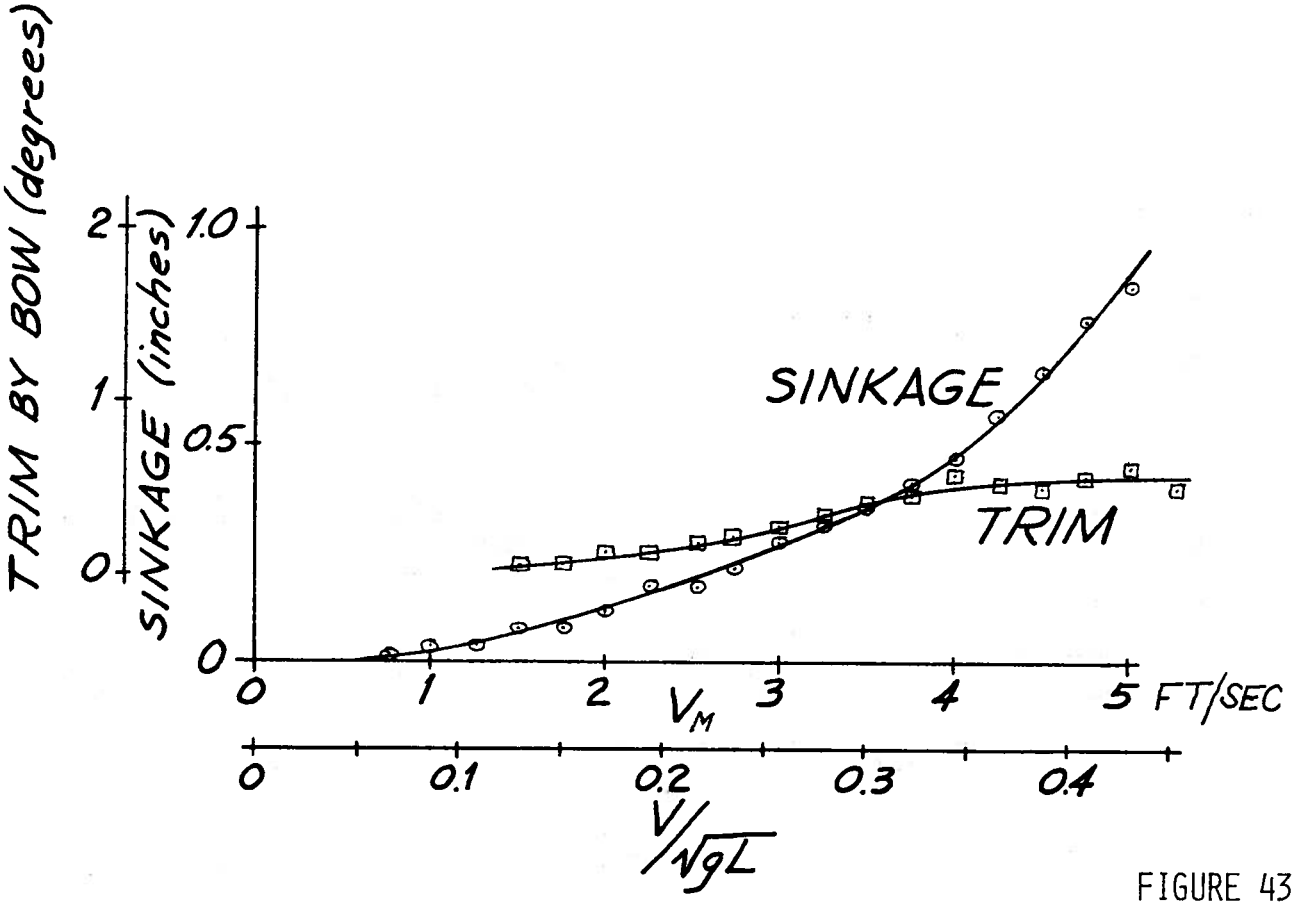

FIGURE 43

SINKAGE AND TRIM

ONR Amphibious Vehicles

MODEL Nº 6

$L/B = 4.5$ (BOW AND STERN)

$B/H = 4.0$

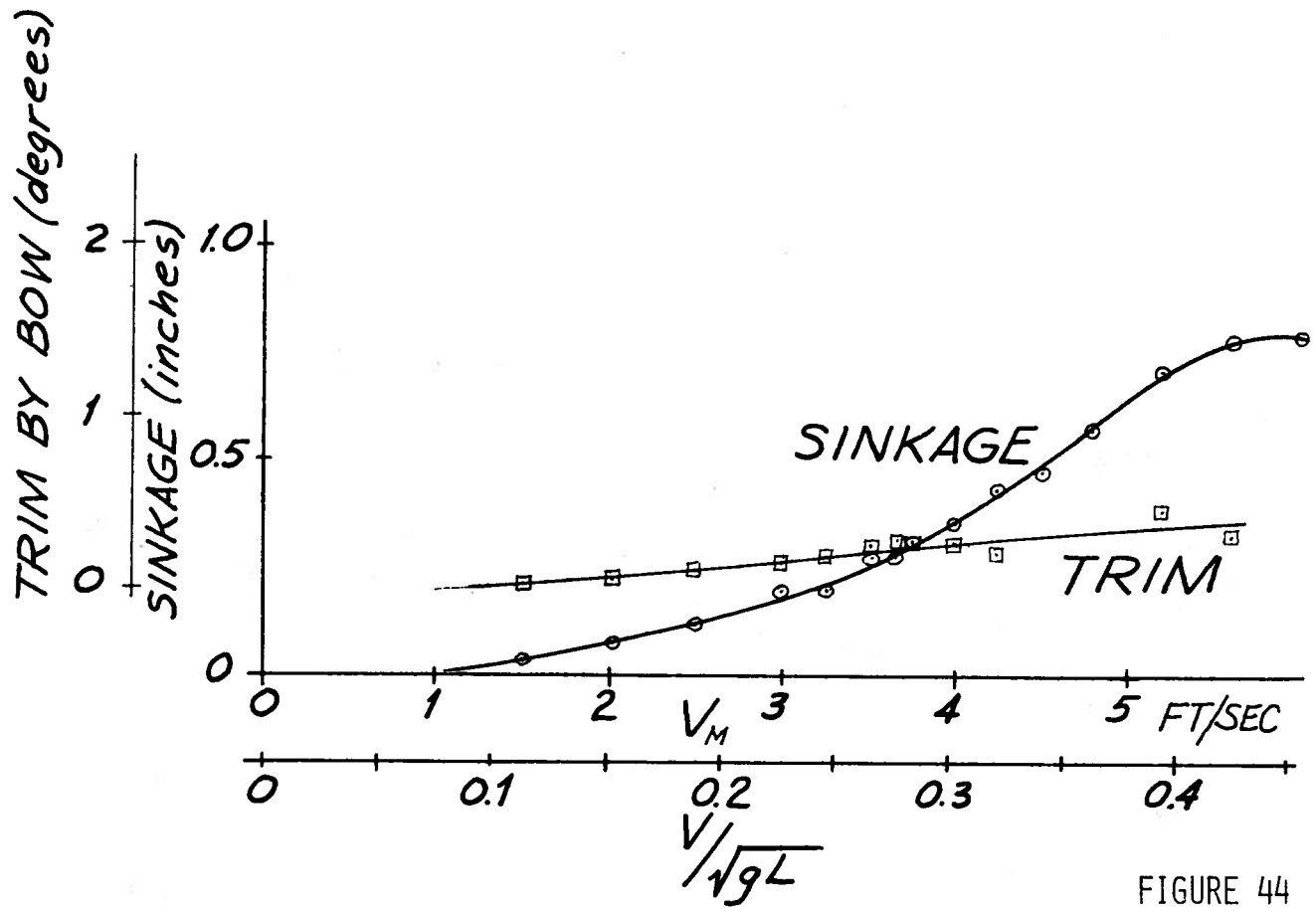

FIGURE 44

SINKAGE AND TRIM

ONR Amphibious Vehicles

MODEL Nº 6

$L/B = 4.5$ (BOW AND STERN)

$B/H = 3.0$

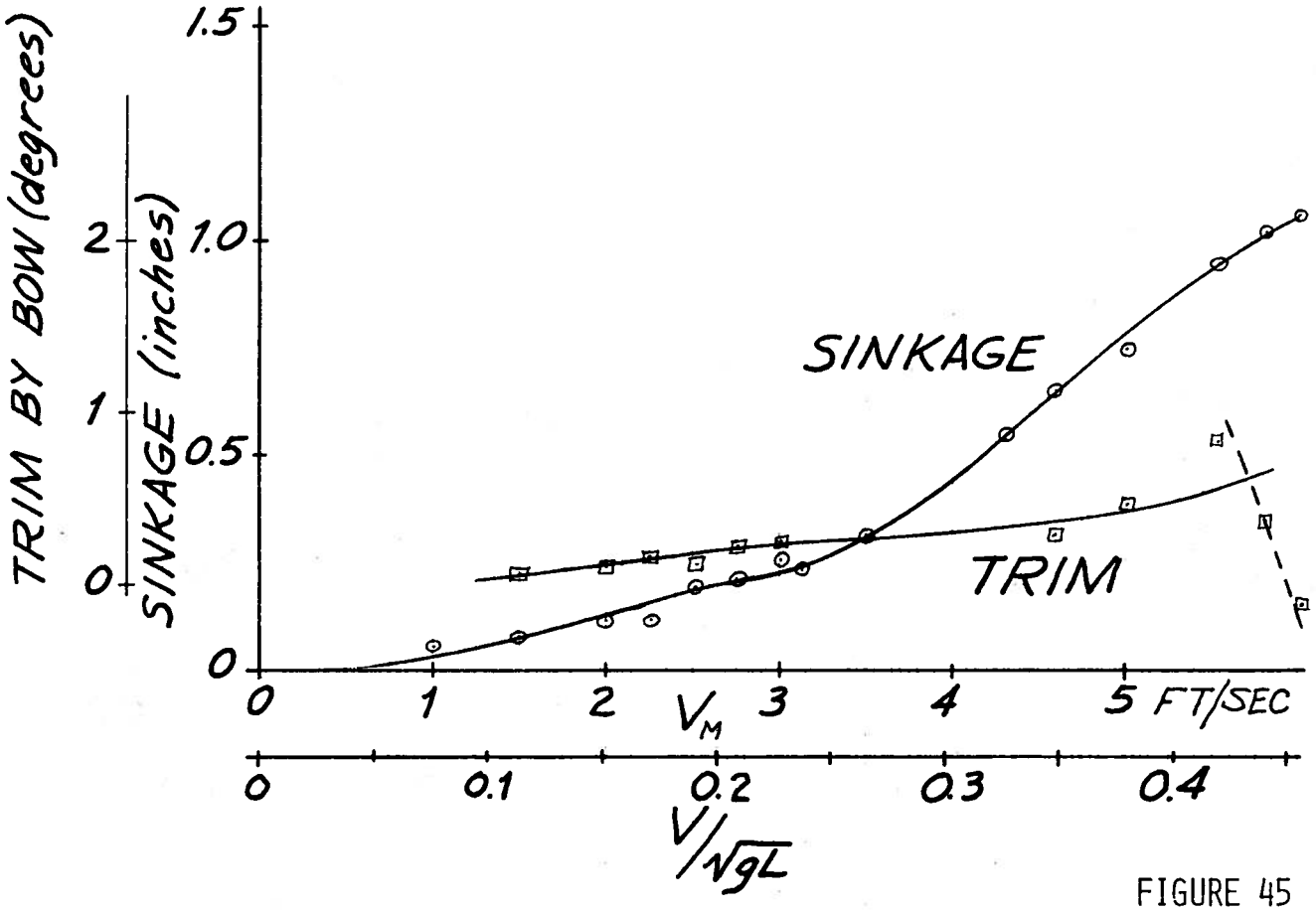

FIGURE 45

SINKAGE AND TRIM

ONR Amphibious Vehicles
MODEL Nº 6
$L/B = 4.5$ (BOW AND STERN)
$B/H = 2.0$

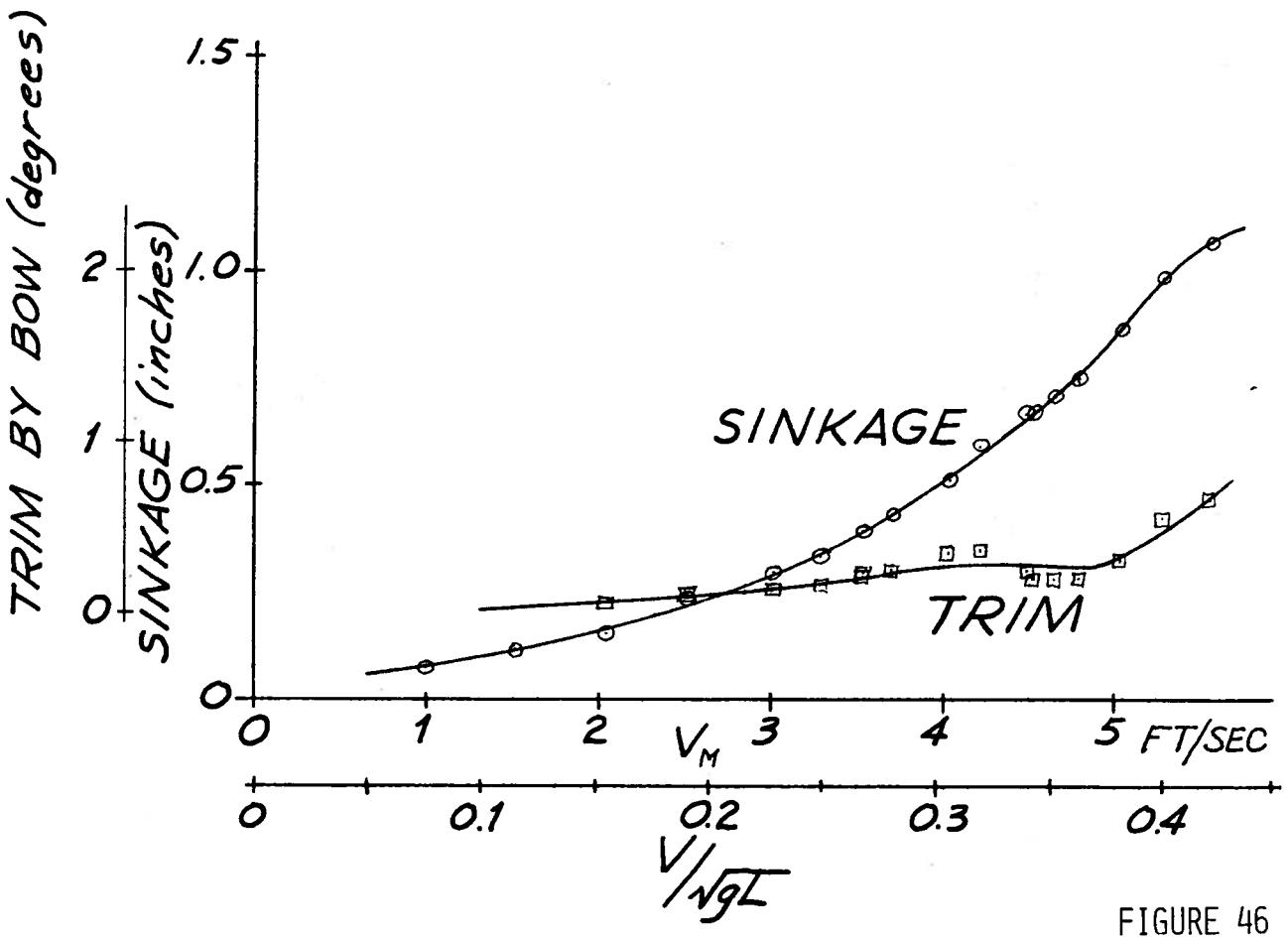

FIGURE 46

SINKAGE AND TRIM

ONR Amphibious Vehicles

MODEL Nº 7

$L/B = 2.5$

$B/H = 3.0$

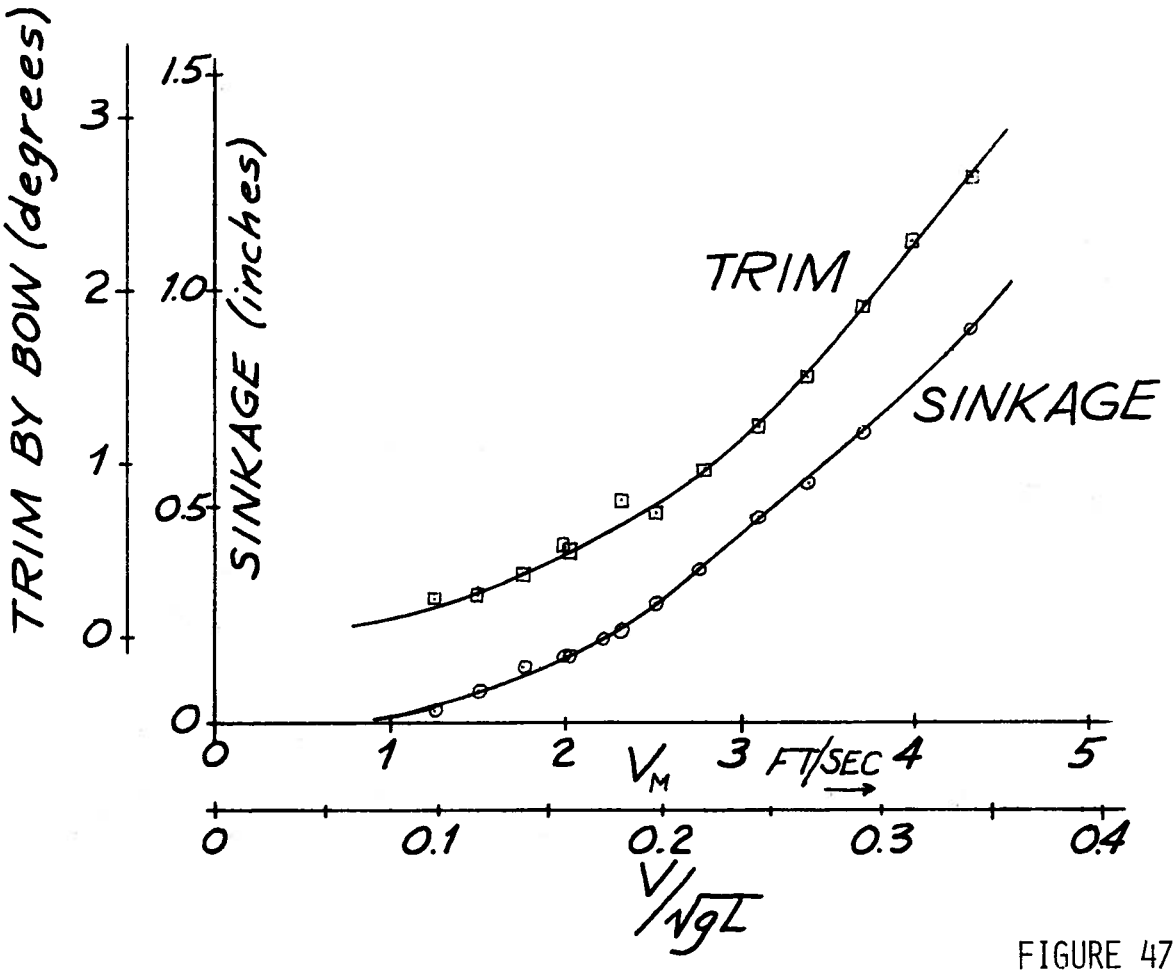

FIGURE 47

SINKAGE AND TRIM

ONR Amphibious Vehicles

MODEL Nº 7

$L/B = 2.5$

$B/H = 2.0$

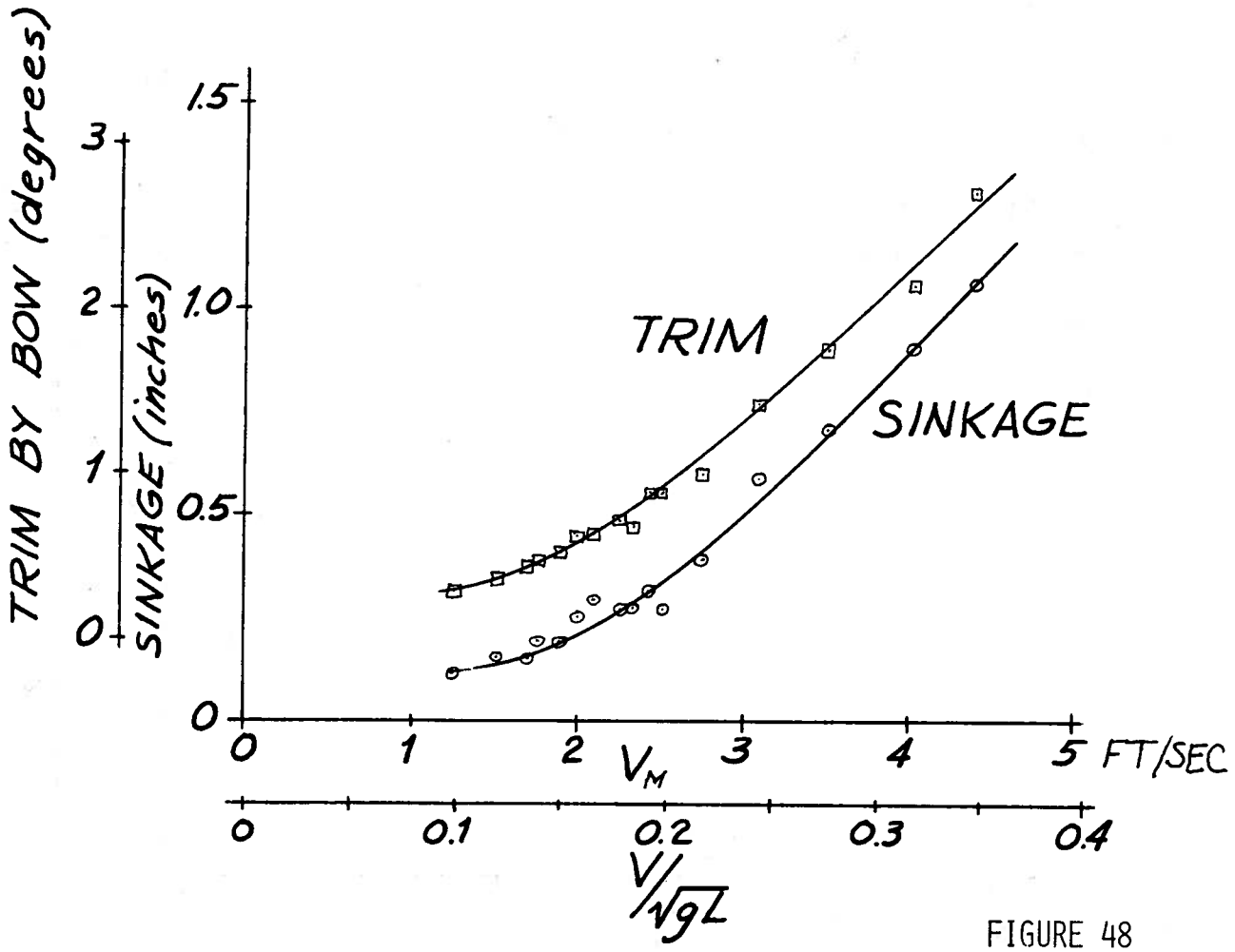

FIGURE 48

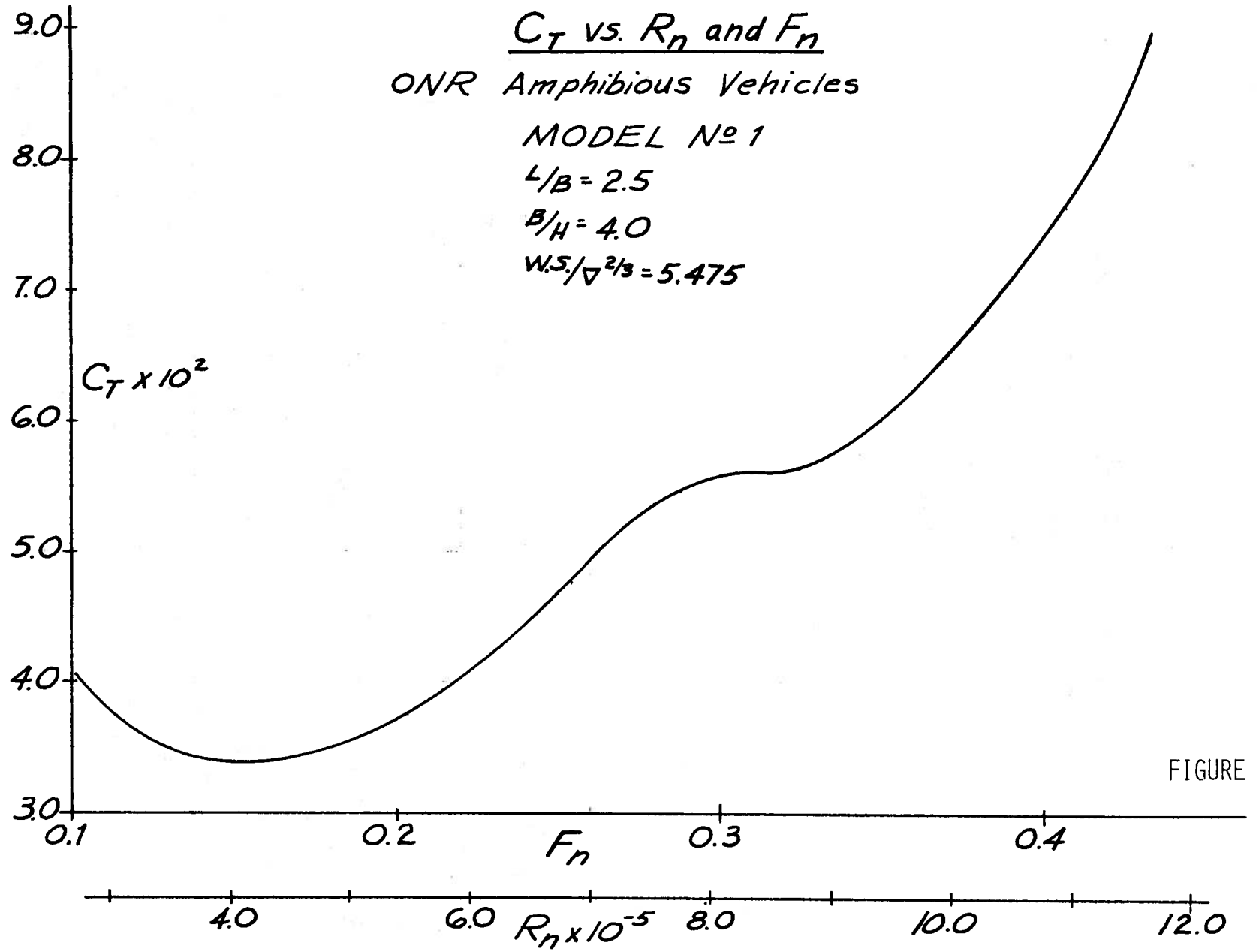
C_T vs. R_n and F_n
ONR Amphibious Vehicles
MODEL Nº 1
$L/B = 2.5$
$B/H = 4.0$
$W.S./\nabla^{2/3} = 5.475$
$C_T \times 10^2$
9.0
8.0
7.0
6.0
5.0
4.0
3.0
0.1
0.2
0.3
0.4
F_n
4.0
6.0
8.0
10.0
12.0
$R_n \times 10^{-5}$

FIGURE 49

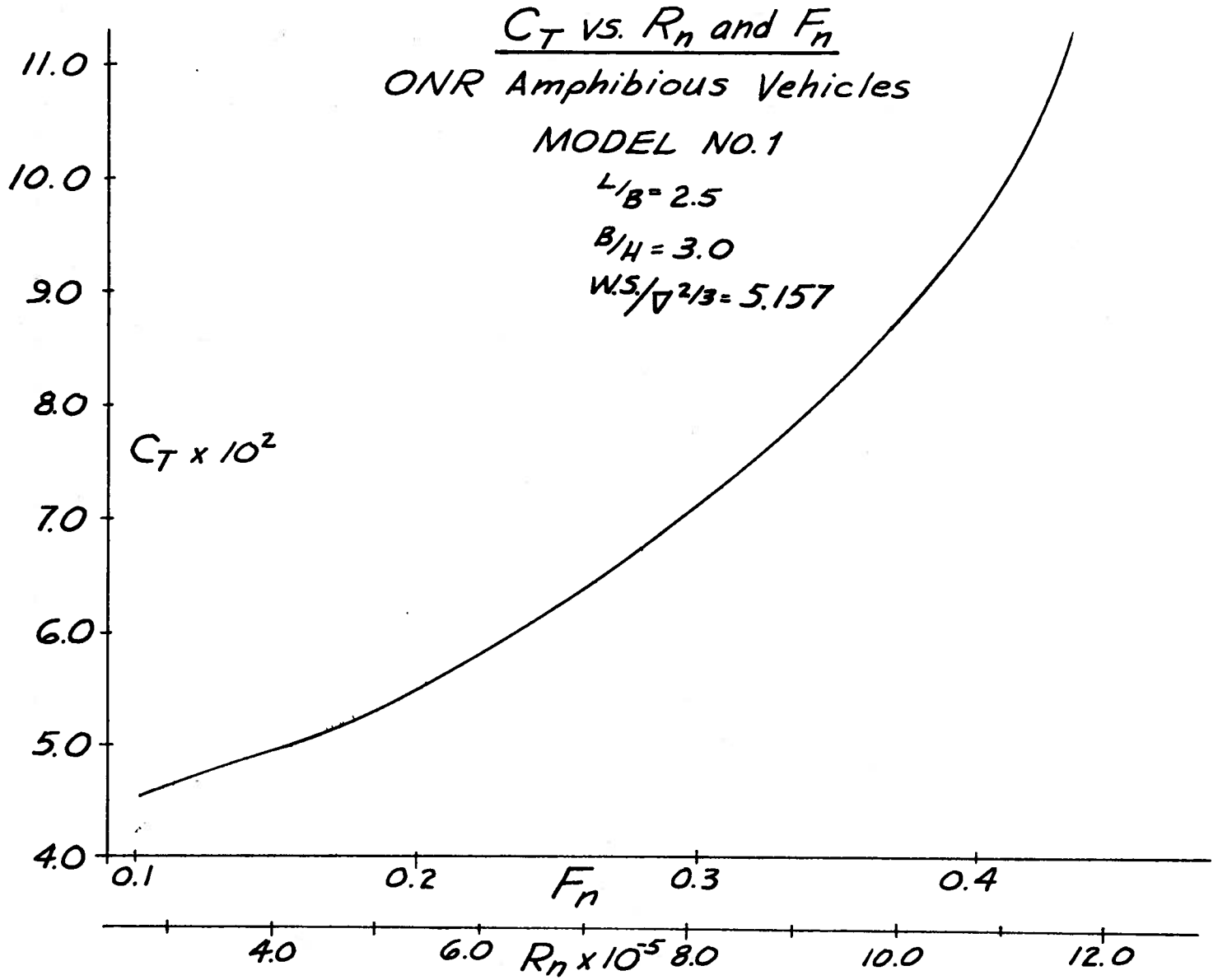
C_T vs. R_n and F_n
ONR Amphibious Vehicles
MODEL NO. 1
$L/B = 2.5$
$B/H = 3.0$
$W.S./\nabla^{2/3} = 5.157$
$C_T \times 10^2$
11.0
10.0
9.0
8.0
7.0
6.0
5.0
4.0
0.1
0.2
F_n
0.3
0.4
4.0
6.0
$R_n \times 10^{-5}$
8.0
10.0
12.0

FIGURE 50

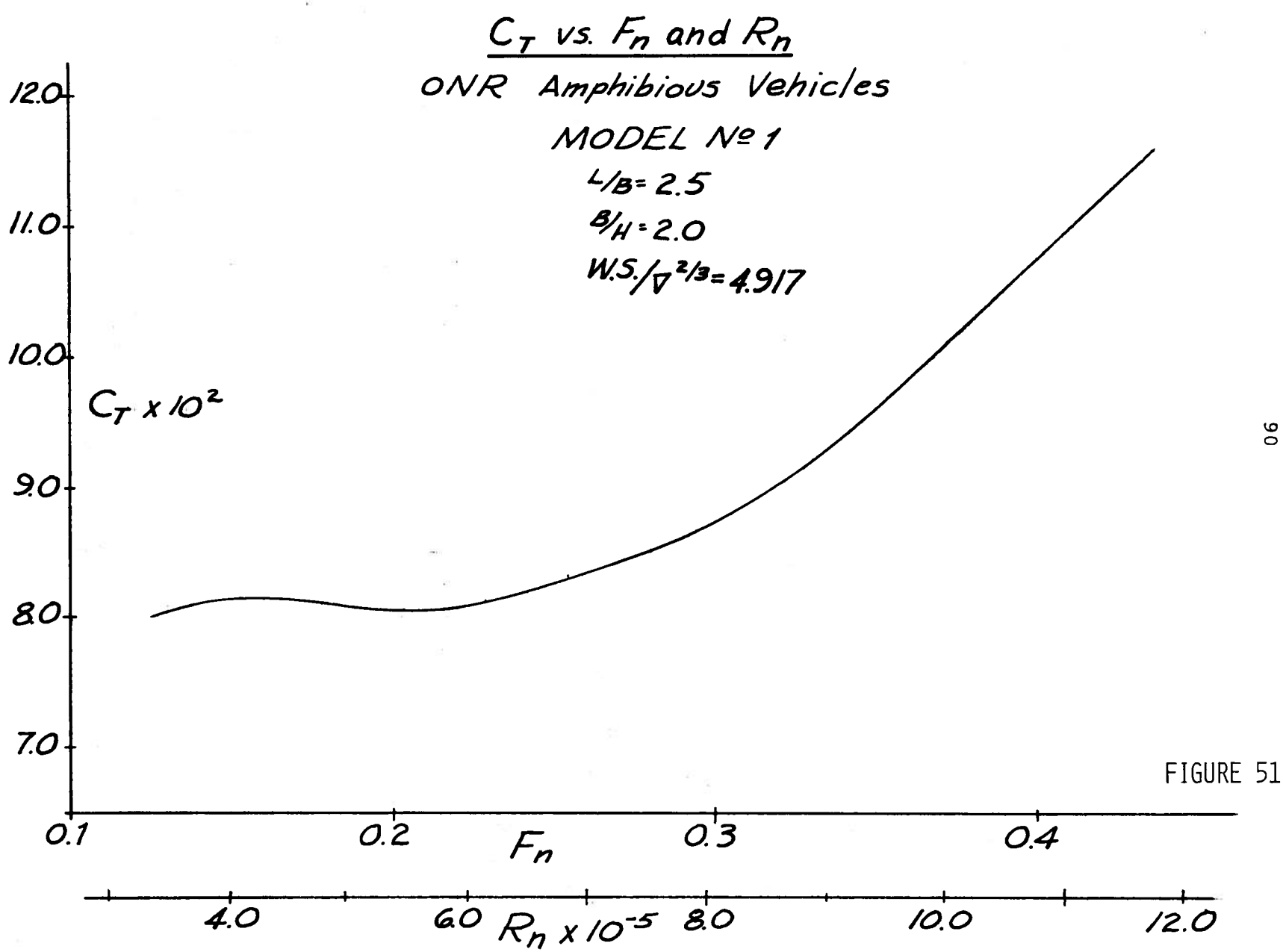
C_T vs. F_n and R_n
ONR Amphibious Vehicles
MODEL Nº 1
L/B = 2.5
B/H = 2.0
W.S./$\nabla^{2/3}$ = 4.917
12.0
11.0
10.0
9.0
8.0
7.0
$C_T \times 10^2$
0.1
0.2
0.3
0.4
F_n
4.0
6.0
8.0
10.0
12.0
$R_n \times 10^{-5}$

FIGURE 51

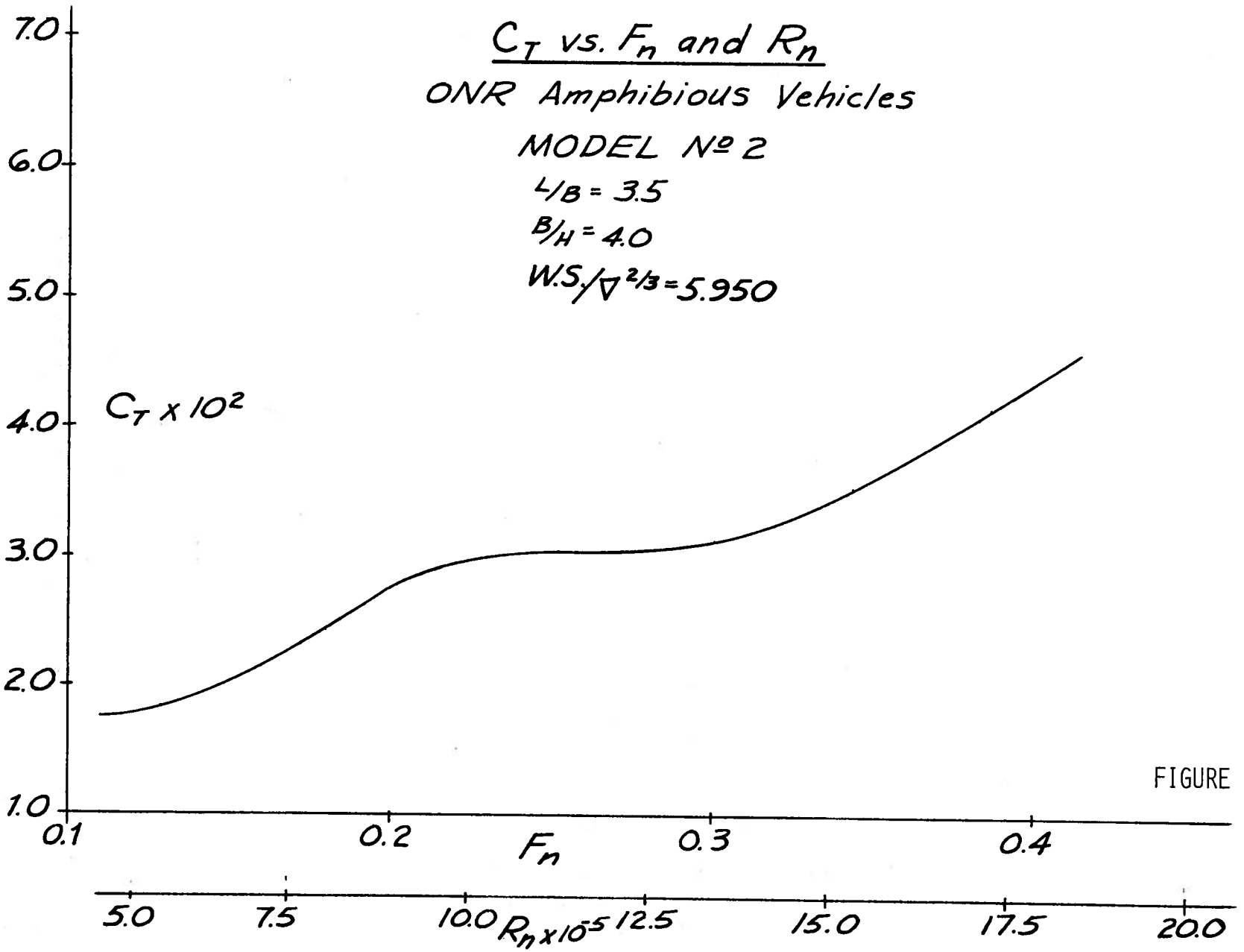
C_T vs. F_n and R_n
ONR Amphibious Vehicles
MODEL Nº 2
L/B = 3.5
B/H = 4.0
W.S./$\nabla^{2/3}$ = 5.950
$C_T \times 10^2$
7.0
6.0
5.0
4.0
3.0
2.0
1.0
0.1
0.2
0.3
0.4
F_n
5.0
7.5
10.0
12.5
15.0
17.5
20.0
$R_n \times 10^5$

FIGURE 52

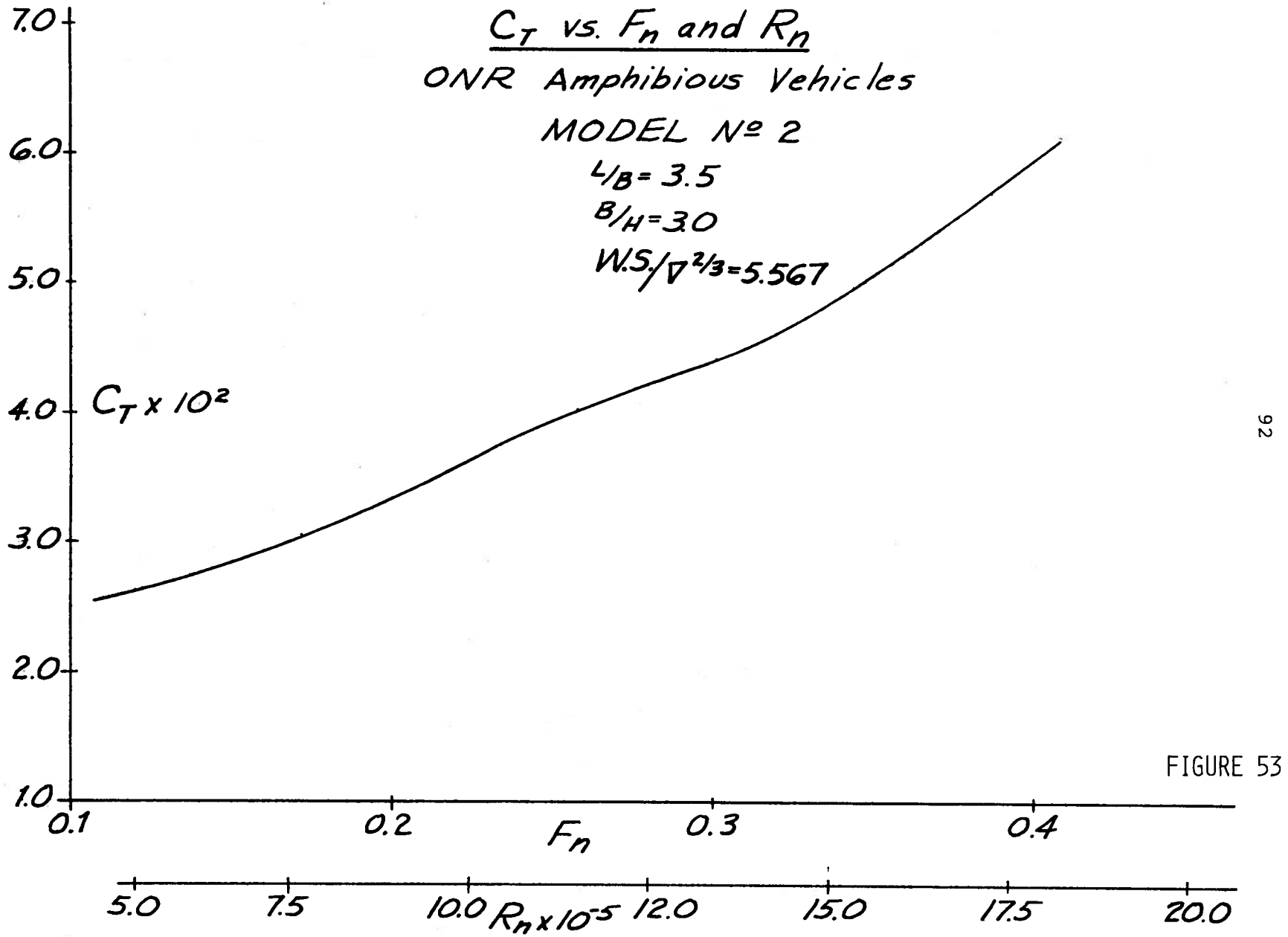
C_T vs. F_n and R_n
ONR Amphibious Vehicles
MODEL Nº 2
$L/B = 3.5$
$B/H = 3.0$
$W.S./\nabla^{2/3} = 5.567$
$C_T \times 10^2$
7.0
6.0
5.0
4.0
3.0
2.0
1.0
0.1
0.2
0.3
0.4
F_n
5.0
7.5
10.0
12.0
15.0
17.5
20.0
$R_n \times 10^{-5}$

FIGURE 53

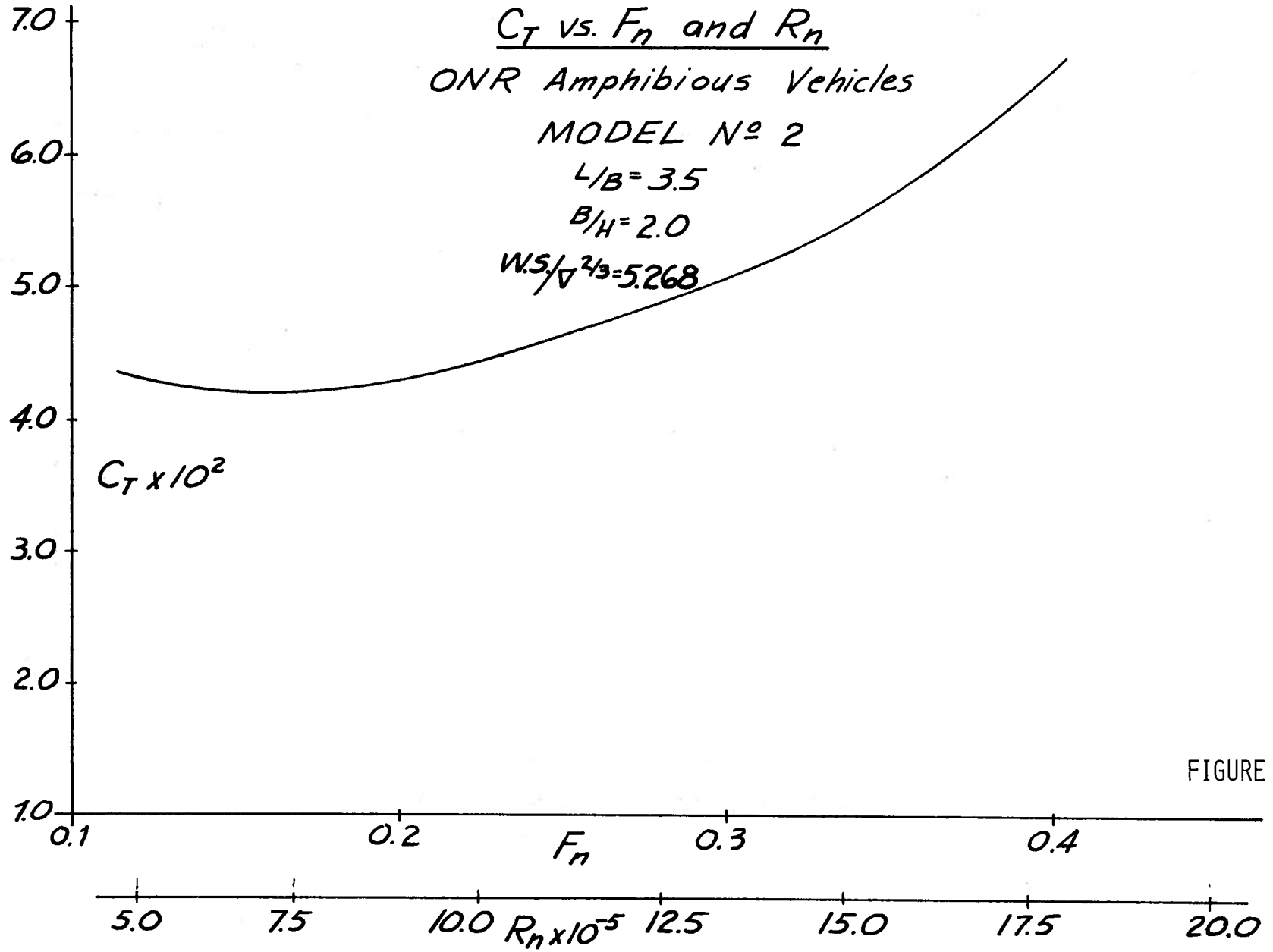
C_T vs. F_n and R_n
ONR Amphibious Vehicles
MODEL Nº 2
L/B = 3.5
B/H = 2.0
W.S./∇^2/3 = 5.268
7.0
6.0
5.0
4.0
3.0
2.0
1.0
$C_T \times 10^2$
0.1
0.2
0.3
0.4
F_n
5.0
7.5
10.0
12.5
15.0
17.5
20.0
$R_n \times 10^{-5}$

FIGURE 54

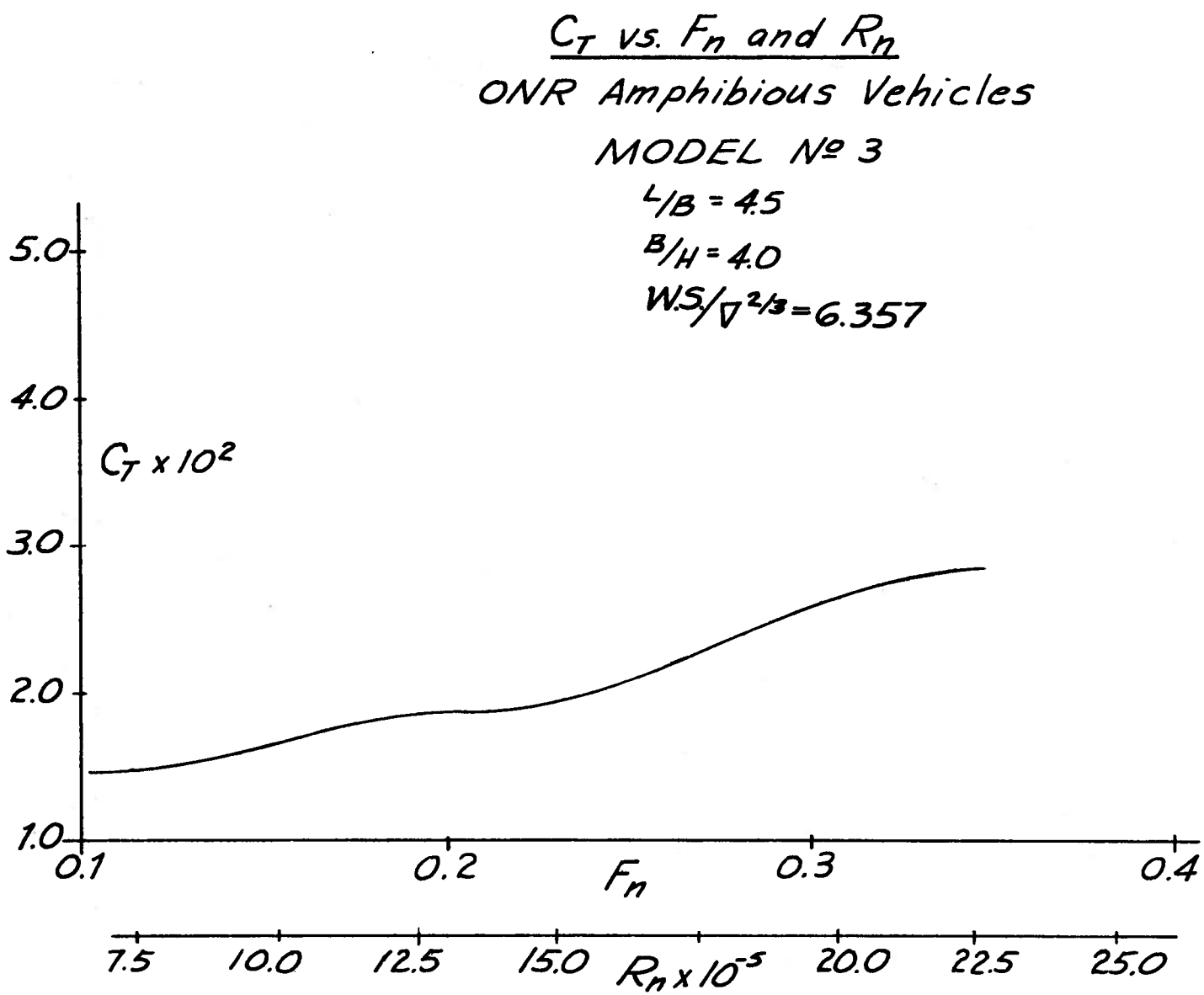
C_T vs. F_n and R_n
ONR Amphibious Vehicles
MODEL Nº 3
L/B = 4.5
B/H = 4.0
W.S./$\nabla^{2/3}$ = 6.357
5.0
4.0
3.0
2.0
1.0
$C_T \times 10^2$
0.1
0.2
0.3
0.4
F_n
7.5
10.0
12.5
15.0
20.0
22.5
25.0
$R_n \times 10^{-5}$

FIGURE 55

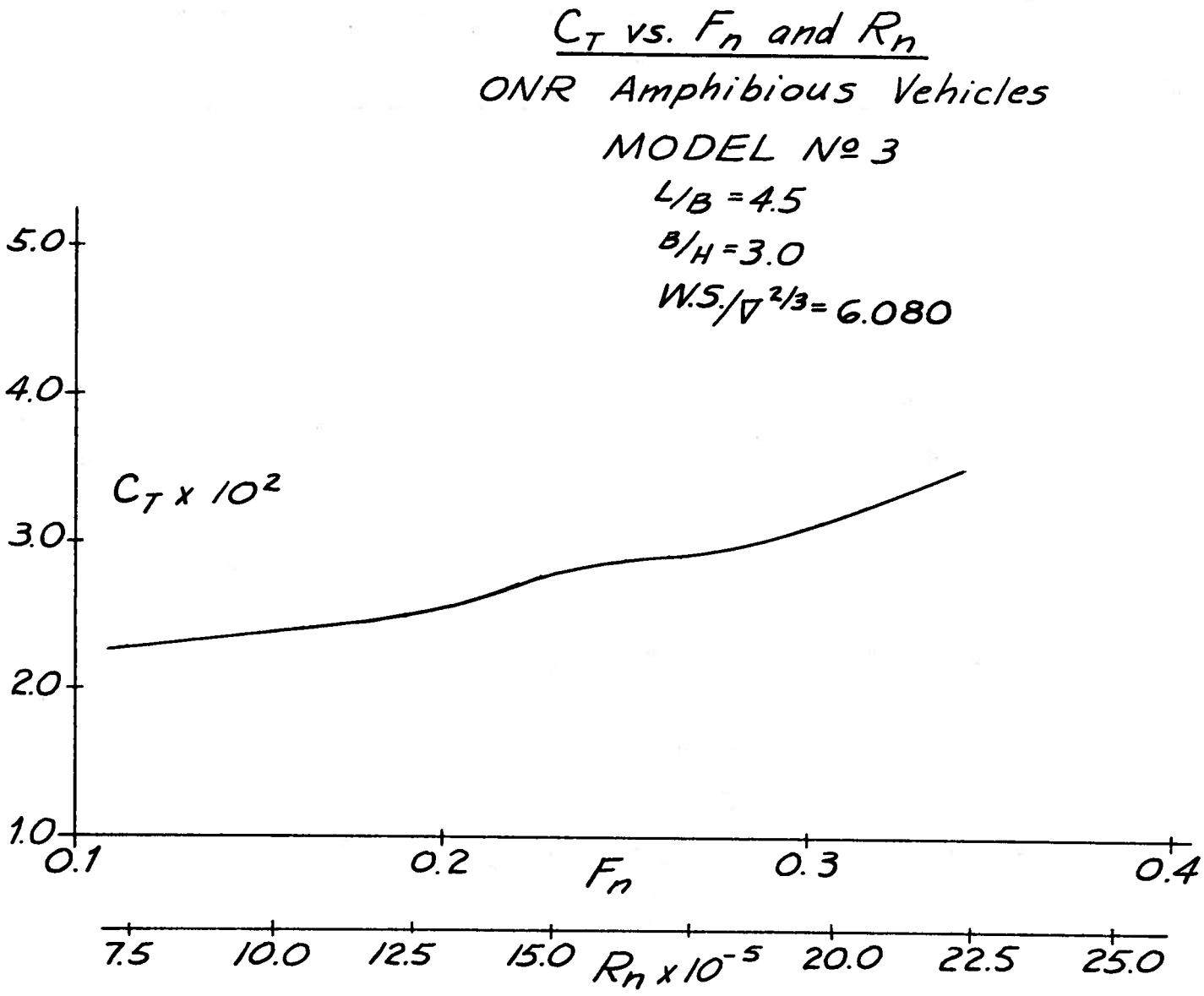
C_T vs. F_n and R_n
ONR Amphibious Vehicles
MODEL Nº 3
$L/B = 4.5$
$B/H = 3.0$
$W.S./\nabla^{2/3} = 6.080$
5.0
4.0
3.0
2.0
1.0
$C_T \times 10^2$
0.1
0.2
0.3
0.4
F_n
7.5
10.0
12.5
15.0
20.0
22.5
25.0
$R_n \times 10^{-5}$

FIGURE 56

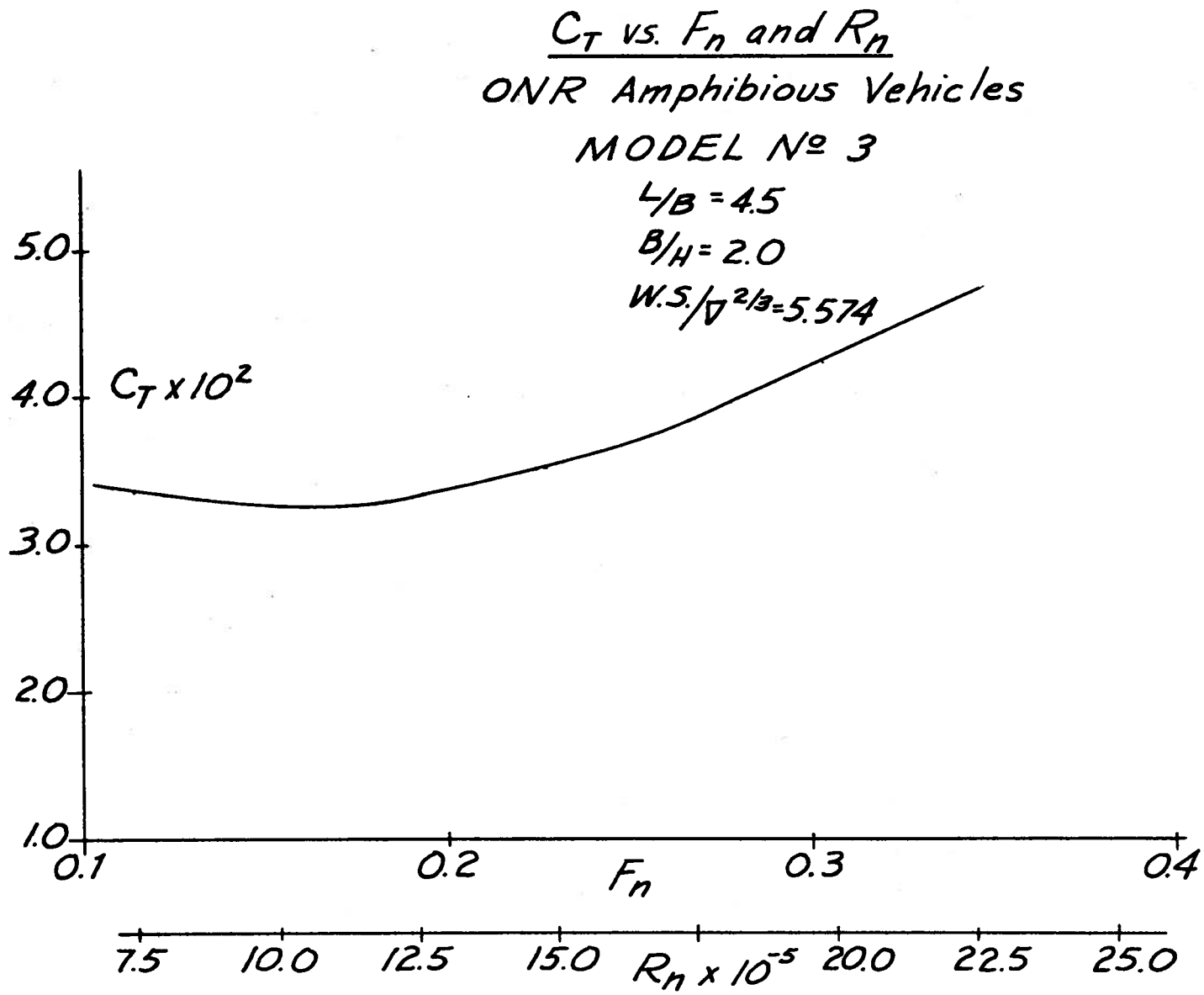
C_T vs. F_n and R_n
ONR Amphibious Vehicles
MODEL Nº 3
L/B = 4.5
B/H = 2.0
W.S./∇^2/3 = 5.574
5.0
4.0
3.0
2.0
1.0
$C_T \times 10^2$
0.1
0.2
0.3
0.4
F_n
7.5
10.0
12.5
15.0
$R_n \times 10^{-5}$
20.0
22.5
25.0

FIGURE 57

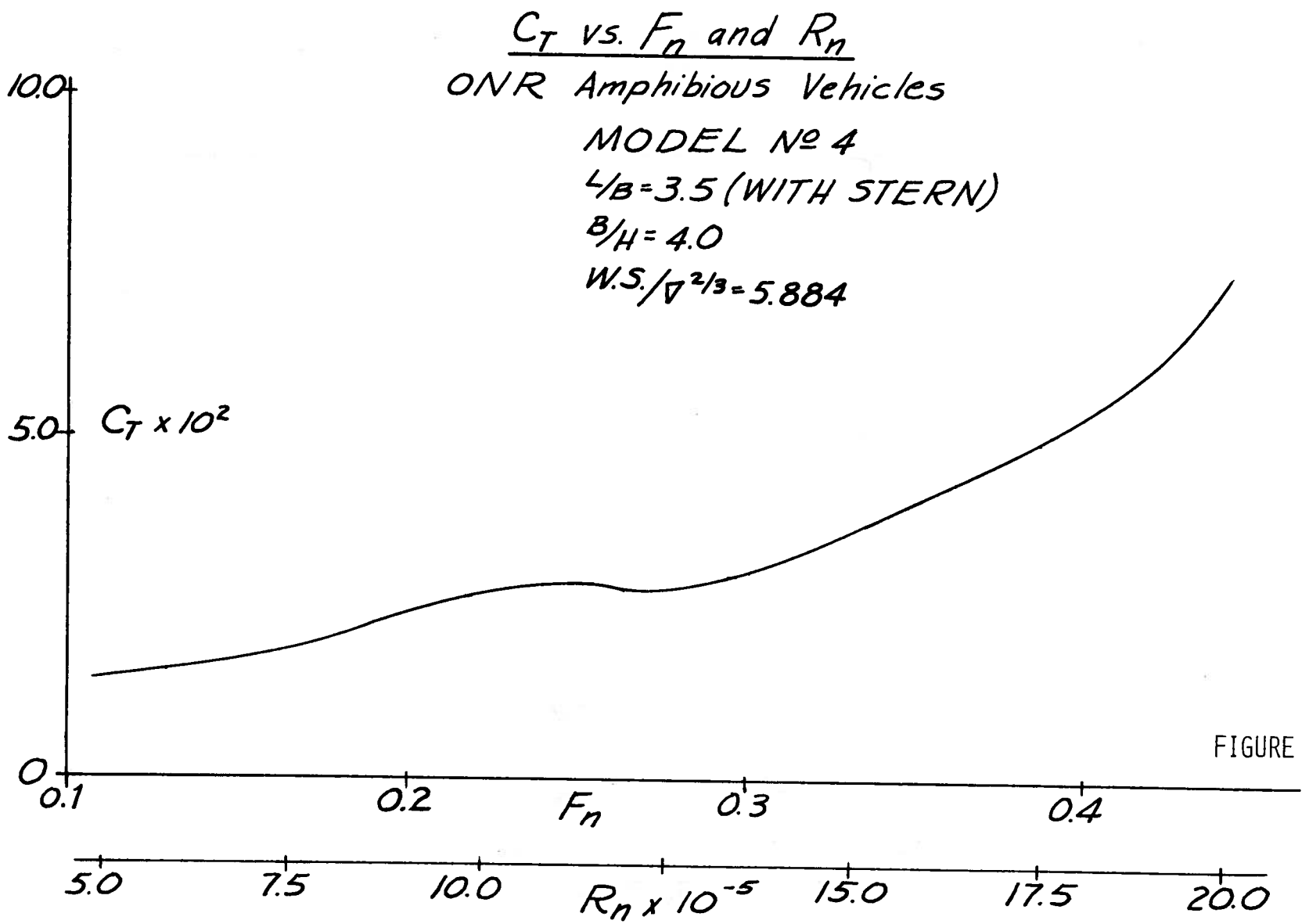
C_T vs. F_n and R_n
ONR Amphibious Vehicles
MODEL Nº 4
$L/B = 3.5$ (WITH STERN)
$B/H = 4.0$
$W.S./\nabla^{2/3} = 5.884$
10.0
5.0
0
$C_T \times 10^2$
0.1
0.2
0.3
0.4
F_n
5.0
7.5
10.0
15.0
17.5
20.0
$R_n \times 10^{-5}$

FIGURE 58

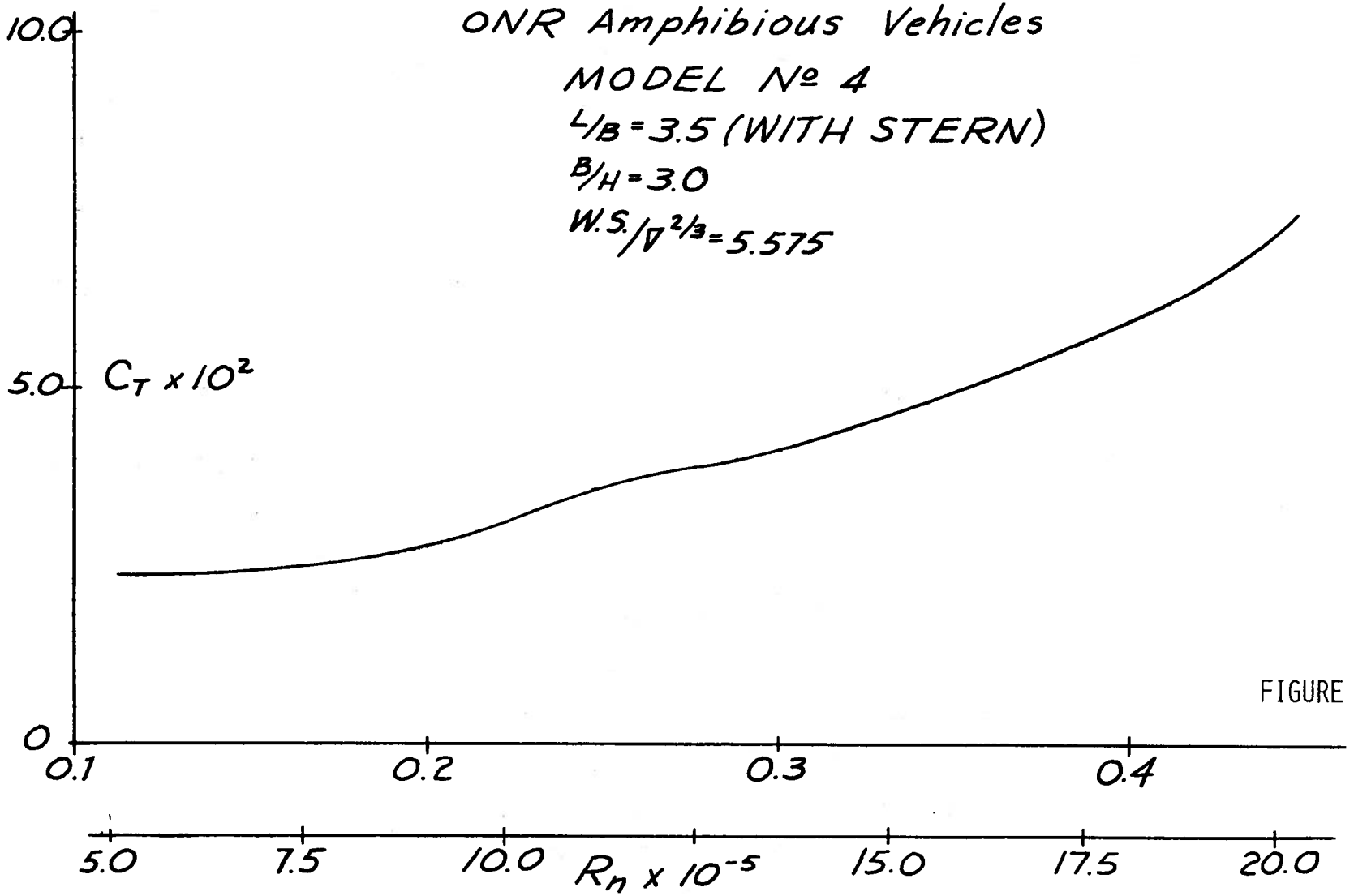
C_T vs. F_n and R_n
ONR Amphibious Vehicles
MODEL Nº 4
L/B = 3.5 (WITH STERN)
B/H = 3.0
W.S./$\nabla^{2/3}$ = 5.575
10.0
5.0
$C_T \times 10^2$
0
0.1
0.2
0.3
0.4
5.0
7.5
10.0
$R_n \times 10^{-5}$
15.0
17.5
20.0

FIGURE 59

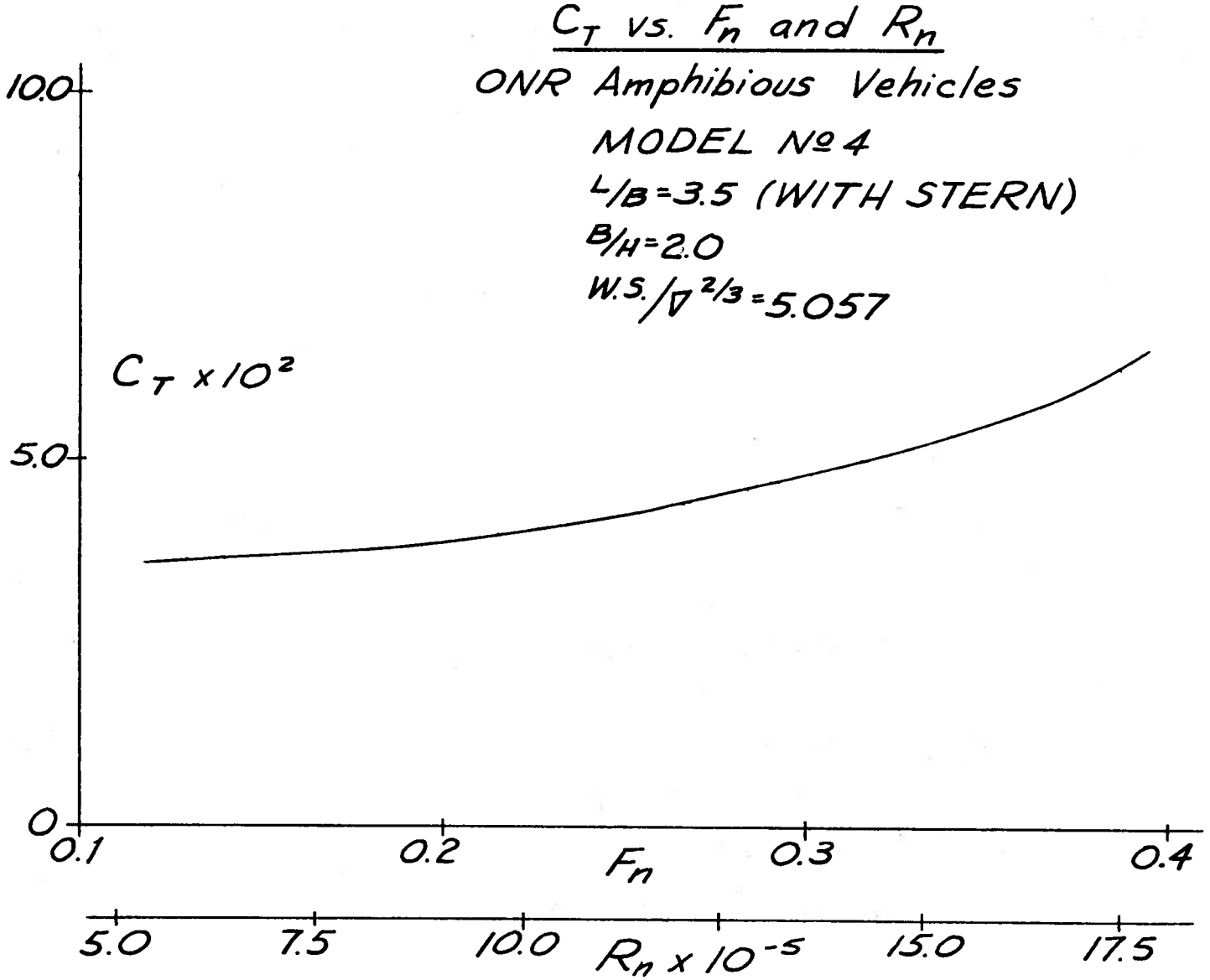
C_T vs. F_n and R_n
ONR Amphibious Vehicles
MODEL Nº 4
$L/B = 3.5$ (WITH STERN)
$B/H = 2.0$
$W.S./\nabla^{2/3} = 5.057$
$C_T \times 10^2$
10.0
5.0
0
0.1
0.2
0.3
0.4
F_n
5.0
7.5
10.0
15.0
17.5
$R_n \times 10^{-5}$

FIGURE 60

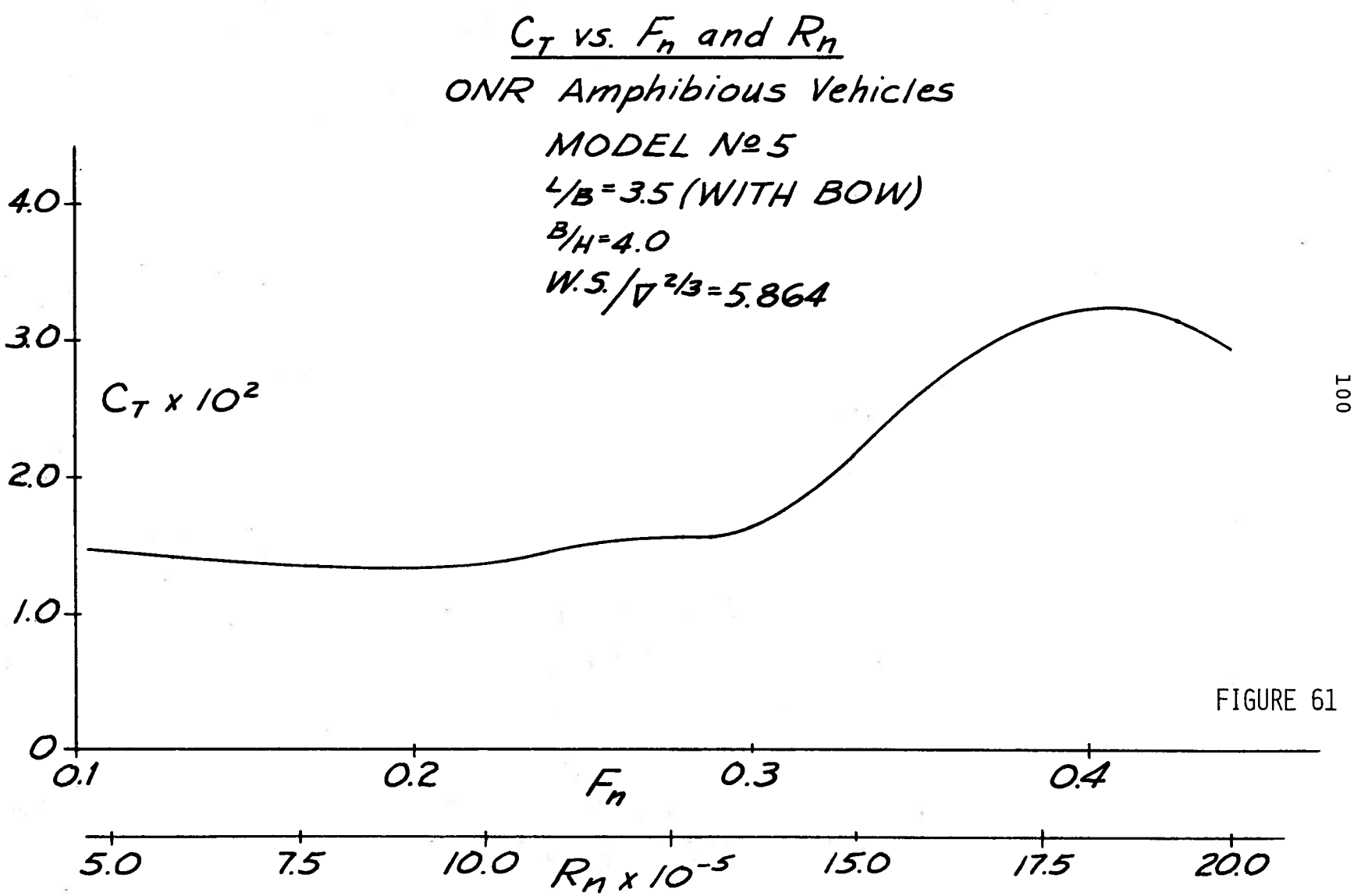
C_T vs. F_n and R_n
ONR Amphibious Vehicles
MODEL №5
L/B=3.5 (WITH BOW)
B/H=4.0
W.S./$\nabla^{2/3}$=5.864
4.0
3.0
2.0
1.0
0
$C_T \times 10^2$
0.1
0.2
0.3
0.4
F_n
5.0
7.5
10.0
15.0
17.5
20.0
$R_n \times 10^{-5}$

FIGURE 61

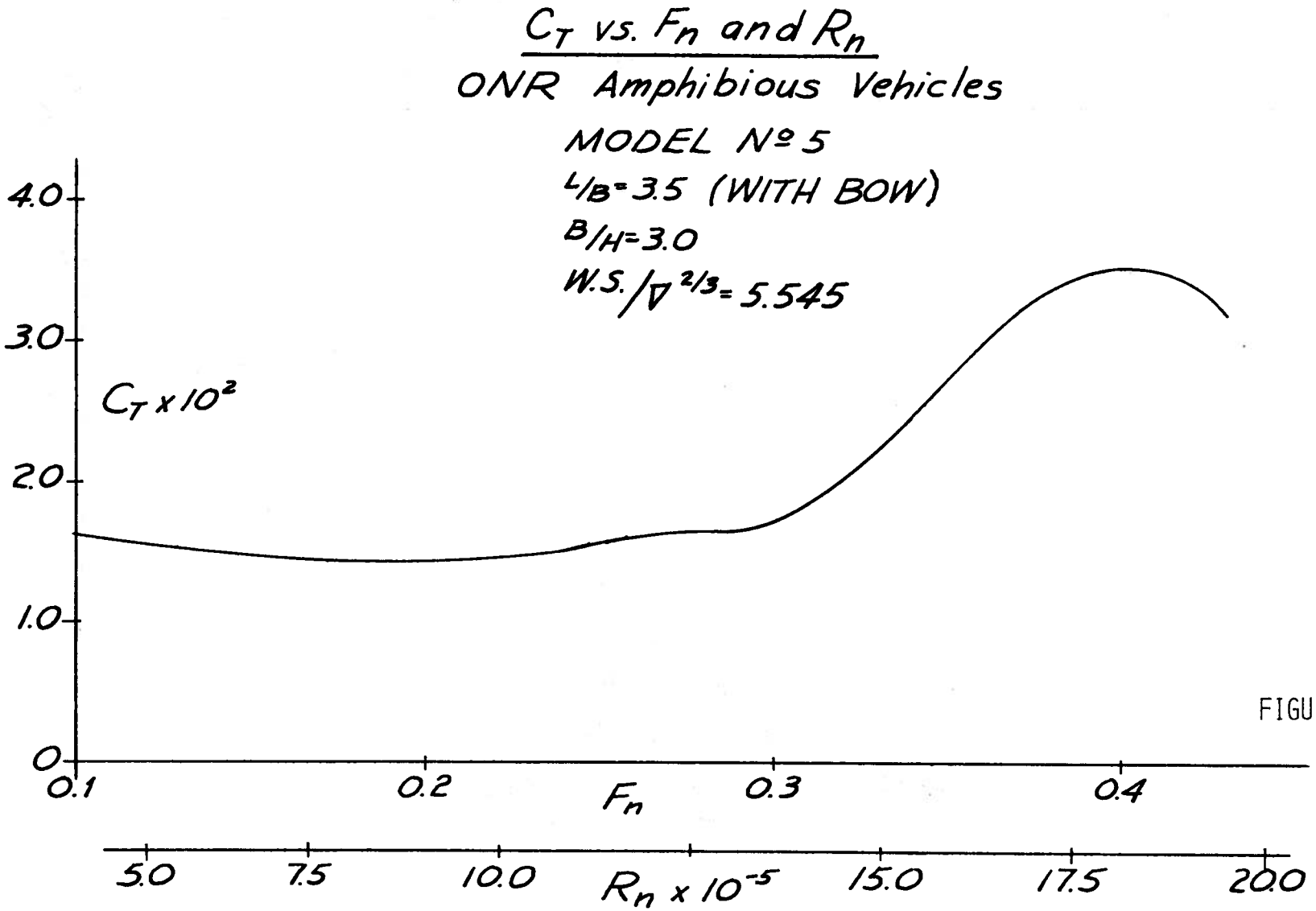
C_T vs. F_n and R_n
ONR Amphibious Vehicles
MODEL Nº 5
$L/B = 3.5$ (WITH BOW)
$B/H = 3.0$
$W.S./\nabla^{2/3} = 5.545$
4.0
3.0
2.0
1.0
0
$C_T \times 10^2$
0.1
0.2
0.3
0.4
F_n
5.0
7.5
10.0
15.0
17.5
20.0
$R_n \times 10^{-5}$

FIGURE 62

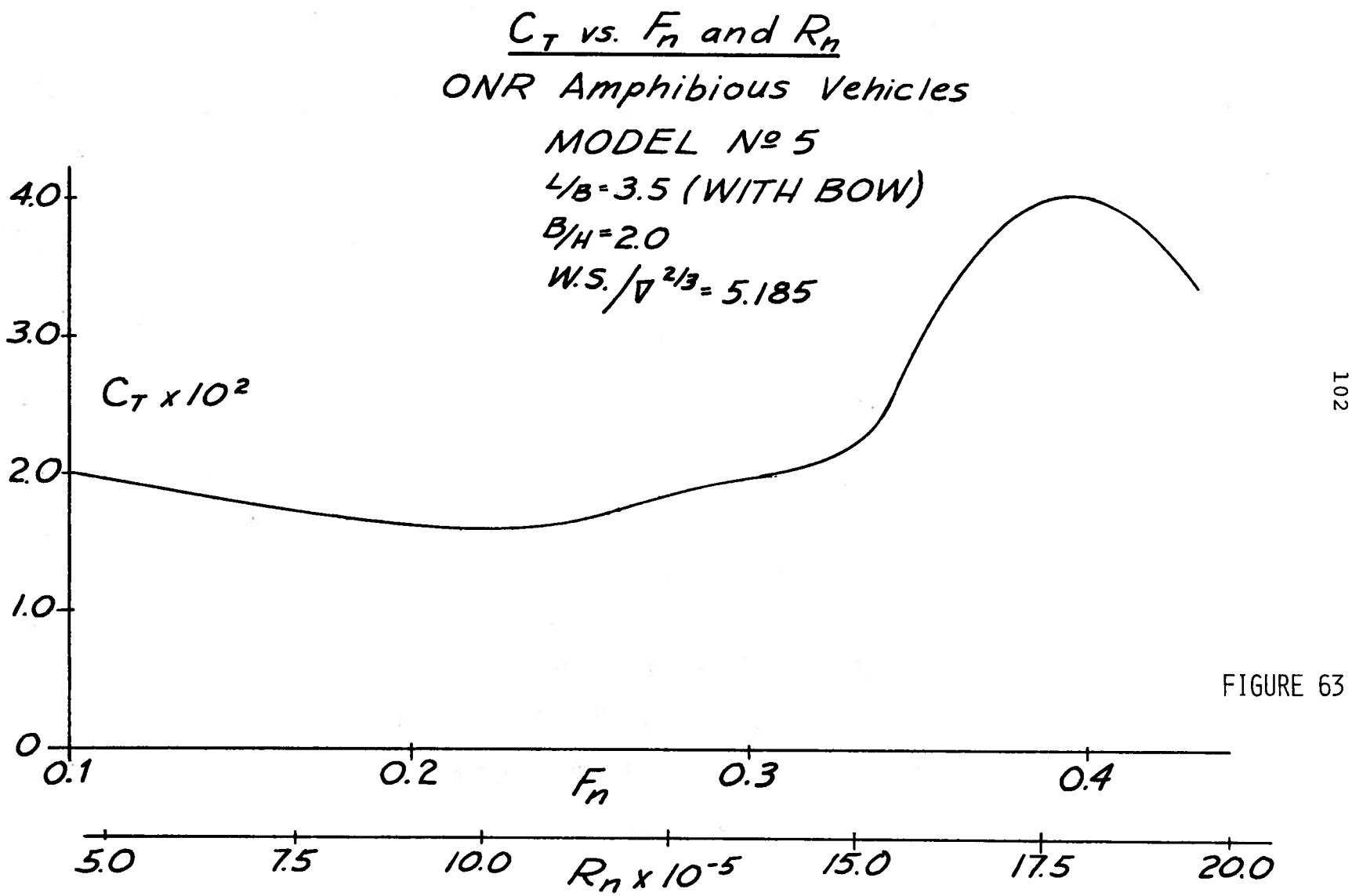
C_T vs. F_n and R_n
ONR Amphibious Vehicles
MODEL Nº 5
L/B = 3.5 (WITH BOW)
B/H = 2.0
W.S./$\nabla^{2/3}$ = 5.185
4.0
3.0
2.0
1.0
0
$C_T \times 10^2$
0.1
0.2
0.3
0.4
F_n
5.0
7.5
10.0
15.0
17.5
20.0
$R_n \times 10^{-5}$

FIGURE 63

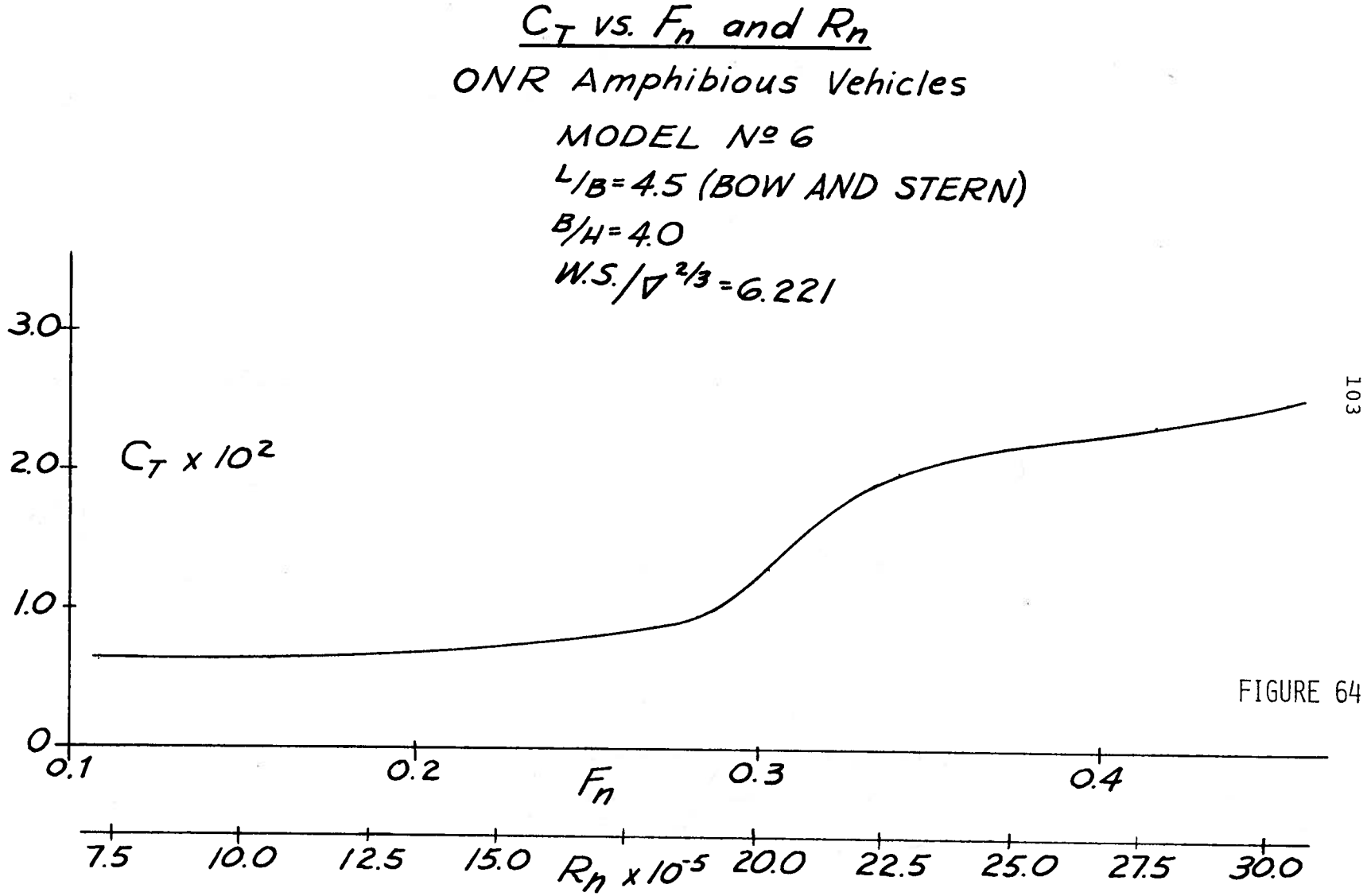
C_T vs. F_n and R_n
ONR Amphibious Vehicles
MODEL Nº 6
$L/B = 4.5$ (BOW AND STERN)
$B/H = 4.0$
$W.S./\nabla^{2/3} = 6.221$
3.0
2.0
1.0
0
$C_T \times 10^2$
0.1
0.2
0.3
0.4
F_n
7.5
10.0
12.5
15.0
$R_n \times 10^{-5}$
20.0
22.5
25.0
27.5
30.0

FIGURE 64

C_T vs. F_n and R_n

ONR Amphibious Vehicles

MODEL Nº 7

$L/B = 2.5$

$B/H = 3.0$

$W.S./\nabla^{2/3} = 5.157$

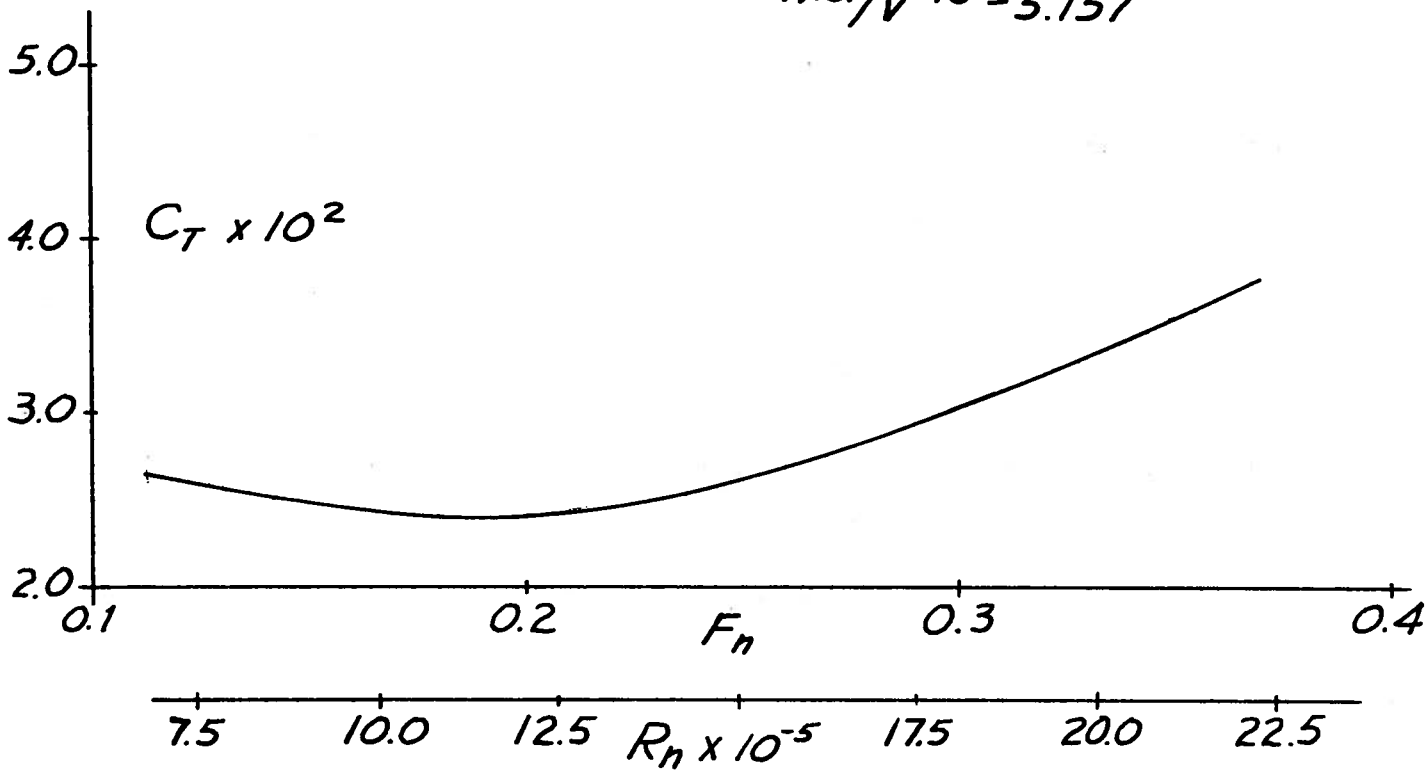

FIGURE 67

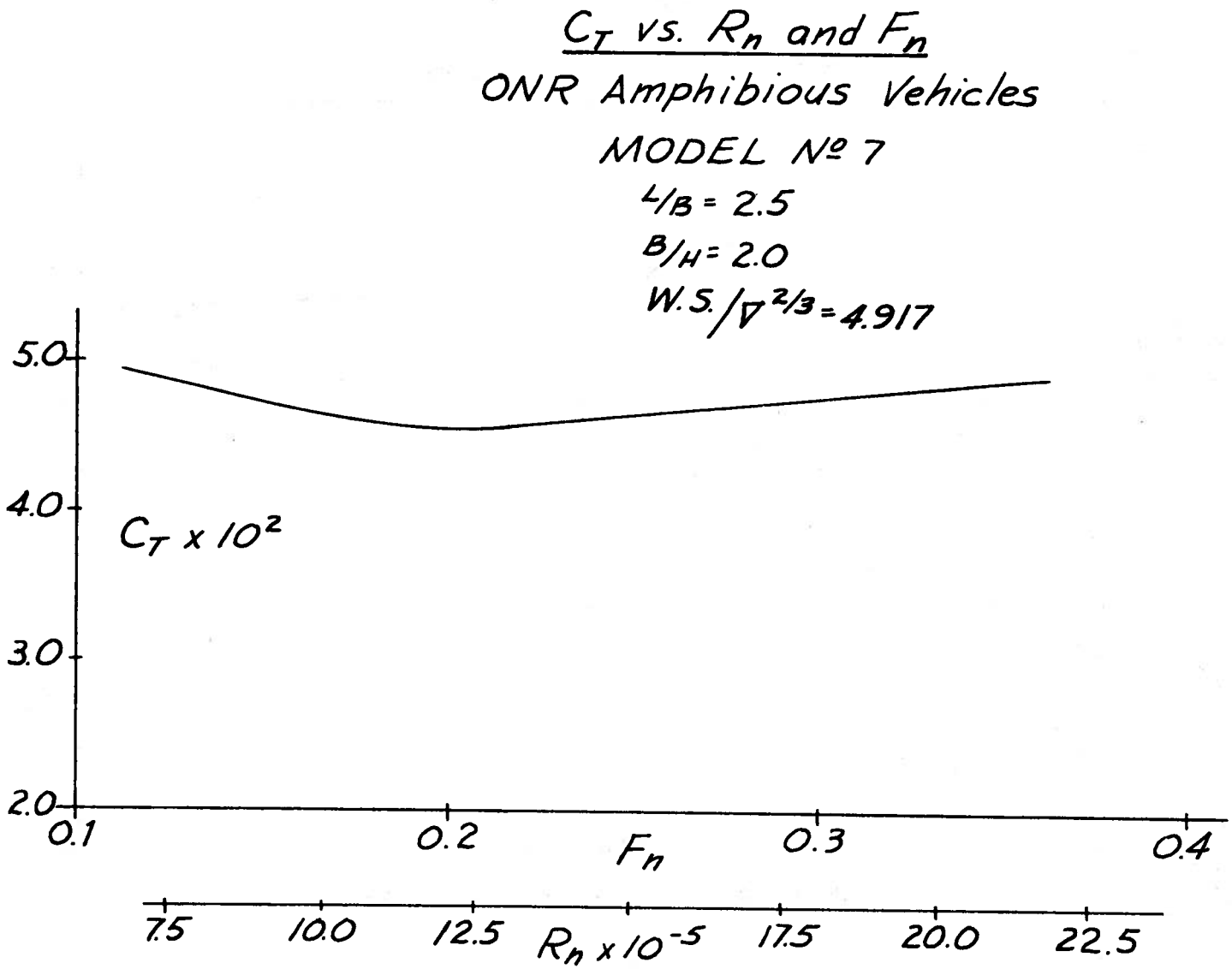
C_T vs. R_n and F_n
ONR Amphibious Vehicles
MODEL Nº 7
$L/B = 2.5$
$B/H = 2.0$
$W.S./\nabla^{2/3} = 4.917$
5.0
4.0
3.0
2.0
$C_T \times 10^2$
0.1
0.2
0.3
0.4
F_n
7.5
10.0
12.5
$R_n \times 10^{-5}$
17.5
20.0
22.5

FIGURE 68

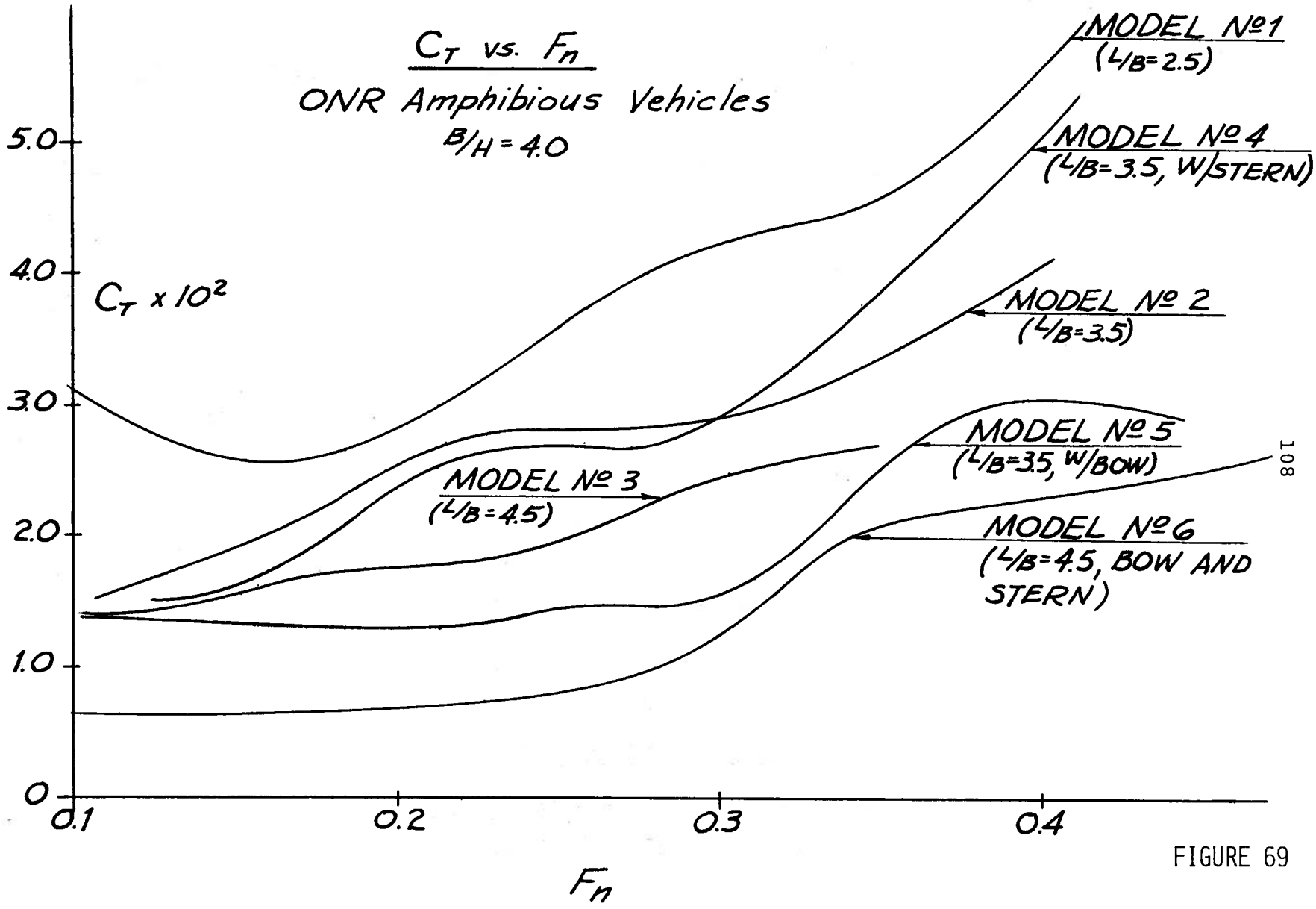
C_T vs. F_n
ONR Amphibious Vehicles
B/H = 4.0
MODEL Nº1
(L/B=2.5)
MODEL Nº4
(L/B=3.5, W/STERN)
MODEL Nº 2
(L/B=3.5)
MODEL Nº 3
(L/B=4.5)
MODEL Nº 5
(L/B=3.5, W/BOW)
MODEL Nº 6
(L/B=4.5, BOW AND STERN)
$C_T \times 10^2$
5.0
4.0
3.0
2.0
1.0
0
0.1
0.2
0.3
0.4
F_n

FIGURE 69

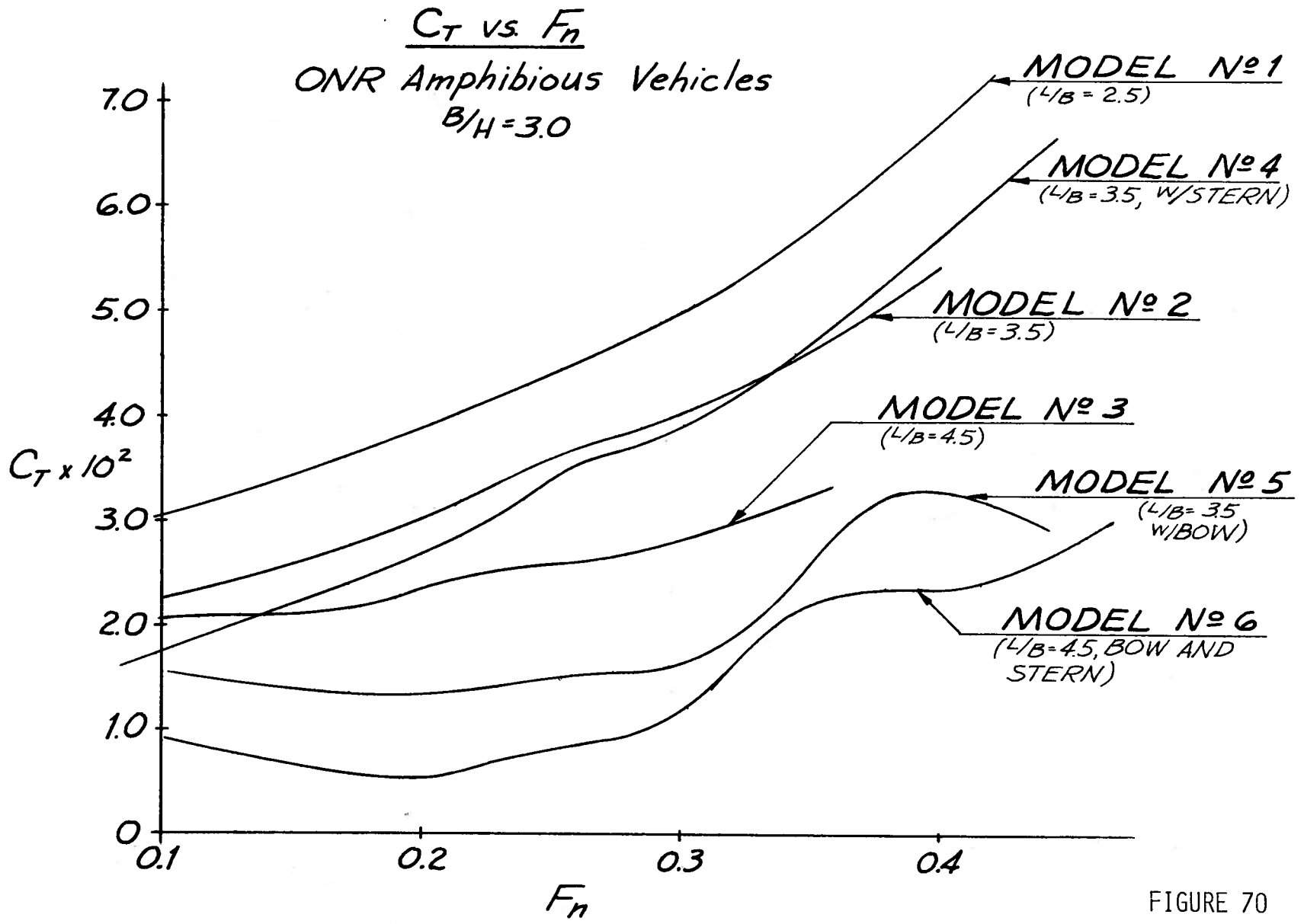
C_T vs. F_n
ONR Amphibious Vehicles
B/H = 3.0
MODEL Nº 1
(L/B = 2.5)
MODEL Nº 4
(L/B = 3.5, W/STERN)
MODEL Nº 2
(L/B = 3.5)
MODEL Nº 3
(L/B = 4.5)
MODEL Nº 5
(L/B = 3.5 W/BOW)
MODEL Nº 6
(L/B = 4.5, BOW AND STERN)
$C_T \times 10^2$
7.0
6.0
5.0
4.0
3.0
2.0
1.0
0
0.1
0.2
0.3
0.4
F_n

FIGURE 70

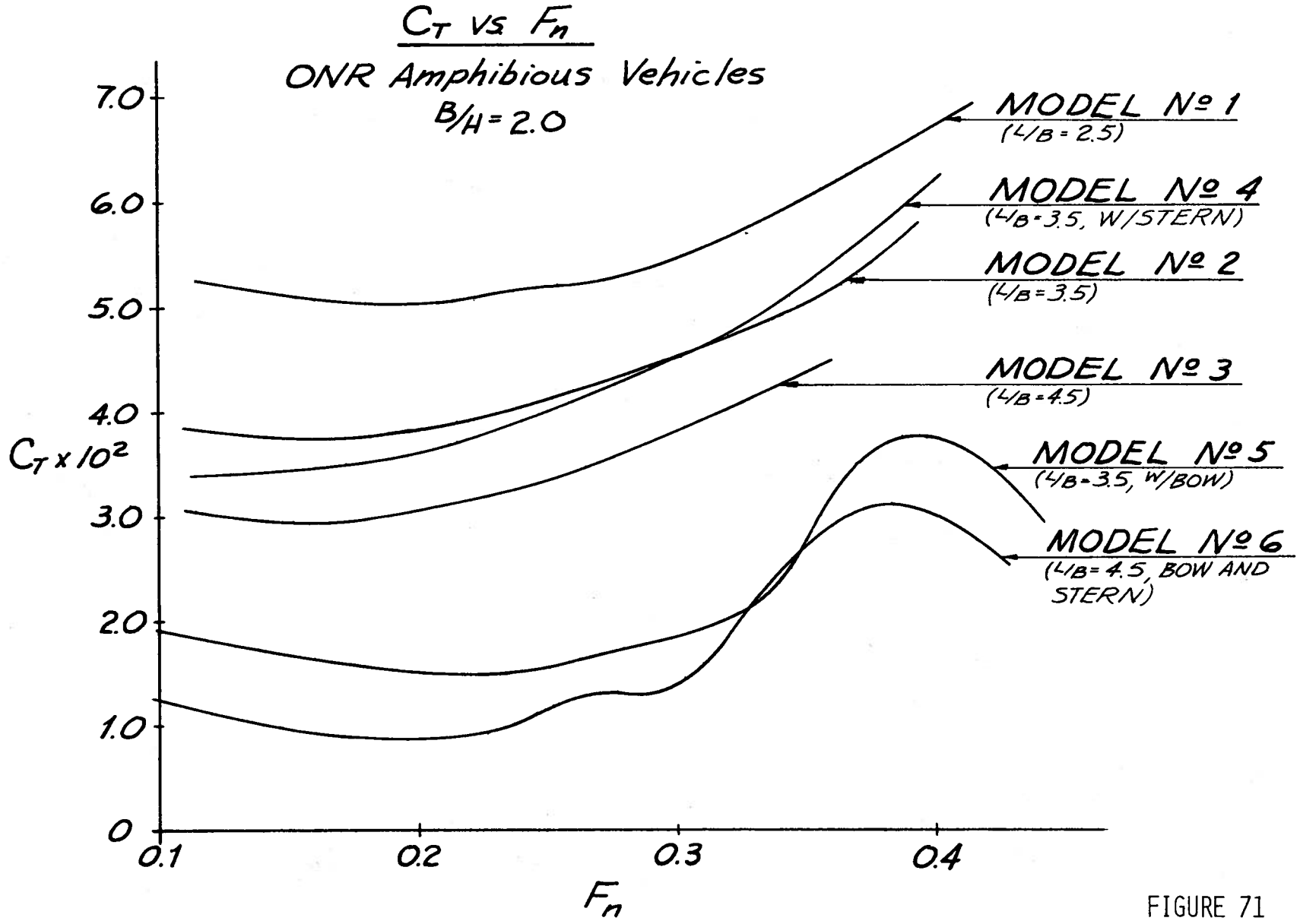
C_T vs F_n
ONR Amphibious Vehicles
B/H = 2.0
MODEL Nº 1
(L/B = 2.5)
MODEL Nº 4
(L/B = 3.5, W/STERN)
MODEL Nº 2
(L/B = 3.5)
MODEL Nº 3
(L/B = 4.5)
MODEL Nº 5
(L/B = 3.5, W/BOW)
MODEL Nº 6
(L/B = 4.5, BOW AND STERN)
$C_T \times 10^2$
7.0
6.0
5.0
4.0
3.0
2.0
1.0
0
0.1
0.2
0.3
0.4
F_n

FIGURE 71

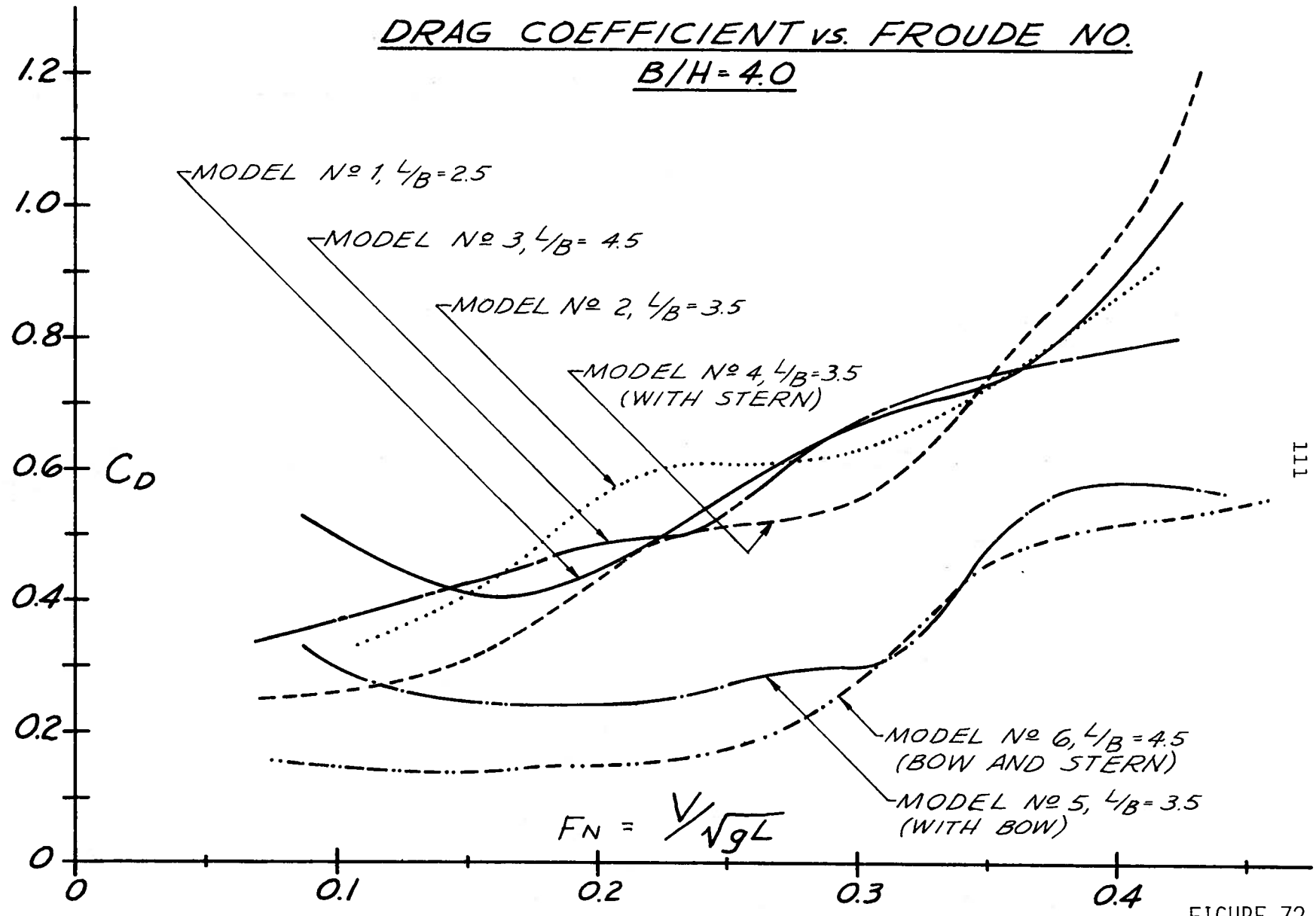
DRAG COEFFICIENT vs. FROUDE NO.
B/H = 4.0
MODEL Nº 1, L/B = 2.5
MODEL Nº 3, L/B = 4.5
MODEL Nº 2, L/B = 3.5
MODEL Nº 4, L/B = 3.5
(WITH STERN)
MODEL Nº 6, L/B = 4.5
(BOW AND STERN)
MODEL Nº 5, L/B = 3.5
(WITH BOW)
C_D
$F_N = V/\sqrt{gL}$
1.2
1.0
0.8
0.6
0.4
0.2
0
0
0.1
0.2
0.3
0.4

FIGURE 72

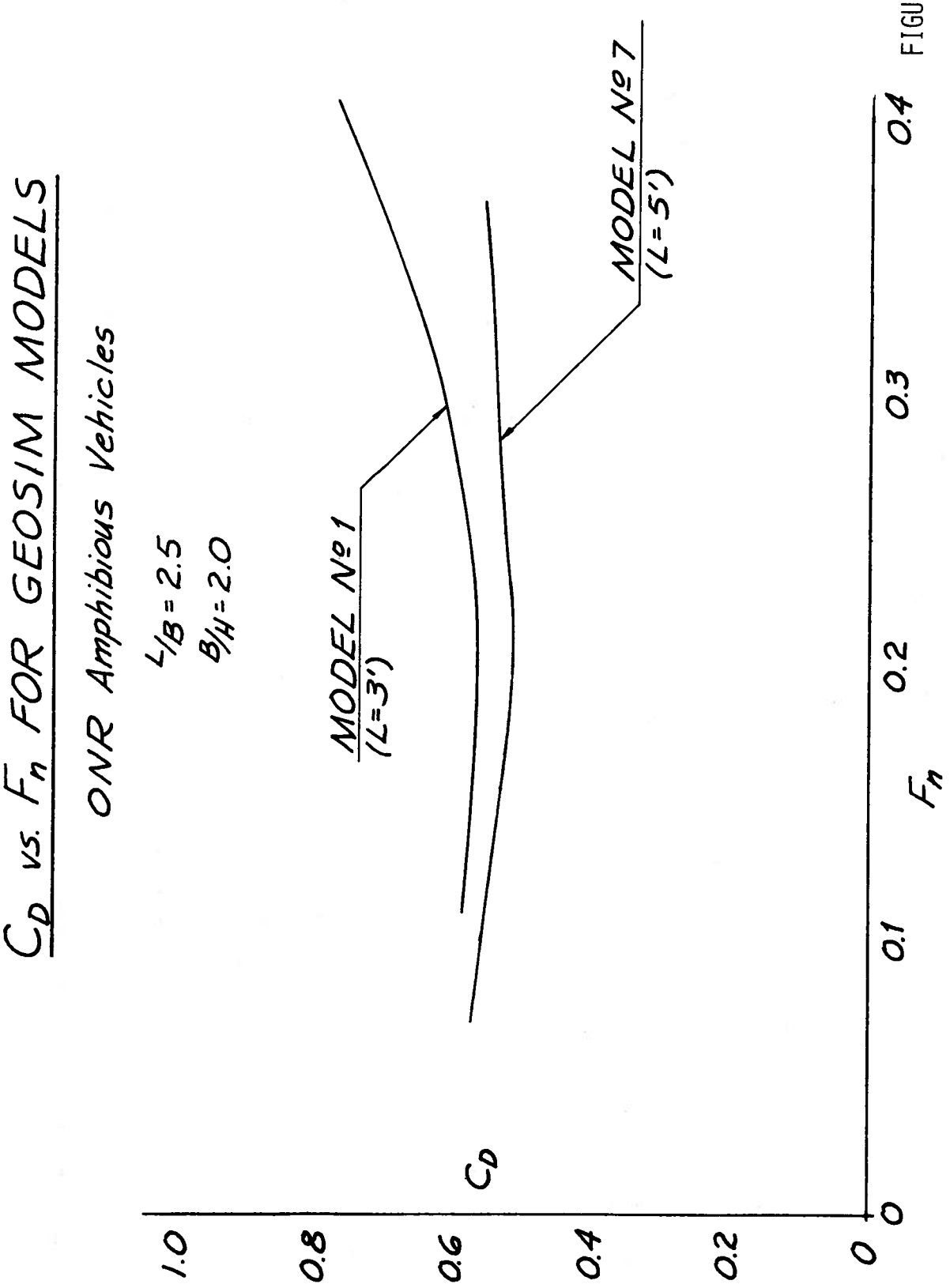
C_D vs. F_n FOR GEOSIM MODELS
ONR Amphibious Vehicles
$L/B = 2.5$
$B/H = 2.0$
MODEL Nº 1
(L=3')
MODEL Nº 7
(L=5')
C_D
1.0
0.8
0.6
0.4
0.2
0
0
0.1
0.2
0.3
0.4
F_n

FIGURE 75

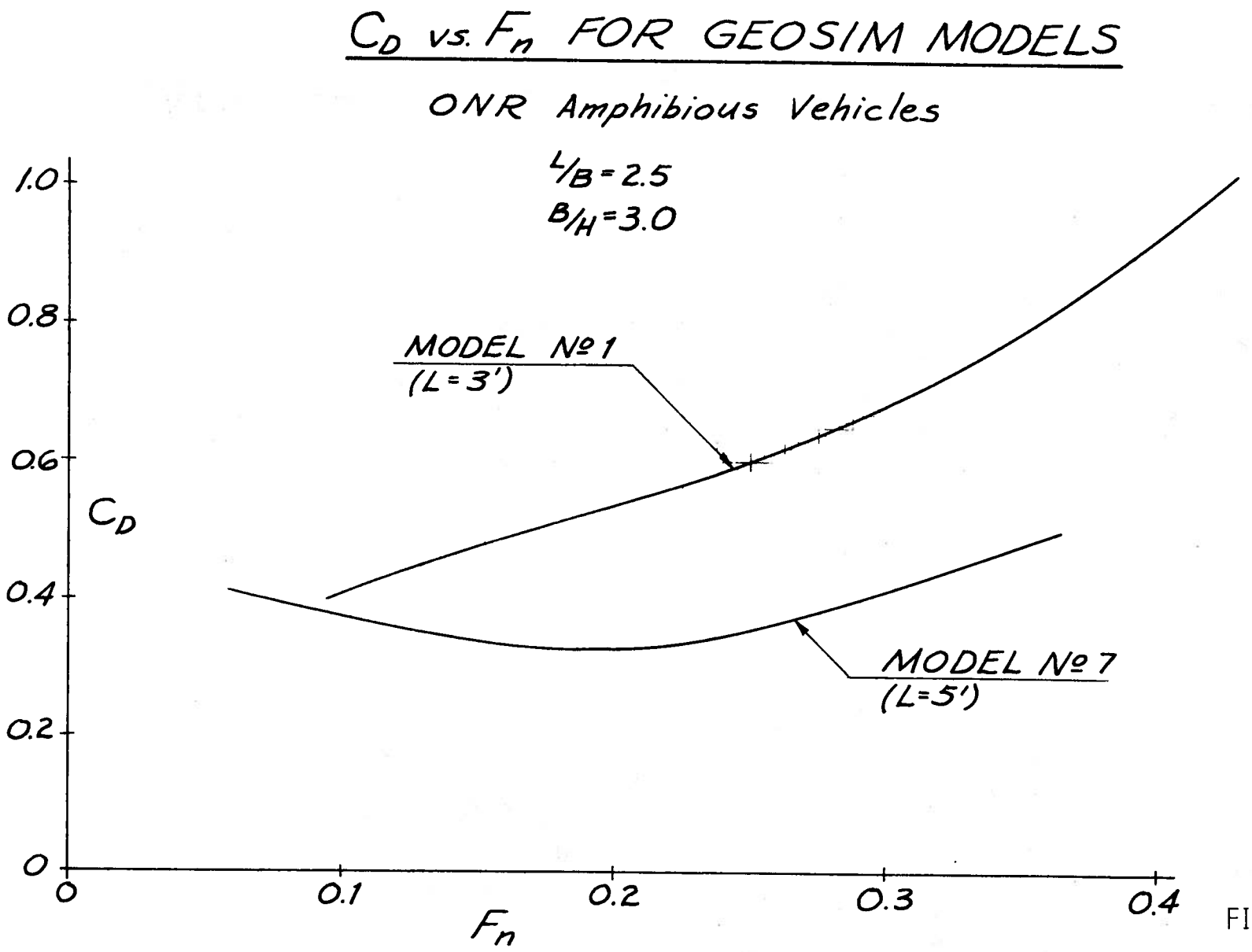
C_D vs. F_n FOR GEOSIM MODELS
ONR Amphibious Vehicles
$L/B = 2.5$
$B/H = 3.0$
MODEL Nº 1
(L = 3')
MODEL Nº 7
(L = 5')
C_D
F_n
1.0
0.8
0.6
0.4
0.2
0
0.1
0.2
0.3
0.4

FIGURE 76

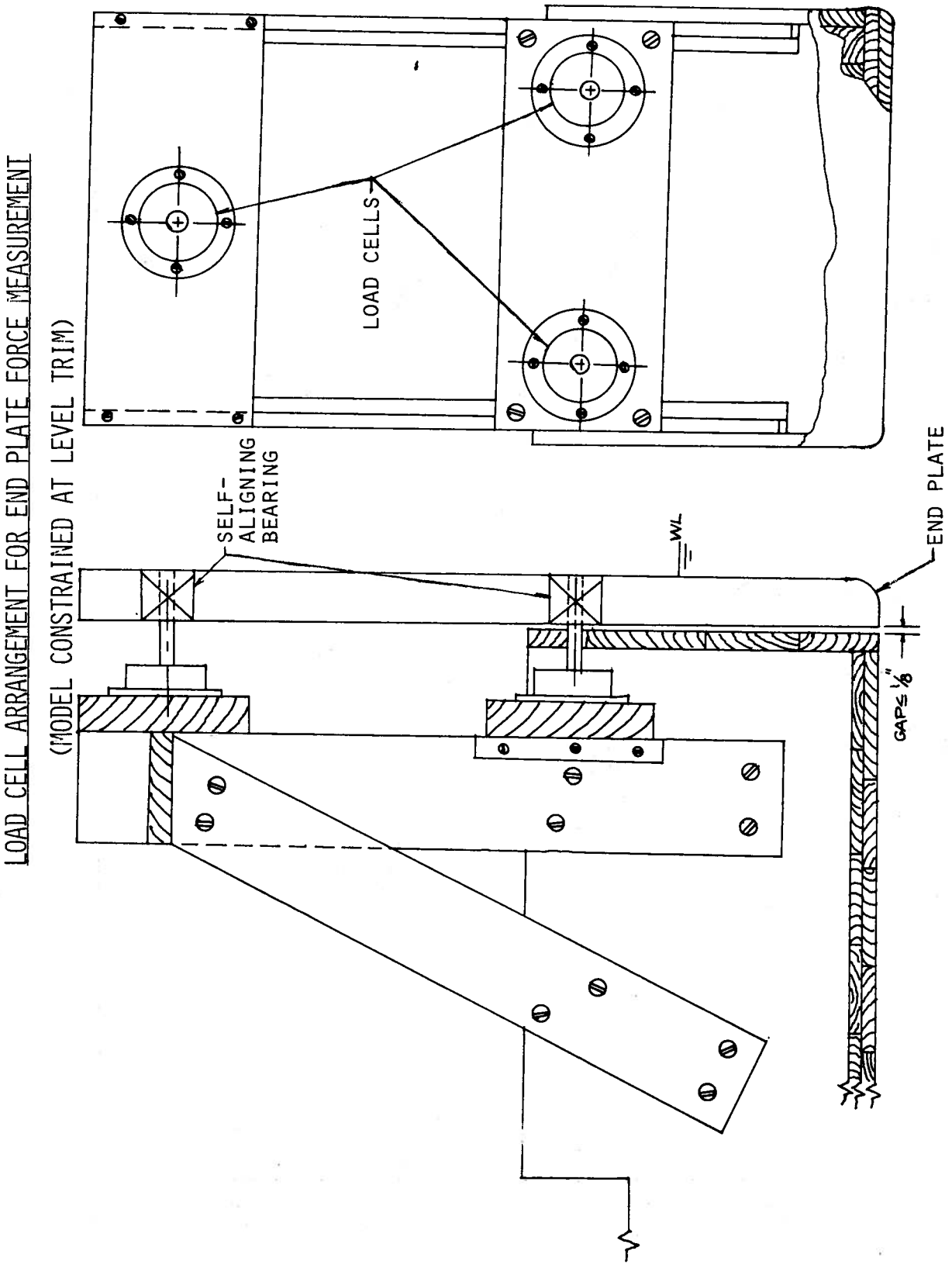
LOAD CELL ARRANGEMENT FOR END PLATE FORCE MEASUREMENT
(MODEL CONSTRAINED AT LEVEL TRIM)
LOAD CELLS
SELF-ALIGNING BEARING
WL
END PLATE
GAP ≤ 1/8"

FIGURE 77

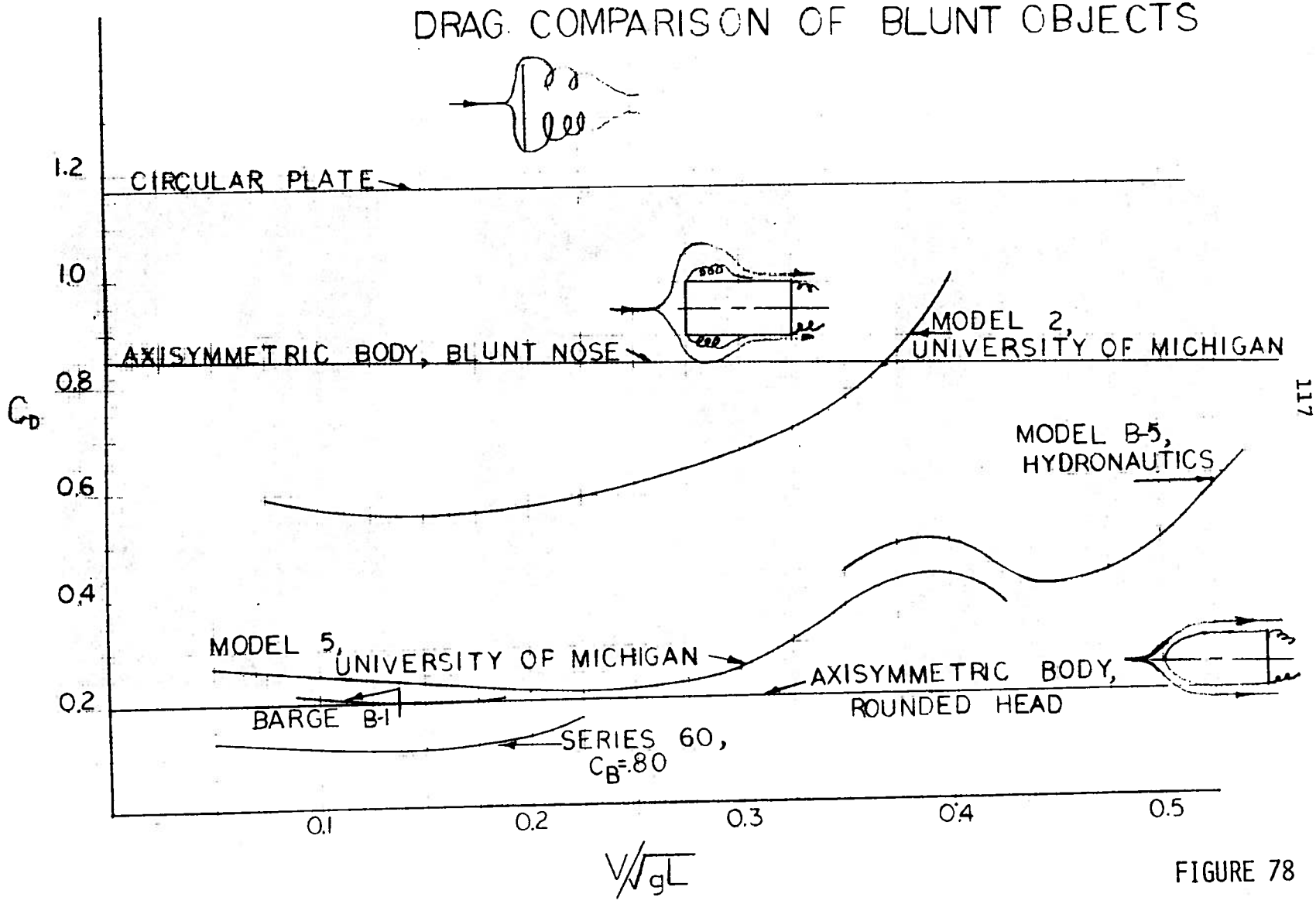
DRAG COMPARISON OF BLUNT OBJECTS
1.2
1.0
0.8
0.6
0.4
0.2
C_D
CIRCULAR PLATE
AXISYMMETRIC BODY, BLUNT NOSE
MODEL 2, UNIVERSITY OF MICHIGAN
MODEL B-5, HYDRONAUTICS
MODEL 5, UNIVERSITY OF MICHIGAN
BARGE B-1
SERIES 60, C_B=.80
AXISYMMETRIC BODY, ROUNDED HEAD
0.1
0.2
0.3
0.4
0.5
$V/\sqrt{gL}$

FIGURE 78

(1)

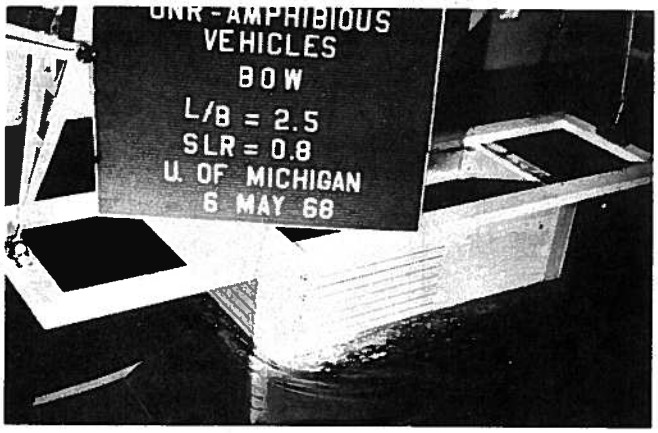

(2)

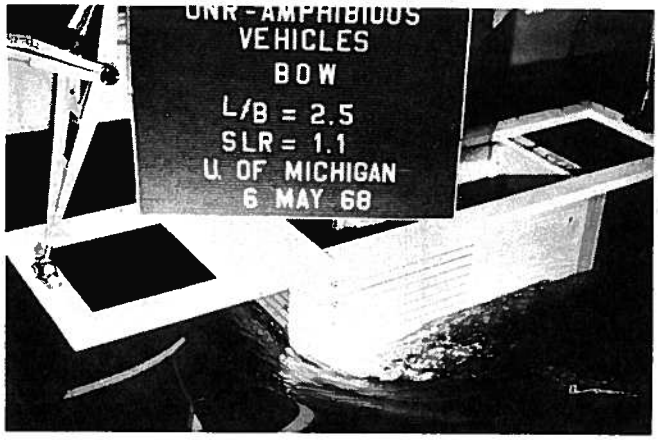

(3)

FIGURES 1-3. MODEL 1, BOW VIEW AT THREE SPEED-LENGTH RATIOS (SLR)

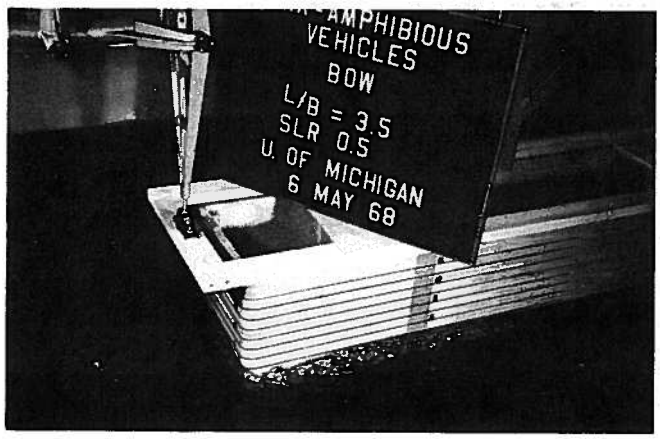

(4)

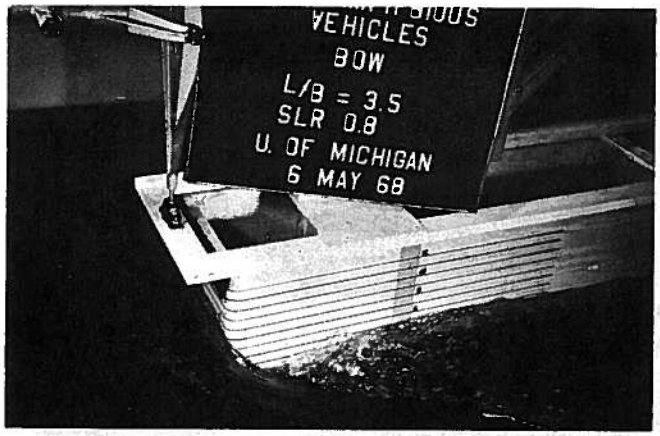

(5)

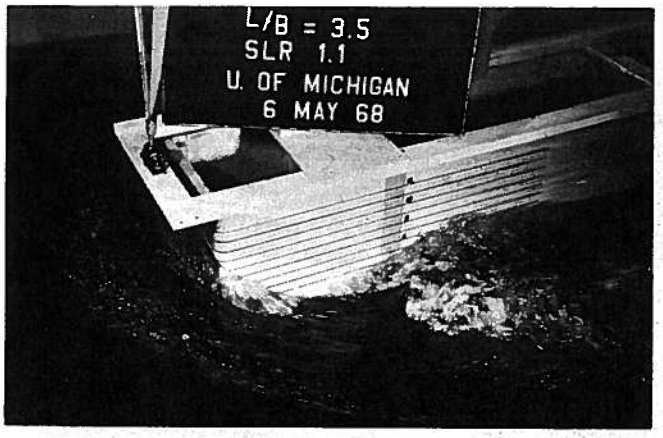

(6)

FIGURES 4-6. MODEL 2, BOW VIEW AT THREE SPEED-LENGTH RATIOS (SLR)

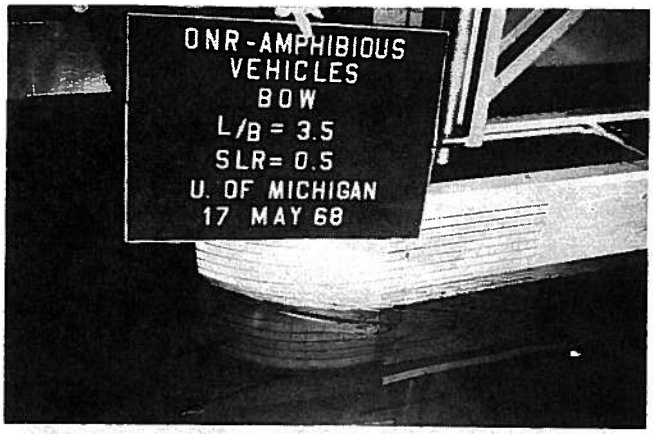

(7)

(8)

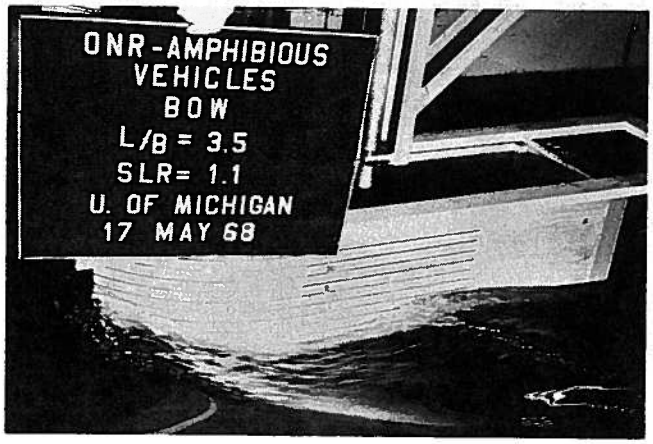

(9)

FIGURES 7-9. MODEL 5, BOW VIEW, AT THREE SPEED-LENGTH RATIOS (SLR)

Security Classification

121

DOCUMENT CONTROL DATA - R & D

(Security classification of title, body of abstract and indexing annotation must be entered when the overall report is classified)

1. ORIGINATING ACTIVITY *(Corporate author)*

The University of Michigan
Ship Hydrodynamics Laboratory

2a. REPORT SECURITY CLASSIFICATION

2b. GROUP

3. REPORT TITLE

Experiments on the Resistance of a Family of Box-Like Hull Forms for Amphibious Vehicles

4. DESCRIPTIVE NOTES *(Type of report and inclusive dates)*

Final report, September 1968

5. AUTHOR(S) *(First name, middle initial, last name)*

Horst Nowacki, James L. Moss
Eric D. Snyder, Bernard J. Young

6. REPORT DATE	7a. TOTAL NO. OF PAGES	7b. NO. OF REFS
September, 1968	121	6

8a. CONTRACT OR GRANT NO.

ONR-Nonr-1224(64)

b. PROJECT NO.

08216

c.

d.

9a. ORIGINATOR'S REPORT NUMBER(S)

9b. OTHER REPORT NO(S) *(Any other numbers that may be assigned this report)*

10. DISTRIBUTION STATEMENT

This document has been approved for public release and sale; its distribution is unlimited.

11. SUPPLEMENTARY NOTES

12. SPONSORING MILITARY ACTIVITY

Office of Naval Research

13. ABSTRACT

Resistance, trim, and sinkage were measured for a family of hull shapes derived from a simple box-like parent similar to present amphibians. The data were analyzed to derive conclusions as to the feasibility of major resistance reductions, the effects of drastic variations in hull proportions, and the presence of scale effects.

DD FORM 1 NOV 65 1473 (PAGE 1)

S/N 0101-807-6811

Security Classification

14 KEY WORDS	LINK A		LINK B		LINK C	
	ROLE	WT	ROLE	WT	ROLE	WT

DD FORM 1 NOV 65 1473 (BACK)

S/N 0101-807-6821